Production of particles with large transverse momenta and models of hard collisions

G. Ranft and J. Ranft

Physics Faculty, Karl Marx University, Liepzig, German Democratic Republic
Fiz. Elem. Chastits At. Yadra **10**, 90–190 (January-February 1979)

The results of investigations of the production of particles with large transverse momenta in hadron–hadron collisions at high energies are considered. The main experimental data are given on the total cross sections, the multiplicities, and the single-particle and two-particle spectra of the secondary particles. These data are analyzed in the framework of models of hard collisions.

PACS numbers: 13.85.Kf

1. BASIC EXPERIMENTAL FACTS

Single-Particle Distributions. The first indications of a somewhat unexpected behavior of the particle production probability at large transverse momenta ($p_\perp > 2$ GeV/c) were reported in 1972 by the CCR group (CERN, Columbia University, Rockefeller University).[1,2] Using the colliding beams of the CERN ISR, it was found that the cross section of the reaction $pp \to \pi^0 + X$ at $p_\perp \approx 6$ GeV/c, $\sqrt{s} = 52.7$ GeV, and $\theta_{cm} = 90°$ exceeds by seven orders of magnitude the value obtained by extrapolating the then adopted exponential law $Ed^3\sigma/d^3p \sim \exp(-6p_\perp)$ (Fig. 1).

Since then, the results of these measurements have been confirmed more than once and also in the case of other secondary particles such as $\pi^\pm, K^\pm, p, \bar{p}, \eta$; moreover, this has been done not only in the energy range of the CERN ISR[1-18] but also in the FNAL (Fermi National Accelerator Laboratory, Batavia) energy range.[19-24] The obtained data can be parametrized by a power-law function of $p_\perp$ and a scale-invariant function of $x_\perp = 2p_\perp/\sqrt{s}$:

$$Ed^3\sigma/d^3p \sim f(x_\perp)/p_\perp^n, \tag{1}$$

where

$$n \approx 8; \tag{2}$$

in the range of the CERN ISR[2]

$$f(x_\perp) \sim \exp(-Dx_\perp), \quad D \approx 13, \tag{3}$$

and at the FNAL energies[19,20]

$$f(x_\perp) \sim (1-x_\perp)^b, \quad b \approx 9. \tag{4}$$

The data shown in Fig. 2 suggest that at large $p_\perp$ the function $p_\perp^8 Ed^3\sigma/d^3p$ tends to a scale-invariant limit. A similar behavior was also found in the case of the η resonance, whose spectrum $Ed^3\sigma/d^3p$ as a function of $p_\perp$ repeats the π^0-meson spectrum except for a normalization factor 0.58, which reduces the absolute number of η mesons at $p_\perp \gtrsim 3$ GeV/c.[12]

At large transverse momenta, the fraction of heavy particles increases in comparison with its value at small $p_\perp$, as is reflected in Fig. 3. Figure 4 gives data on the relative yields of the particles as a function of $p_\perp$ obtained in the joint experiment of the Chicago-Princeton group.[20]

Jet Structure of Events at Large $p_\perp$. Investigations of the two- and many-particle distributions revealed a strong correlation between the particle with large $p_\perp$ (trigger particle) and the other particles detected in the same hemisphere and also in the opposite hemisphere with respect to the azimuthal angle. The majority of the experimental facts indicate that the particle production at large $p_\perp$ proceeds through a mechanism involving jets (possibly two).

Coplanarity. It is found that particles produced in the hemisphere with azimuthal angle opposite to the hemisphere with the trigger particle (particle 1 in Fig. 5) have rather small transverse momenta relative to the scattering plane (determined by the momentum of the initial particle and the momentum of the trigger particle). Let p_{out} be the momentum component of the secondary particles perpendicular to the scattering plane; the p_{out} distribution decreases exponentially, approximately as (Fig. 6)

$$dN/d|p_{out}| \sim \exp(-2|p_{out}|). \tag{5}$$

The mean value of p_{out} is $\langle p_{out}\rangle \approx 0.5$ GeV/c.[10]

Jet in the forward hemisphere. Study of the behavior of two particles with large $p_\perp$ in the same hemisphere revealed the following.

1. The invariant two-particle distribution as a function of $(p_{\perp_1} + p_{\perp_2})$ in the reactions $pp \to \pi_1^0\pi_2^0 X$ behaves like the single-particle distribution at large $p_\perp$ (Fig. 7)[10]:

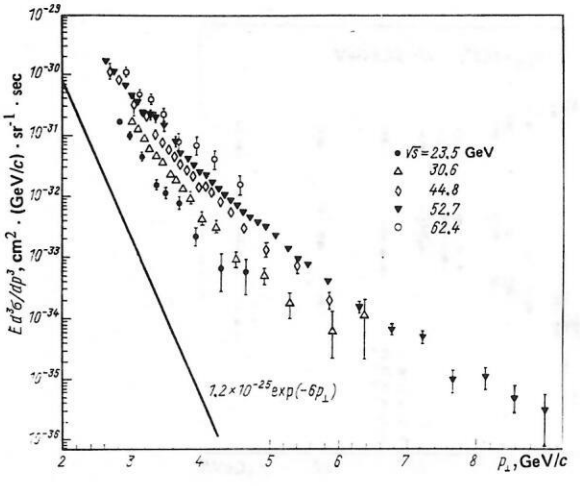

FIG. 1. Dependence of the invariant cross section on the transverse momentum in the energy range of the CERN ISR.[2]

 0090-4759/79/010035-36$02.80

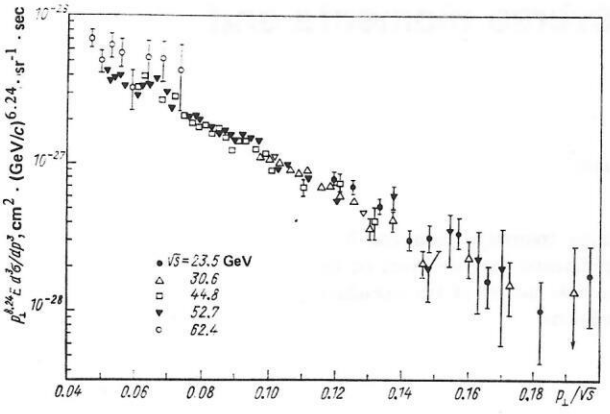

FIG. 2. Factorization of the inclusive cross section of π^0-meson production at $\theta_{cm}=90°$ and energies $23.4 \le \sqrt{s} \le 63$ GeV.[2]

$$E_1 E_2 \frac{d^6\sigma}{d^3p_1 d^3p_2} \sim (p_{\perp_1} - p_{\perp_2})^{-n} f(x_{\perp_1} - x_{\perp_2}). \qquad (6)$$

Here, n and $f(x_{\perp_1}+x_{\perp_2})$ are analogous to the same quantities for the single-particle distributions. This suggests that the production of two particles with a large value of $p_\perp = p_{\perp_1} + p_{\perp_2}$ is just as improbable as the production of one particle with the same value of the momentum.

2. The correlations between the transverse momenta reveal an appreciable positive correlation between the momentum of the pions with large $p_\perp$ and the momentum of charged particles produced in the forward hemisphere.

For the joint experiment of the CCRS group (CERN, Columbia, Rockefeller, Saclay)[12] this connection was expressed by means of the function

$$F(p^0_{\perp_1},\ p_{\perp_2}) = \frac{\int_{-\Delta\varphi_1}^{\Delta\varphi_1} d\varphi_1 \int_{-\Delta\varphi_2}^{\Delta\varphi_2} d\varphi_2 \int_{-\Delta y_1}^{\Delta y_1} dy_1 \int_{-\Delta y_2}^{\Delta y_2} dy_2 \int_{p^0_{\perp_1}}^{\sqrt{s}/2} dp_{\perp_1} \frac{d^6\sigma}{dy_1 dp_{\perp_1} d\varphi_1 dy_2 dp_{\perp_2} d\varphi_2}}{\int_{-\Delta\varphi_1}^{\Delta\varphi_1} d\varphi_1 \int_{-\Delta y_1}^{\Delta y_1} dy_1 \int_{p^0_{\perp_1}}^{\Delta\sqrt{s}/2} dp_{\perp_1} \frac{d^3\sigma}{dy_1 dp_{\perp_1} d\varphi_1}} \qquad (7)$$

(the limits of integration are determined by the geometrical acceptance of the detector), which gives the number of charged particles in unit intervals of momentum and the angle φ observed together with a trigger particle with large $p_\perp$ (particle 1 in Fig. 5) as a function of the transverse momentum $p^0_{\perp_1}$ of this particle and the transverse momentum $p_{\perp_2}$ of particle 2. Such a two-particle correlation function is appreciably larger than the inclusive single-particle distribution (Fig. 8), i.e., with increasing $p_{\perp_2}$ it decreases slower than the completely inclusive distribution. With increasing $\sqrt{s}$, the function F increases.

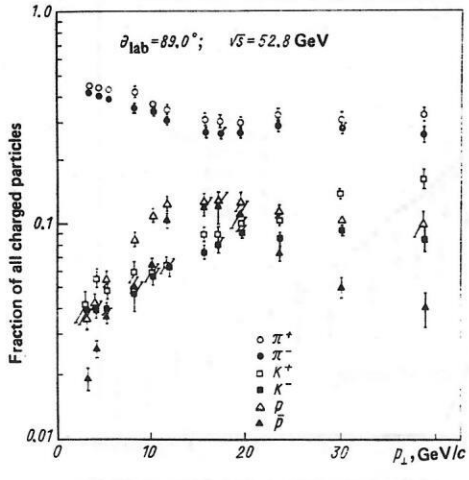

FIG. 3. Relative values of production cross sections of different charged particles as functions of $p_\perp$.[14]

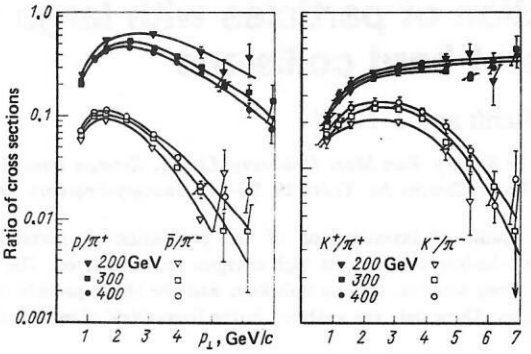

FIG. 4. Ratios of production cross sections of different species of hadrons as functions of $p_\perp$.

The distribution with respect to the transverse momenta in the direction of the jet is limited and is reminiscent of the analogous distributions from the physics of small $p_\perp$ (Fig. 9), where $\langle q_\perp \rangle \approx 0.3$ GeV/c ($q_\perp$ is the transverse momentum relative to the direction of the jet).[7,10]

In the language of the rapidity distribution of the particles of the forward hemisphere in the center-of-mass system, this boundedness of $q_\perp$ is equivalent to a shrinkage of the y distribution with increasing $|p_x| = p_\perp$ (Ref. 10) (p_x is the component of the transverse momentum in the scattering plane) (Fig. 10). It can be expressed in terms of the correlation length $L \sim 1/p_\perp$.

The boundedness of $q_\perp$ has the consequence that the rapidity distribution of particles of the forward hemisphere repeats the rapidity distribution of the trigger particle. This can be seen in Figs. 11a and 11b, which show the rapidity distributions of the particles of the forward hemisphere.[7]

Jet in the backward hemisphere. To all appearances, the secondary particles also form a jet in the backward

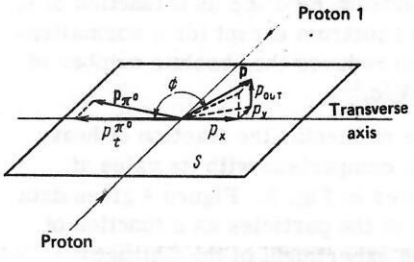

FIG. 5. Definition of p_{out} and p_x for secondary particle in the hemisphere opposite to the hemisphere with the trigger particle[10]; S is the scattering plane of the π^0 meson.

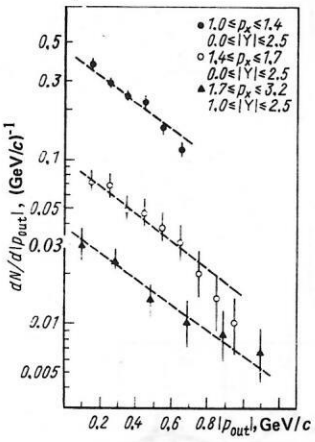

FIG. 6. Distribution of the secondary particles in the backward hemisphere with respect to p_{out} for different $|p_x|$ intervals.[27]

hemisphere.

In the majority of experiments, this jet behaves completely independently of the jet in the forward hemisphere. It is not collinear (not antiparallel) with the jet in the direction of the trigger particle. This is well demonstrated in Fig. 12: Independently of the rapidity of the trigger particle, the maximum of the y distribution is at $y = 0$. The data of the experiment of Ref. 11, in which the momenta of the secondary particles were not analyzed, indicate a certain back-to-back correlation with the rapidity maximum of the trigger particle.

In the backward hemisphere too there is a large positive correlation of the momenta; this can be seen in Fig. 13, which shows the function $F(p_{\perp}^0, p_{\perp_2})$ defined by Eq. (7) for the backward hemisphere.

In Fig. 14, the distribution with respect to the transverse momentum component p_x, which equalizes the transverse momentum $p_{\perp_1}$ of the trigger particle, is plotted as dN/dx_e (Ref. 27) as a function of $x_e = |p_x|/p_{\perp_1}$. Darriulat *et al.*[27] compared this distribution with the analogous fragmentation distributions of jets in the reactions $e^+e^- \to$ hadrons and for deep inelastic scattering and found much that was similar in the behavior of these quantities; this suggests that there is a single mechanism at the basis of these phenomena.

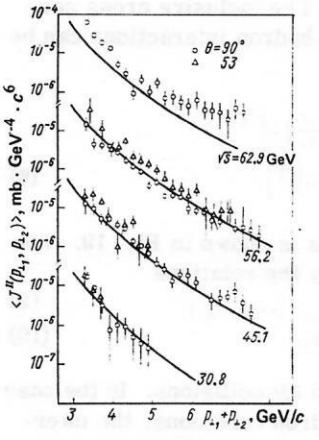

FIG. 7. Invariant two-particle distribution for the reaction $pp \to \pi_1^0\pi_2^0 X$ at different energies as a function of $p_{\perp_1}+p_{\perp_2}$. The curves correspond to the dependence $(p_{\perp_1}+p_{\perp_2})^{-n}\exp[-B(x_{\perp_1}+x_{\perp_2})]$ for $n = 7.1 \pm 0.5$, which follows from the $p_{\perp}$ behavior of the single-particle spectra.[9]

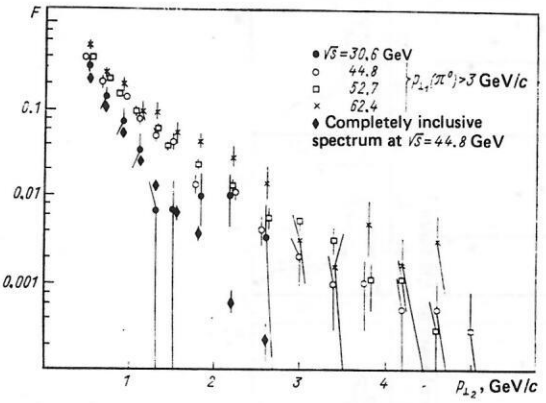

FIG. 8. Two-particle correlation function with respect to the transverse momenta $F(p^0{}_{\perp_1}, p_{\perp_2})$ defined by Eq. (7) as a function of the $p_{\perp}$ of the charged particle comoving with the trigger π^0 (forward hemisphere).

In Ref. 18 there was reported to be a strong decrease of dN/dx_e with increasing transverse momentum $p_{\perp_1}$ of the detected particle, especially at small $x_e (x_e \lesssim 0.6)$ (Fig. 15).

Jet trigger. The first experimental information about the behavior of the jet cross section at momentum 200 GeV/c was obtained at FNAL in a recent experiment with jet trigger.[30] In this experiment, two calorimeters (consisting of four modules) were used and placed in front of the trigger and behind it; they were sensitive to electron-photon (π^0) and hadron ($\pi^{\pm}$) showers. A jet with large $p_{\perp}$ was defined by the condition that the total transverse momentum measured by one of the calorimeters exceeds a certain given value ($p_{\perp}^{tot} \gtrsim 3.4$ or 4.5 GeV/c). Using only one module, it was possible to measure simultaneously the cross section by a single-particle trigger. It was found that the cross section measured by the jet trigger was approximately 100 times as large as the cross section measured by the single-particle trigger (Fig. 16); this effect is dis-

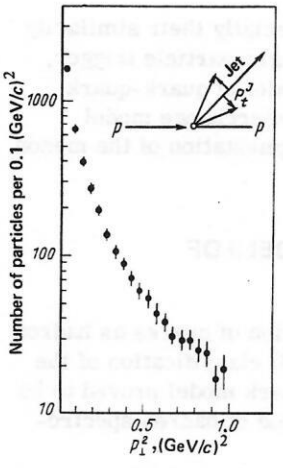

FIG. 9. Distribution of the number of particles of the forward hemisphere jet containing the trigger particle as a function of the square of the transverse momentum.[7]

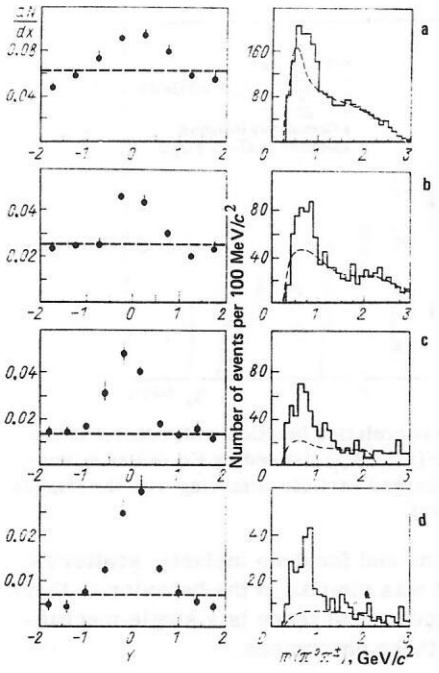

FIG. 10. Distributions of the forward hemisphere particles with respect to the rapidity and invariant mass for $|\varphi| \leq 27°$. a) $0.4 < p_x < 0.6$ GeV/c; b) $0.6 < p_x < 0.8$; c) $0.8 < p_x < 1.1$; d) $1.1 < p_x < 1.7$.

cussed in Sec. 2.

Let p_x' be the component of the charged particle's transverse momentum in the plane of the jet (i.e., the plane determined by the directions of the jet momentum P and the momentum of the incident hadron); the distribution $(1/\sigma)\, d\sigma/dz$, where $z = p_x'/p_\perp$, is shown in Fig. 17 and contains information about the fraction of the jet momentum carried away by individual charged particles; it is very similar to the distribution for reactions induced by leptons.

The analogous graph for the case of the backward hemisphere considered in the previous section is shown in Fig. 18 [note that in Fig. 18 we plot $(1/\sigma)\, d\sigma/dz$ as a function of $z = -p_x'/p_\perp$]. Note the manifest similarity of the behavior of the distributions measured by means of the single-particle and jet triggers.

These experimental data, especially their similarity to the data obtained using the single-particle trigger, can be understood in both the model of quark-quark scattering[31] and the constituent interchange model (CIM),[32] in which one allows fragmentation of the meson in the final state.[33,34]

2. BASIC PROPERTIES OF MODELS OF HARD COLLISIONS

Quark-Parton Model. The notion of quarks as hadron constituents is based on the $SU(3)$ classification of the hadrons.[35,36] The low-energy quark model proved to be particularly successful in the field of hadron spectroscopy.[37]

The parton model was proposed by Feynman[38] to interpret the Bjorken scaling observed in deep inelas-

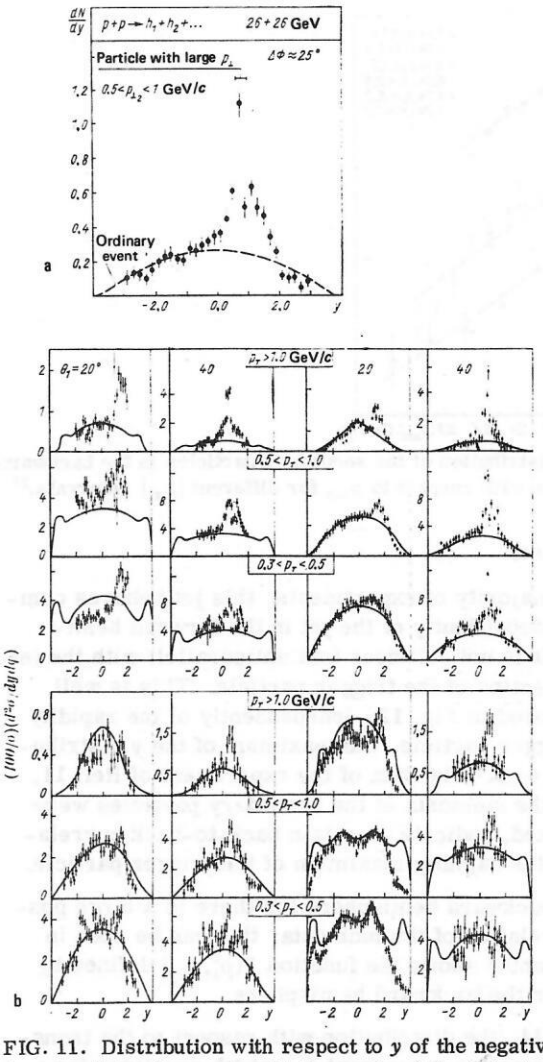

FIG. 11. Distribution with respect to y of the negative secondary particles in events with large $p_\perp$ of the detected particle at $\theta_1 = 45°$ (i.e., $y_1 \approx 1$) and $p_{\perp 1} > 2$ GeV/c (a) and the rapidity distributions in the forward hemisphere (b). On the left for negative trigger particles (positive and negative secondary particles); on the right for positive trigger particles (negative and positive secondary particles). For the secondary particles $|\varphi| \leq 25°$ relative to the direction of the trigger particle.

tic lepton-hadron collisions. The inclusive cross section for deep inelastic lepton-hadron interactions can be written in the form

$$\frac{d^2\sigma^{(\nu)}_{(\bar\nu)}}{dx\,dy} = \frac{G^2 M E_1}{\pi}\left[\left(1 - y - \frac{1}{2}xy\frac{M}{E_1}\right)G_2^{(\nu)_{(\bar\nu)}} + xy^2 G_1^{(\nu)_{(\bar\nu)}} \mp xy\left(1 - \frac{1}{2}y\right)G_3^{(\nu)_{(\bar\nu)}}\right]. \quad (8)$$

The kinematics of the process is shown in Fig. 19. The variables x and y are given by the relations

$$x = 1/\omega = -q^2/2\nu M = -q^2/2Mq_0, \quad 0 \leq x \leq 1; \quad (9)$$

$$y = \nu/E_1 = 1 - E_2/E_1. \quad (10)$$

Equation (8) applies to νN and $\bar\nu N$ collisions. In the case of deep inelastic electron-hadron collisions, the interference $V-A$ term with G_3, which does not conserve parity, is absent, and the coupling constant G^2 of the weak interactions is replaced by

$$G^2 \to (1/2)\,(e^2/q^2)^2 = 8\pi^2\alpha^2/(q^2)^2. \quad (11)$$

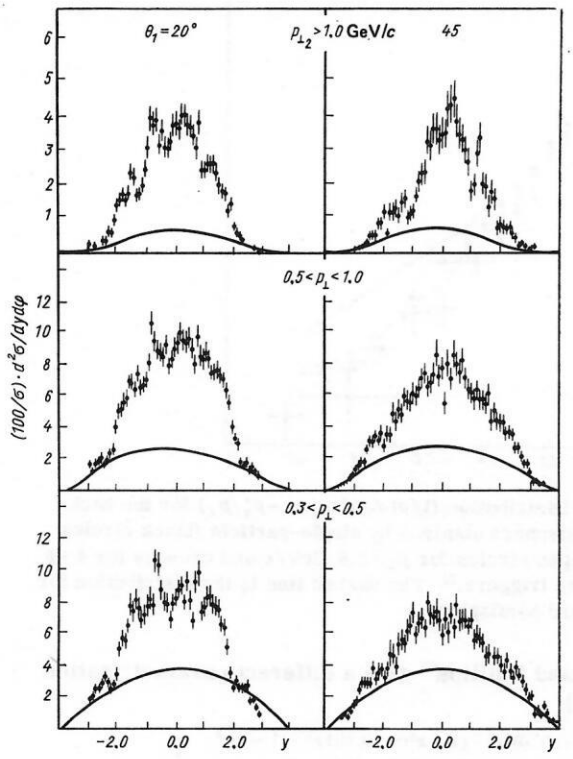

FIG. 12. Rapidity distribution of negative secondary particles of the backward hemisphere for large $p_\perp$ values of the trigger particle. The continuous curve corresponds to the distribution from ordinary events.

In the general case, the structure functions depend on ω and q: $G_i(\omega, q^2)$. Bjorken's prediction of the scaling behavior[39]

$$\lim_{|q^2|\to\infty} G_i(\omega, q^2) = F_i(x), \quad i = 1, 2, 3. \tag{12}$$

where x is fixed, agrees to within a 20% error with the majority of the currently known experimental data (Fig. 20).

In the quark-parton model, it is assumed that the partons are the quarks. The structure functions $F_i(x)$ are related to the distributions $f_i(x)$ and $f_{\bar{i}}(x)$ of the

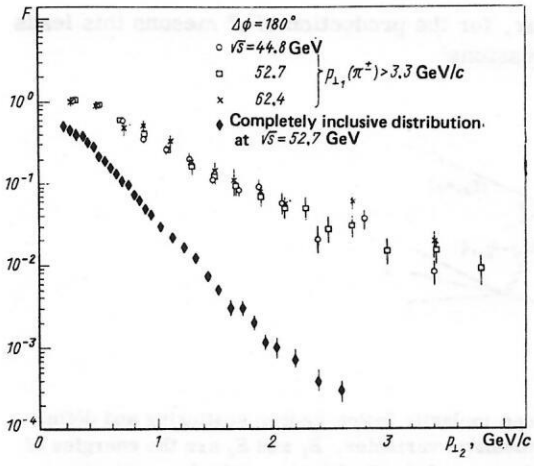

FIG. 13. Dependence of the two-particle momentum correlation function $F(p^0_{\perp 1}, p_{\perp 2})$ on the $p_{\perp 2}$ of the charged particle in the backward hemisphere.

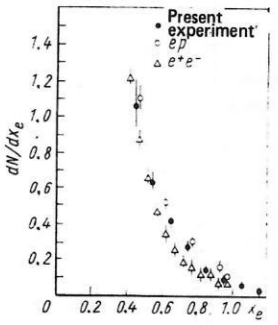

FIG. 14. Comparison of the distribtuion dN/dx_e for secondary particles of the backward hemisphere with the x distributions observed in the reaction $e^+e^- \to$ hadrons [at $\sqrt{s} = 4.8$ GeV (Ref. 28)] and in deep inelastic scattering $ep \to e +$ hadrons (Ref. 29) [at $\sqrt{s}$ in the interval from 3.5 to 5.5 GeV and $1 < q^2 < 2$ $(\text{GeV}/c)^2$ (Ref. 10)].

charged partons i and charged antipartons $\bar{i}$, respectively, in the hadron. Here, the variable x is the fraction of the longitudinal momentum of the hadron carried by the parton. For example, in the case of inelastic electron scattering

$$2xF_1(x) = F_2(x) = x\sum_i e_i^2 [f_i(x) - f_{\bar{i}}(x)]. \tag{13}$$

We denote the distributions of the u, d, and s quarks in the proton by

$$\left.\begin{aligned} u(x) &= x f_u(x), \\ d(x) &= x f_d(x), \\ s(x) &= x f_s(x) \end{aligned}\right\} \tag{14}$$

and find, for example, the following expressions for deep inelastic electron-proton scattering:

$$F_2^{ep}(x) = (4/9)[u(x) + \bar{u}(x)] + (1/9)[d(x) + \bar{d}(x)] + (1/9)[s(x) + \bar{s}(x)]; \tag{15}$$

$$F_2^{en}(x) = (4/9)[d(x) + \bar{d}(x)] + (1/9)[u(x) + \bar{u}(x)] + (1/9)[s(x) + \bar{s}(x)]. \tag{16}$$

For neutrino and antineutrino scattering,

$$F_2^{\nu p}(x) = 2[d(x) + \bar{u}(x)]; \quad F_2^{\bar{\nu} p}(x) = 2[u(x) + \bar{d}(x)]; \tag{17}$$

$$F_2^{\nu n}(x) = 2[u(x) + \bar{d}(x)]; \quad F_2^{\bar{\nu} n}(x) = 2[d(x) + \bar{u}(x)]. \tag{18}$$

The quark distribution functions satisfy a number of sum rules:

$$\int_0^1 [u(x) - \bar{u}(x)]\frac{dx}{x} = 2; \tag{19a}$$

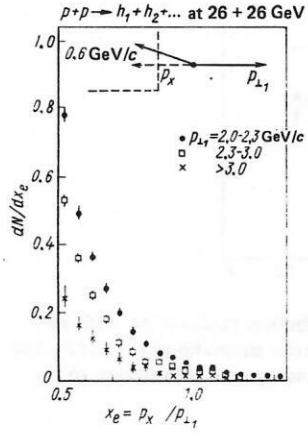

FIG. 15. Distribution dN/dx_e ($x_e = |p_x|/p_{\perp 1}$, particle 1 is the distinguished particle).[18]

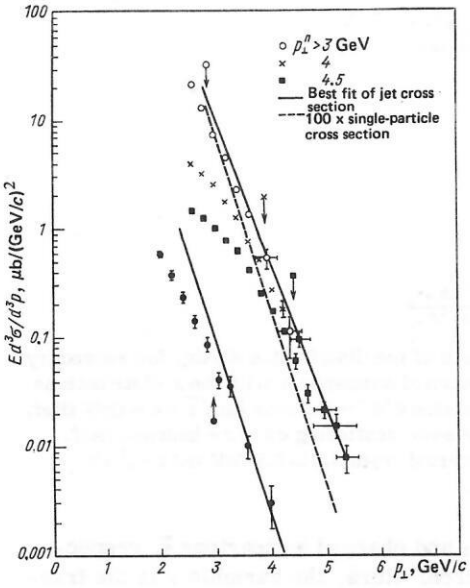

FIG. 16. Sum of the production cross sections of all charged particles for the given experiment (black circles) and the experiment of the Chicago-Princeton group (open circles).[30] The arrows indicate the systematic errors due to the trigger bias effect.

$$\int_0^1 [d(x)-\bar{d}(x)]\frac{dx}{x}=1;$$
$$\int_0^1 [s(x)-\bar{s}(x)]\frac{dx}{x}=0. \qquad (19b)$$

Empirical fitting of the data on deep inelastic scattering for the quark-parton distributions was carried out, for example, in Ref. 41 by McElhaney and Tuan:

$$\left.\begin{aligned} u(x)&=1.74\sqrt{x}\,(1-x)\,(1+2.3x)+0.1\,(1-x)^{7/2}x^2;\\ d(x)&=1.11\sqrt{x}\,(1-x)^{3.1}+0.1\,(1-x)^{7/2};\\ \bar{u}(x)&=\bar{d}(x)=s(x)=\bar{s}(x)=0.1\,(1-x)^{7/2}. \end{aligned}\right\} \qquad (20)$$

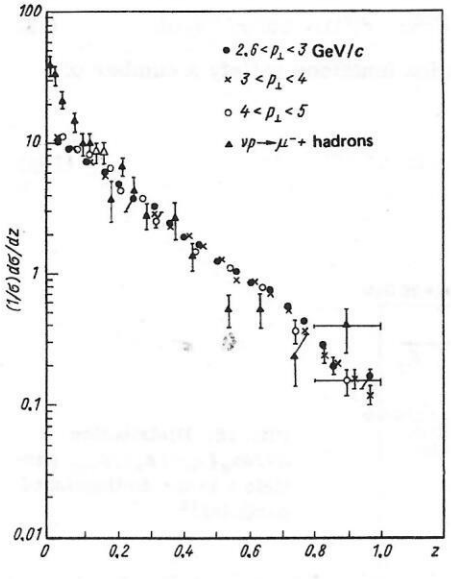

FIG. 17. Comparison of the distribution $(1/\delta)\,d\sigma/dz$ with respect to the fraction of the transverse momentum $z = p_x'/p_\perp$ for the forward hemisphere with the analogous distribution in the case of neutrino scattering.[30]

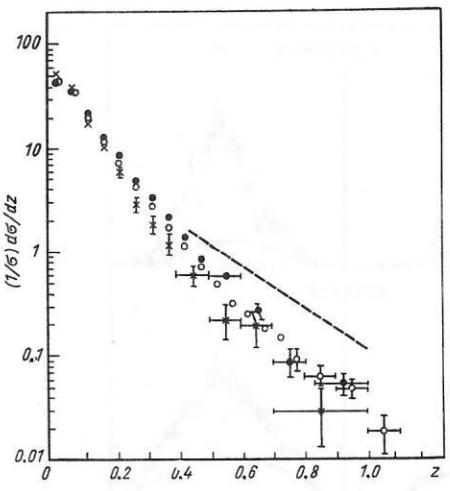

FIG. 18. Distribution $(1/\sigma)\,d\sigma/dz$ $(z=-p_x'/p_\perp)$ for the backward hemisphere obtained by single-particle (black circles) and jet (open circles for $p_\perp > 2.6$ GeV/c and crosses for $4 < p_\perp < 5$ GeV/c) triggers.[30] The dashed line is the distribution for the forward hemisphere.

Barger and Phillips[42] give a different parametrization (Fig. 21):

$$\left.\begin{aligned} u(x)&=0.594x^{1/2}(1-x^2)^3+0.461x^{1/2}(1-x^2)^5\\ &\quad+0.621x^{1/2}(1-x^2)^7+s(x);\\ d(x)&=0.072x^{1/2}(1-x^2)^3+0.206x^{1/2}(1-x^2)^5\\ &\quad+0.621x^{1/2}(1-x^2)^7+s(x);\\ \bar{u}(x)&=\bar{d}(x)=s(x)=\bar{s}(x)=0.145\,(1-x)^9. \end{aligned}\right\} \qquad (21)$$

In the fragmentation region of lepton-proton scattering, the probability of finding hadrons in the final state is proportional to the product of the parton distribution function in the proton and the distribution function $D_h^i(z)$ for the "decay" of parton i into hadrons h. The inclusive cross section of hadron production has the form

$$\frac{1}{\sigma_{\text{tot}}}\frac{d\sigma^{ep\to ehX}}{dz}=\frac{\sum_i e_i^2\,[f_i(x)+f_{\bar{i}}(x)]\,D_h^i(z)}{\sum_i e_i^2\,[f_i(x)+f_{\bar{i}}(x)]}. \qquad (22)$$

Remembering that the Cabibbo angle is small, $\theta_C \ll 1$, and ignoring charm, we obtain for νp collisions

$$\frac{1}{\sigma_{\text{tot}}}\frac{d\sigma^{\nu p\to\mu^- hX}}{dz}=\frac{d(x)\,D_h^u(z)+\bar{u}(x)\,D_h^{\bar{d}}(z),3}{d(x)+\bar{u}(x),3}. \qquad (23)$$

In particular, for the production of $\pi^\pm$ mesons this leads to the expressions

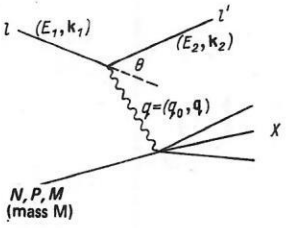

FIG. 19. Deep inelastic lepton-hadron scattering and definition of the kinematic variables. E_1 and E_2 are the energies of the incident lepton and the final lepton; θ is the scattering angle of lepton l in the laboratory system: $-q^2 = Q^2 = 4E_1E_2\sin^2(\theta/2)$; $\nu = E_1 - E_2 = qP/M$; $W^2 = (p+q)^2$.

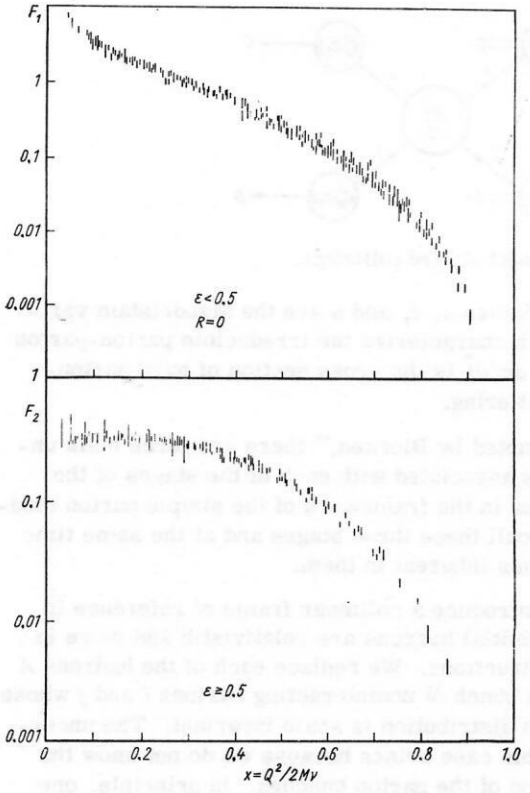

FIG. 20. Bjorken scaling for the functions F_1 and F_2 in the case of proton scattering with $Q^2 > 1\,\text{GeV}^2$ and $W^2 > 4\,\text{GeV}^2$.[40]

$$(1/\sigma_{\text{tot}})\, d\sigma^{\nu p \to \mu^- \pi^\pm X}/dz = D^u_{\pi^\pm}(z) \tag{24}$$

and

$$(1/\sigma_{\text{tot}})\, d\sigma^{\bar{\nu} p \to \mu^+ \pi^\pm X}/dz = D^d_{\pi^\pm}(z) = D^u_{\pi^\mp}(z). \tag{25}$$

The production of hadrons in e^+e^- annihilation is described by

$$(1/\sigma_{\text{tot}})\, d\sigma^{e^+e^- \to hX}/dz = \frac{\sum_i e_i^2 \left[D_h^i(z) + D_h^{\bar{i}}(z)\right]}{\sum_i e_i^2}. \tag{26}$$

The momentum distributions of the hadrons h from the decay of parton i can also be represented in the form

$$D_h^i(z) = G_h^i(z)/z, \tag{27}$$

where z is the fraction of the momentum of the parton carried by the hadron h, $z = p_h/p_i$. These distributions

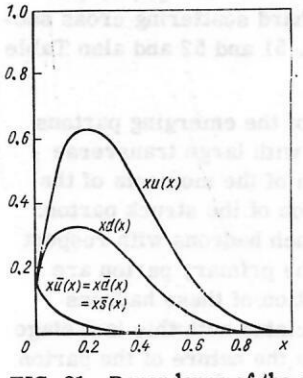

FIG. 21. Dependence of the parton distribution functions parametrized by Barger and Phillips[42] on the scaling variable x.

satisfy a sum rule for the momenta:

$$\sum_h \int_0^1 G_h^i(z)\, dz = 1, \tag{28}$$

and the integral of $D_h^i(z)$ gives the mean multiplicity of hadrons of type h emitted from parton i:

$$\langle n_h \rangle = \int_{z_{\min}}^1 G_h^i(z)\, \frac{dz}{z}. \tag{29}$$

Since the decay function behaves near the point $z = 0$ like $1/z$, the multiplicity increases from some fixed momentum $p_h^0 = p_i/z_{\min}$ logarithmically with increasing quark momentum p_i. Invariance under isotopic and charge conjugation reduces the number of independent functions $D_h^i(z)$; for example, for the pions

$$G^u_{\pi^-}(z) = G^d_{\pi^-}(z) = G^{\bar{u}}_{\pi^-}(z) = G^{\bar{d}}_{\pi^+}(z); \tag{30a}$$

$$G^d_{\pi^+}(z) = G^u_{\pi^-}(z) = G^{\bar{d}}_{\pi^-}(z) = G^{\bar{u}}_{\pi^+}(z); \tag{30b}$$

$$G^s_{\pi^-}(z) = G^{\bar{s}}_{\pi^-}(z) = G^{\bar{s}}_{\pi^+}(z) = G^{\bar{s}}_{\pi^-}(z) \tag{30c}$$

and, in addition,

$$G^i_{\pi^0}(z) = \tfrac{1}{2}\left[G^i_{\pi^+}(z) - G^i_{\pi^-}(z)\right]. \tag{31}$$

An empirical representation for the quark fragmentation functions can be obtained using data on electron and neutrino production. This was done by Sehgal[43]:

$$G^u_{\pi^+}(z) = 0.83\,(1-z); \tag{32}$$

$$G^d_{\pi^+}(z) = 0.41\,(1-z)^{3/2}. \tag{33}$$

Kripfganz,[44] using a model of successive decay with isospin conservation, obtained the distributions

$$G^u_{\pi^+}(z) = 2/3 - 4z/15 - 2z^{8/3}/5; \tag{34}$$

$$G^u_{\pi^-}(z) = 2/3 - 16z\ 15 + 2z^{8/3}/5; \tag{35}$$

$$G^u_{\pi^0}(z) = 2/3 - 2z/3. \tag{36}$$

As is shown in Fig. 22, these distributions agree fairly well with the experimental data.

In the expressions given above, only the component of the hadron momentum parallel to the parton momentum is important. In the direction of motion of the parton, the hadrons have limited transverse momentum. The authors of the present paper proposed the following formula for the fragmentation of a quark into charged particles, with allowance for the transverse momenta and the departure from scaling:

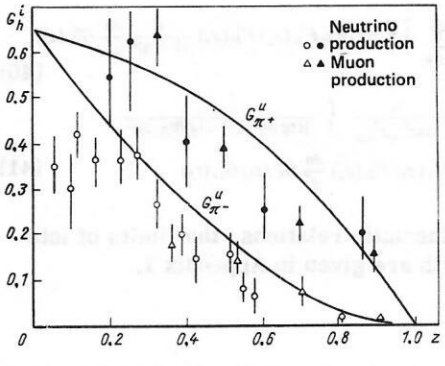

FIG. 22. Comparison of the parametrizations (33)–(35) for the quark fragmentation functions with the data obtained from lepton-hadron collisions.[33]

$$p_0^h \frac{d^3n}{d^3p_h} = B\left(1 - \frac{p_{\parallel h}}{p_i + \frac{A_2}{p_i}}\right)^F \exp\left(-\frac{p_{\parallel h}^2}{b^2 + \frac{p_i^4}{M^2}} - \frac{p_{\perp h}^2}{b^2}\right) \quad (37)$$

with the parameters

$$A = 1.6,\ M = 0.9\ \text{GeV}/c,\ F = 1,\ b = 0.355\ \text{GeV}/c. \quad (38)$$

Model of Hard Scattering for Inclusive Production of Particles with Large $p_\perp$. The production of particles with large transverse momentum was predicted by Bjorken, Berman, and Kogut[45] in the framework of models of hard collisions. In Ref. 45, the main attention was devoted to electromagnetic interactions of partons. At the same time, the existing experimental data indicate that processes of purely strong interaction are predominant. The general structure of models of hard scattering is illustrated in Fig. 23. In collisions of the hadrons A and B, the secondary hadrons C and D, which have large transverse momenta, are produced by the hard scattering of point constituents, the partons i and j.

The partons i and j are fragments of the colliding hadrons A and B. The momentum distributions of partons i and j in the hadrons are $F_A^i(x_1)/x_1$ and $F_B^j(x_2)/x_2$, in which x_1 determines the fraction of the hadron momentum carried by parton i: $x_1 = p_i/p_A$. The scattered partons k and l are usually not observed directly if, for example, they carry quark quantum numbers. The observed hadrons C and D are due to the "decay" of partons k and l into hadrons. The momentum distributions of the hadrons in the parton fragmentation process are given by the functions $G_C^k(z_1)/z_1$ and $G_D^l(z_2)/z_2$, where where z_1 and z_2 are the fractions of the parton momentum carried by the hadrons C and D, respectively: $z_1 = p_C/p_k$.

The inclusive cross sections in this model were also considered by Bjorken[46] and by Ellis and Kislinger.[47] Ignoring the transverse momenta of the parton in the hadron jets and the transverse momenta of the hadron in the parton jets, we obtain for the cross section for the production of the two jets k and l the expression

$$E_l E_k \frac{d^6\sigma_J}{d^3p_l d^3p_k} = \frac{1}{\pi} \sum_{i,j} F_A^i(x_1) F_B^j(x_2) \frac{d\sigma}{d\hat{t}} \delta^{(2)}(p_{\perp l} + p_{\perp k}). \quad (39)$$

In accordance with this picture, the inclusive single-particle and two-particle distributions are given by the expression (Refs. 46 and 47)[1)]

$$E_C = \frac{d^3\sigma}{d^3P_C} \approx \frac{4}{\pi x_{\perp C}^2} \sum_{i,j,k} \int\int dx_1 dx_2 F_A^i(x_1) F_B^j(x_2) \frac{\eta}{(1+\eta)^2} \frac{d\sigma}{d\hat{t}} G_C^k(z); \quad (40)$$

$$E_C E_D \frac{d^6\sigma}{d^3p_C d^3p_D} \approx \frac{16}{\pi s x_{\perp C}^2 x_{\perp D}^2} \int \frac{x_1 dx_1}{[\text{ctg}(\theta_C/2) + \text{ctg}(\theta_D/2)]^2} \times \sum_{ijkl} F_A^i(x_1) F_B^j(x_2) \frac{d\sigma}{d\hat{t}} G_C^k(z_1) G_D^l(z_2). \quad (41)$$

All details, the kinematic relations, the limits of integration and so forth are given in Appendix 1.

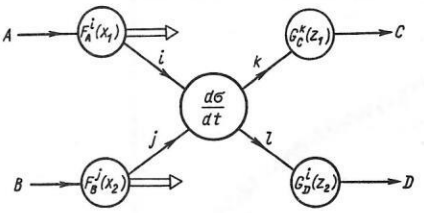

FIG. 23. Model of hard collisions.

The variables s, t, and u are the Mandelstam variables which characterize the irreducible parton-parton collision; $d\sigma/d\hat{t}$ is the cross section of hard parton-parton scattering.

As was noted by Bjorken,[46] there are three main uncertainties associated with each of the stages of the calculations in the framework of the simple parton model. We recall these three stages and at the same time the problems inherent in them.

1. We introduce a collinear frame of reference in which the initial hadrons are relativistic and move in opposite directions. We replace each of the hadrons A and B by a bunch of noninteracting partons i and j whose momentum distribution is scale invariant. The uncertainty in this case arises because we do not know the composition of the parton bunches. In principle, one can determine from experiment the charged quark-parton composition and the momentum distribution. However, approximately 50% of the hadron momentum is not transported by charged partons. It is assumed that this momentum must be transported by the massless neutral gluons.

The momentum distribution of the gluons is not known.

Besides this, there exist hard scattering models in which the interacting partons i and j are not quarks but mesons, baryons, or diquarks.[48]

2. We shall regard the collision as a two-particle collision of the partons of each of the bunches, assuming that the scattering cross section depends only on the variables s and t for the pair of interacting partons. This uncertainty is the most unpleasant. We do not know the strong interaction dynamics of the partons.

Frequently, dimensional analysis is used to determine the form of the hard scattering cross section.[49,50] However, one also uses expressions of a purely phenomenological nature for the hard scattering cross sections (see, for example, Refs. 51 and 52 and also Table V).

3. The momentum of each of the emerging partons that has undergone scattering with large transverse momentum is equal to the sum of the momenta of the hadrons emitted in the direction of the struck parton. The transverse momenta of such hadrons with respect to the direction of motion of the primary parton are small. The inclusive distribution of these hadrons scales. The uncertainty associated with this last stage arises because we do not know the nature of the parton fragmentation into hadrons. Data on reactions with the participation of leptons can give information about

[1)] *Translator's Note:* The Russian notation for the trigonometric, inverse trigonometric, hyperbolic trigonometric functions, etc., is retained here and throughout the article in the displayed equations.

the fragmentation of charged quark-partons. However, such data do not give any information about neutral partons. Moreover, constituents with baryon or meson quantum numbers can also be observable hadrons, and hadron resonances or hadron jets having properties analogous to the properties of the quark jets.

The distribution functions $F_h^i(x)$ and $G_h^i(z)$ satisfy the momentum conservation law

$$\sum_{i\in A}\int_0^1 dx F_A^i(x)=1 \tag{42}$$

and accordingly the expression (28) for the function $G_h^i(z)$. The sum rule which characterizes the conservation of the quantum numbers has the form

$$\sum_{i\in A}\int_0^1 \frac{dx}{x} Q^i F_A^i(x)=Q_A. \tag{43}$$

The convolution formula can be written in the form

$$F_A^i(x)=\int_x^1 \frac{dz}{z}\sum_{j\in A} F_j^i\left(\frac{x}{z}\right) F_A^j(z). \tag{44}$$

From the Gribov-Lipatov relations[53] between the structure functions of deep inelastic electron production and electron-positron annihilation into hadrons, one can obtain parton-nucleon reciprocal relations.[54,55] They relate the functions $G_A^i(z)$, which describe the fragmentation of parton i into hadron A, and the momentum distribution $F_A^i(x)$ of the partons in hadron A:

$$G_A^i(z=x)=F_A^i(x). \tag{45}$$

As $x\to 0$, the behavior of the parton distribution functions $F_A^i(x)/x$ is related to the Regge behavior of the total cross sections. For example, if $\sigma_A^i\sim s^{\alpha-1}$, then $F_A^i(x)/x\sim cx^{-\alpha}$ as $x\to 0$. By the optical theorem, the structure functions of deep inelastic lepton-nucleon scattering are proportional to the imaginary parts of the amplitudes of elastic scattering of the weak or electromagnetic currents on the nucleons at zero angle. In the model of valence quarks and "sea" quarks, the contributions of the "sea" quarks correspond to Pomeron exchange, and the contributions of the valence quarks to exchanges in the t channel of a secondary Regge pole.[56] If the Regge behavior

$$F_i(Q^2,\ \nu)\sim\beta(Q^2)\,\nu^{\alpha(0)} \tag{46}$$

at large ν is to be compatible with scaling at small x, it is necessary that

$$(1/x)\,F_A^i(x)\sim cx^{-\alpha(0)}, \tag{47}$$

where we have also used the relation between the structure function of deep inelastic scattering and the parton distribution.

Dimensional Analysis. Different applications of the rules of dimensional analysis have been reviewed from all sides in Ref. 48. Such an analysis was first proposed by Matveev, Muradyan, and Tavkhelidze[49] and Brodsky and Farrar.[50]

We consider the hard scattering model shown schematically in Fig. 23. In accordance with this, the inclusive single-particle distributions have the form (40). Since all the fragmentation functions are scale invariant, at large $p_\perp$ the scaling of the inclusive distribution reflects the scaling of the cross section $d\sigma/d\hat{t}$ in the elementary hard scattering event. Depending on the models, the interacting partons i, j, k, and l may be quarks, hadrons, or diquarks. The basic rule for reactions with large $p_\perp$ is as follows.[57,58]

We count the number of active quarks participating in the elementary scattering event with large $p_\perp$:

$$n_{\text{act}}=n_i+n_j+n_k+n_l \tag{48}$$

and the number of quark spectators or passive quarks in hadrons A, B, or C:

$$n_{\text{pas}}=n(\bar{i}A)+n(\bar{j}B)+n(\bar{k}C). \tag{49}$$

Being guided by the behavior of the Born diagrams of renormalizable field theories, we find for the inclusive distribution the representation

$$E_C\frac{d^3\sigma}{d^3p_C}=\sum_r c_r\,(p_\perp^2+m_r^2)^{-N_r}\,(1-x_\perp)^{F_r} f(\theta_{\text{cm}}^C), \tag{50}$$

where the summation takes into account all possible elementary scattering events r;

$$x_\perp=2p_{\perp C}/\sqrt{s};\quad \varepsilon=1-x_\perp. \tag{51}$$

The quantity m_r^2 is a free parameter, and $f(\theta_{\text{cm}}^C)$ is some unknown function. The exponents N_r and F_r refer to the elementary process r and are determined by the relations

$$N_r=n_{\text{act}}-2; \tag{52}$$

$$F_r=2n_{\text{pas}}-1. \tag{53}$$

It should be emphasized that formula (50) is derived only in the limit $x_\perp\to 1$. Near the point $x_\perp=0$, and it is precisely in this region that the majority of measurements is made, the expression (50) is modified by some smooth function of $x_\perp$. The rule for counting the passive quarks is equivalent to

$$F_A^i(x)\sim(1-x)^{2n(\bar{i}A)-1} \tag{54}$$

for $x\to 1$. For small x, the parton distributions $F_A^i(x)$ are known insufficiently well. As an example of the application of these quark counting rules, we have considered the process of kaon production in pp collisions (Fig. 24).[59] The general formula (50) can also be used in the case of arbitrary exclusive two-particle reactions, $n_{\text{pas}}=0$:

$$\frac{d\sigma}{dt}(A+B\to C+D)=\frac{1}{s^{n_A+n_B+n_C+n_D-2}} f(\theta_{\text{cm}}^C). \tag{55}$$

Applied to electron scattering, this gives the following form factor averaged over the spins:

$$F_h(t)\sim t^{1-n_h}, \tag{56}$$

where n_h is the number of partons in the hadron.

Relation between the Distributions of Primary and Secondary Fragments. At large transverse momenta, the single-particle distribution has the form [see, for example, Eq. (50) and also Eq. (1)]

$$Ed^3\sigma/d^3p\sim(1/p_\perp^n)\,f(p/p_{\max},\ \theta_{\text{cm}}). \tag{57}$$

The form of the expression (57) is invariant with respect to decay processes. Such a connection between the distributions of the primary and secondary frag-

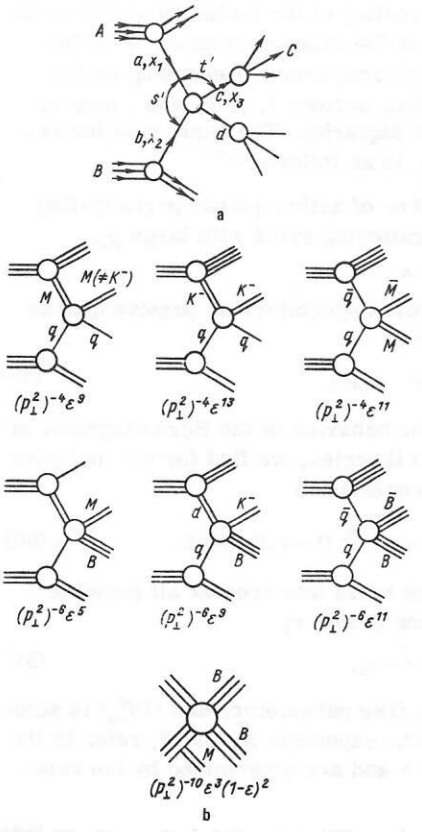

FIG. 24. Examples of the use of the rules of dimensional analysis. a) General diagram of hard scattering of constituents for the reaction $A+B\to C+X$; b) concrete diagrams of the constituent interchange model for the single-particle distributions. All lines are quark lines.[55]

ments was studied by Bjorken.[60]

We consider the inclusive production of a primary particle with large $p_\perp$ ("parent" particle, which we denote by the index p), for example, an isobar or parton, which decays into secondary hadrons ("newly created," denoted by c) with limited $p_\perp$ with respect to the direction of motion of the parent particle. For such decay, we have the scale-invariant representation

$$x dN_c/dx = g_{cp}(x), \tag{58}$$

where

$$x \approx E_c/E_p \approx p_c/p_p \approx p_{\perp c}/p_{\perp p} \tag{59}$$

for sufficiently large $p_\perp$, the angle θ will be the same for the parent and the secondary particle. Substituting Eq. (58) in the expression (57), we arrive at a representation for the distribution of the secondary particles, this having the same form as the representation (57), in which

$$f_c(x,\ \theta_{cm}) = \int_x^1 dz z^{n-3} f_p\left(\frac{x}{z},\ \theta_{cm}\right) g_{cp}(z). \tag{60}$$

At large $p_\perp$, the distribution can be conveniently parametrized by a local power function:

$$E\frac{d^3\sigma}{d^3p} \sim p^{-n_{eff}(p/p_{max},\ \theta_{cm})}. \tag{61}$$

In this case, for the same transverse momenta, we obtain

$$\left(E\frac{d^3\sigma}{d^3p}\right)_c \Big/ \left(E\frac{d^3\sigma}{d^3p}\right)_p \approx \int_0^1 dz z^{n_{eff}-3} g_{cp}(z). \tag{62}$$

Typical values of the parameter n_{eff} are of order 8–12.

For isotropic two-particle decay into particles of negligibly small mass, for example, $\rho\to\pi\pi$ or $\pi^0\to\gamma\gamma$, we have $g_{cp}=2z$ and

$$(Ed^3\sigma/d^3p)_c/(Ed^3\sigma/d^3p)_p = 2/(n_{eff}-1). \tag{63}$$

For parton fragmentation $g_{cp}(z)\approx(1-z)^F$ [see, for example, (27)–(37)], and we obtain

$$(Ed^3\sigma/d^3p)_c/(Ed^3\sigma/d^3p)_p \approx 1/(n_{eff})^{F+1}. \tag{64}$$

Thus, the newly created secondary particles resulting from the decay of the parent particles are to a high degree distinguished objects in the inclusive spectra. Equation (64) expresses the effect of the trigger error due to the selection of events of special type, and this will be considered in more detail below.

Trigger Bias Effect. This systematic effect is a consequence of the fact that the single-particle trigger used in the experiments at large $p_\perp$ selects rather specific jets. In these cases, a large fraction of the total momentum of the jet is transported by one particle.

A very important alternative to the single-particle triggers is provided by jet triggers that use hadron calorimeters. Experiments of this kind are currently being made, and the first results are already known[30]; we have mentioned them in Sec. 1. The trigger bias effect was studied by Bjorken[61] and other authors.[62,63,64] We shall follow Ref. 63.

We restrict ourselves to considering production at $\theta_{cm}=90°$; for the jet distribution function we choose the parametrization obtained by fitting to data on the single-particle distributions at large $p_\perp$ (see, for example, Refs. 1 and 3). By $p_\perp$ and E we denote the transverse momentum and energy of the jet, respectively. The scaled variable of the jet is

$$X_{\perp_J} = 2P_\perp/\sqrt{s}. \tag{65}$$

We write the jet production cross sections in the form

$$\frac{d^3\sigma_J}{d\Phi dY dP_\perp} = \frac{c}{P_\perp^N}\exp(-DX_{\perp_J}) = \frac{c}{P_\perp^N}\exp\left(-\frac{2DP_\perp}{\sqrt{s}}\right), \tag{66}$$

where Y is the rapidity of the jet in the center-of-mass system.

We shall describe the jet fragmentation by the distribution (37). If, however, we replace P_J by $P_{\perp_J}$ in Eq. (37), the departure from scaling will be correctly described only for the case of production at $\theta=90°$, when $P_J=P_{\perp_J}$. In the same central rapidity region in which the jet distribution (66) is true, we arrive at the following distribution of the pions from jet decays with respect to the transverse momentum and the rapidity y in the center-of-mass system:

$$\frac{d^3\sigma}{dy\,d\Phi\,dp_\perp} = \int_{p_\perp}^\infty \frac{d^3\sigma}{dY\,d\Phi\,dP_{\perp_J}}\frac{dn}{P_{\perp_J}dx}dP_{\perp_J}, \tag{67}$$

where $P_{\perp_J}dx = dp_\perp$.

It follows from (67) that the pion rapidity y is equal to the jet rapidity Y. This is true at $\theta = 90°$. But if the pion mass can be ignored compared with the transverse momentum, then the given representation will also be a good approximation in the neighborhood of $\theta = 90°$. Substituting Eq. (37) in the expression (67) and going over to the variable of integration $x = p_\perp / P_{\perp J}$, we obtain

$$\frac{d\sigma}{dp_\perp} = \Delta y \Delta\varphi c \int_0^1 \frac{x^{N-2}}{p_\perp^{N-1}} dx \exp\left(-\frac{2Dp_\perp}{x\sqrt{s}}\right) \pi^{3/2} bB \left(1 - \frac{x}{1 + A^2 x^2 / p_\perp^2}\right)^F \times \exp\left(-\frac{p_-^2}{b^2 + \frac{p_\perp^2}{x^4 M^2}}\right) \exp\left(\frac{p_\perp^2}{b^2}\right) \left[\operatorname{erf}\left(\frac{p_\perp}{xb}\right) - \operatorname{erf}\left(\frac{p_\perp}{b}\right)\right]. \quad (68)$$

We have introduced the quantities Δy and $\Delta\varphi$ corresponding to the spectrometer acceptance, and we have assumed that within the resolution the cross section does not depend on Δy and $\Delta\varphi$.

To be able to integrate in a closed form in (68), we restrict ourselves to the case when the pion transverse momenta satisfy $p_\perp > 2$ GeV/c. Then the integrand in Eq. (68) can be simplified, and we obtain

$$d\sigma / dp_\perp = \Delta y \Delta\varphi \pi b^2 Bc \, (p_\perp^{N-1} \sqrt{p_\perp^2 + m^2})^{-1} I, \quad (69)$$

where

$$I = \int_0^1 dx x^{N-2} \exp\left(-\frac{2Dp_\perp}{x\sqrt{s}}\right)(1-x)^F. \quad (70)$$

This integral has the form[47]

$$I = \left(\frac{2Dp_\perp}{\sqrt{s}}\right)^{N-1} \exp\left(\frac{2Dp_\perp}{\sqrt{s}}\right) \Gamma(F+1) U\left(F+N, N, \frac{2Dp_\perp}{\sqrt{s}}\right), \quad (71)$$

where $U(a, b, z)$ is the confluent hypergeometric function. In the energy range of the CERN ISR the argument $z = 2Dp_\perp / \sqrt{s}$ is fairly small, and therefore a good approximation for the expression (71) will be

$$I \approx \exp\left(-\frac{2Dp_\perp}{\sqrt{s}}\right) \frac{F!\,(N-2)!}{(F+N-1)!}. \quad (72)$$

Substituting (72) in the expression (69) and using also the asymptotic representation for B,

$$B(F) \xrightarrow[p_\perp \to \infty]{} (F+1)/\pi b^2, \quad (73)$$

we obtain finally

$$\frac{d\sigma}{dp_\perp} = \frac{c\Delta y \Delta\varphi}{p_\perp^N} \exp\left(-\frac{2Dp_\perp}{\sqrt{s}}\right) \frac{(F+1)!(N-2)!}{(F+N-1)!}. \quad (74)$$

This result means that for large transverse momenta $p_\perp$ and high collision energies $\sqrt{s}$ the distribution of the detected pion has the same shape as the distribution (66). For $p_\perp = p_{\perp J}$, the ratio of the pion distribution to the jet distribution

$$\left(\frac{d\sigma}{dp_\perp} \Big/ \frac{d\sigma_J}{dp_{\perp J}}\right)_{p_\perp = P_{\perp J}} = \frac{(F+1)!(N-2)!}{(F+N-1)!} \quad (75)$$

depends on the parameters N and F and is fairly small (for $F = 2$ and $N = 8$, the ratio is 1/84), which is confirmed experimentally.[30] This ratio serves as a measure of the trigger bias. Pions with large $p_\perp$ constitute only a small fraction of the jet. In the detected jets, the mean value of x for the trigger particles is

$$\langle x \rangle = \frac{\int_0^1 dx x^{N-1} \exp\left(-\frac{2Dp_\perp}{x\sqrt{s}}\right)(1-x)^F}{\int_0^1 dx x^{N-2} \exp\left(-\frac{2Dp_\perp}{x\sqrt{s}}\right)(1-x)^F}. \quad (76)$$

Using the approximate formula (72), we find

$$\langle x \rangle = (N-1)/(F+N). \quad (77)$$

Thus, the detected jets contain one particle, which on the average carries approximately 3/4 of the total jet momentum.

Effects due to the Transverse Momenta of the Jet Hadrons: Proof of the Jet Structure. The transverse momenta of the jet hadrons were taken into account by Furmanski and Wosiek[65] and Ranft and Ranft.[66,67] We shall follow Ref. 67.

The jet fragmentation in terms of the variables of the longitudinal momentum (along the jet axis) and the momentum perpendicular to this axis is determined by the expression (37).

In order to calculate the inclusive distribution in which we are interested, we use an approximate function for the jet fragmentation parametrized by means of the c.m.s. variables. In particular, we shall use the rapidity y, the transverse momentum $q_\perp$, and the azimuthal angle φ of the observed hadron and the rapidity Y_J, the transverse momentum $P_\perp$, and the aximuthal angle Φ_J of the jet, referring them to the total center-of-mass system. In addition, we use the variables of the parton-parton center-of-mass system, which we denote by means of a "cap"; for example, the total jet energy $\hat{E}_J = \sqrt{\hat{s}}/2$, the jet rapidity $\hat{Y}_J$, and the polar angle $\hat{\theta}_J$. These variables are related by

$$\operatorname{ch}\hat{Y}_j = \hat{E}_j / P_\perp = 1/\sin\hat{\theta}_j. \quad (78)$$

The invariant mass of the jet satisfies $M_J \approx 0$. In terms of the above variables, the approximate jet fragmentation function has the form

$$\frac{d^3 n(\hat{s})}{dy d\varphi q_\perp dq_\perp} = A\left(\frac{\sqrt{\hat{s}}}{2}\right) \frac{F+1}{q_\perp^2} \left(1 - \frac{q_\perp}{P_\perp}\right)^F \frac{1}{\sqrt{\pi}c} \exp\left[-\frac{(\varphi - \Phi_j)^2}{c^2}\right] \times (1/\sqrt{\pi}c) \exp\left[-(y + Y_j)^2/c^2\right], \quad (79)$$

where

$$c = b/q_\perp. \quad (80)$$

The parameter c characterizes the dependence of the expression (37) on the transverse momentum. The Gaussian functions are chosen for convenience of integration. The widths of the Gaussian distributions are dictated by the results of calculations in Ref. 66. The form of the φ distribution follows from the expression (37) in the approximation $\sin^2(\varphi - \Phi_J) \approx (\varphi - \Phi_J)^2$. The $A(\sqrt{\hat{s}}/2)$ can be determined from the energy sum rule; asymptotically

$$A(\sqrt{\hat{s}}/2) \sim 1. \quad (81)$$

The cross section for the production of two jets is given by Eq. (39) in the framework of the hard collision model. In the present calculation, we shall use the following simple approximation for the two-jet distribution:

$$\frac{d^4\sigma_j(s)}{dY_s dY_0 dP_\perp d\Phi} = C \frac{1}{P_\perp^N} \exp\left(-\frac{2DP_\perp}{\sqrt{s}}\right) \frac{1}{\sqrt{2\pi} B_s} \times \exp\left(-\frac{Y_s^2}{2B_s^2}\right) \frac{1}{\sqrt{2\pi} B_0} \exp\left(-\frac{Y_0^2}{2B_0^2}\right). \quad (82)$$

Here, the rapidities of the jets in the forward and back-

ward hemispheres, Y_s and Y_0, are uncorrelated. This assumption, and also the Gaussian form of the rapidity distributions, are suggested by the data of the experiment of Ref. 7 at the existing transverse momenta of the trigger particles ($x_\perp = P_\perp/(\sqrt{s}/2) \approx 0.1$). As is shown in Ref. 52, at these values of $x_\perp$ of the detected particle the two-jet distribution (39) has exactly the property of uncorrelation. It should, however, be noted that at large momenta of the detected particle a correlation between Y_s and Y_0 arises.[52]

In Appendix 2 we give expressions for the inclusive distributions at large transverse momenta; they are obtained using the expression (82) for the cross section for the production of two uncorrelated jets and the expressions (79) and (A.34). An advantage of our parametrization is that the fairly complicated integral expressions factorize, and the majority of the integrals can be estimated analytically. However, it must be remembered that the expression for the cross section for the production of two uncorrelated jets is justified only in the case of small x of the detected particle, as, for example, in the experiments made recently at CERN.[10] Our expressions will also be valid in the more general case when, for example, one take into account the rapidity distributions of two particles in both the forward and the backward hemispheres.

Two particles emitted from the forward-hemisphere jet are characterized by the distribution with respect to the difference of their rapidities [see (A.25)], this having the form

$$W[(y_1-y_2),\ B_s,\ c_1\ c_2] = \frac{1}{\sqrt{\pi}\sqrt{c_1^2c_2^2/2B_s^2+c_1^2+c_2^2}} \times \exp\left[-\frac{(y_1-y_2)^2}{c_1^2c_2^2/2B_s^2+c_1^2+c_2^2}\right]. \quad (83)$$

The characteristic correlation length is

$$L(q_{\perp_1}, q_{\perp_2}) = (1/\sqrt{2})\sqrt{c_1^2c_2^2/2B_s^2+c_1^2+c_2^2} = (b/\sqrt{2}\,q_{\perp_1}q_{\perp_2})\sqrt{b^2/2B_s^2+q_{\perp_1}^2+q_{\perp_2}^2}. \quad (84)$$

The function $L(q_{\perp_1}, q_{\perp_2})$ decreases with increasing transverse momentum of one or both of the particles. At large $q_{\perp_1}$, the constant term $b^2/2B_s^2$ can be ignored, and we arrive at the limiting behavior

$$L(q_{\perp_1}, q_{\perp_2}) = \begin{cases} b/\sqrt{2}\,q_{\perp_2}, & q_{\perp_1} \gg q_{\perp_2}; \\ b/\sqrt{2}\,q_{\perp_1}, & q_{\perp_2} \gg q_{\perp_1}. \end{cases} \quad (85)$$

In Fig. 25, we compare the dependence of the two-particle distribution on the rapidity of the second particle (for which an analysis with respect to the momentum was made) emitted along the direction of the detected particle with the results of this model. The good agreement can be interpreted as evidence for the existence of a jet in the forward hemisphere. Nevertheless, it is necessary to make a more careful investigation of two- and three-particle resonances.

Recently, the CCHK group[10] at CERN measured correlations with respect to the rapidity of particles emitted in the direction opposite to the detected particle, and also made an analysis with respect to the transverse momenta. The obtained data indicate the existence of a jet in the backward hemisphere. Below,

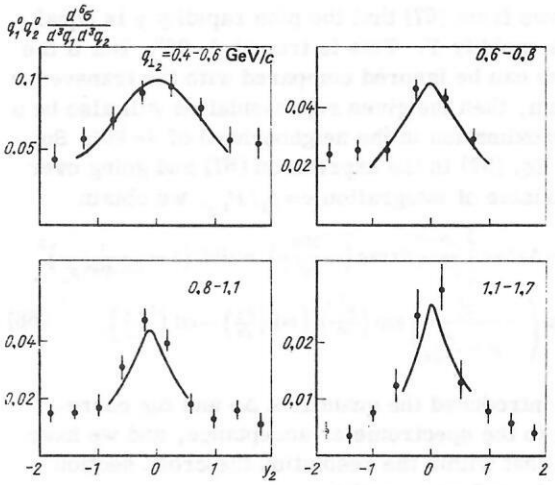

FIG. 25. Two-particle distribution for the forward hemisphere as a function of the rapidity of the second particle.[66] The trigger particle has rapidity $y_1 = 0$ and transverse momentum $q_{\perp_1} = 2\,\text{GeV}/c$. The calculated curves were compared with the data of Ref. 10.

we analyze these data by means of our method. In accordance with Eq. (A.32), the distribution with respect to the difference of the rapidities of the two particles in the backward hemisphere has the same form as the expression (84). The experiment of the CCHK group determined the normalized distribution $dN^c/d(y_2-y_3)$ for two particles of the backward hemisphere and the corresponding normalized uncorrelated distribution $dN^{\text{unc}}/d(y_2-y_3)$, which is obtained when one takes particles from different events. Using these two distributions, we can determine the relative correlation

$$R(\Delta y) = \frac{dN^c}{d(y_2-y_3)} \Big/ \frac{dN^{\text{unc}}}{d(y_2-y_3)}. \quad (86)$$

Data are given for momenta $q_{\perp_1} \approx 2.5\ \text{GeV}/c$ of the trigger particle and transverse momenta of the particles of the backward hemisphere in three ranges: $q_{\perp_2}$ and $q_{\perp_3} \geq 0.3$, 0.6, and 0.9 GeV/c. These distributions are shown in Figs. 26, 27, and 28. It should be noted that at small y the experimental distributions are distorted because of the reduced efficiency for detection of tracks close to each other.[66]

In our approach, the uncorrelated distribution of two particles in the backward hemisphere can be obtained from Eq. (A.26). It has the form

$$\frac{dN^{\text{unc}}}{d(y_2-y_3)} = \frac{1}{\sqrt{\pi}\sqrt{4B_0^2+c_2^2+c_3^2}} \exp\left[-\frac{(y_2-y_3)^2}{4B_0^2+c_2^2+c_3^2}\right]. \quad (87)$$

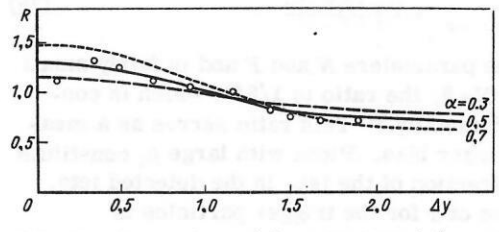

FIG. 26. Comparison of the ratio $R(\Delta y)$ [Eq. (86)] for different values of the parameter α at $q_{\perp_2} = q_{\perp_3} = 0.45\,\text{GeV}/c$ with the data of Ref. 7 for $q_{\perp_2}$ and $q_{\perp_3} \geq 0.3$ GeV/c. The data for $\Delta y \lesssim 0.5$ are strongly displaced because of the restricted acceptance.[67]

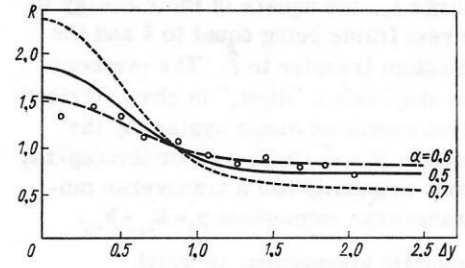

FIG. 27. The ratio $R(\Delta y)$. The theoretical curves are for $q_{\perp_2} = q_{\perp_3} = 0.75$ GeV/c and the experimental data are for $q_{\perp_2}$ and $q_{\perp_3} \geq 0.6$ GeV/c.[67]

In comparing our distribution with the experiment, we must remember that the azimuthal acceptances $A_1(\Delta\phi, c_1, c_2)$ and $A_2(\Delta\phi, c_1, c_2, c_3)$ of the detector [Eqs. (A.27) and (A.33)] are different for the detection of one or two particles of the jet in the backward hemisphere. In Table I, we give the values of the acceptance functions calculated in accordance with Eqs. (A.27) and (A.33). As one would expect, the detector acceptance $A_2(\Delta\phi, c_1, c_2, c_3)$ for the case of detection of two particles in a given angular interval $\Delta\phi$ is smaller than $A_1(\Delta\phi, c_1, c_2)$. For the comparison, we also remembered that not all particles detected in the backward hemisphere arise from the hard scattering process. For the inclusive distribution N, we used a two-component model:

$$N = \alpha N^{\text{h. scat}} + (1-\alpha)\, N^{\text{background of small } q_\perp}. \qquad (88)$$

The quantity α is regarded as a free parameter.

In Figs. 26, 27, and 28 we have compared the results of our calculations with the data for oppositely charged particles. The calculation was made for the fixed mean values of the transverse momenta indicated in the graphs. For reasonable values of α of order 0.5, the calculated curves agree well with the data outside the region $\Delta y = 0$. The width of the peak at small Δy decreases with increasing $q_{\perp_2}$ and $q_{\perp_3}$, which corresponds to the experimental situation. This agreement can be interpreted as evidence for the existence of jets in the opposite hemisphere.

Effects due to the Transverse Momenta of the Partons in the Hadrons. The influence of the transverse momenta of the partons within the hadrons on the production of particles with large $p_\perp$ was taken into account only very recently. From a naive point of view, one could expect that the transverse parton momenta $k_\perp$ are limited and have approximately the same value as the hadron momenta ($\sqrt{\langle k_\perp^2 \rangle} \sim 0.35$ GeV/c). But there are indications that the value of $\sqrt{\langle k_\perp^2 \rangle}$ can be greater than 1 GeV/c.[68] Additional independent information about the transverse momenta of the partons can be obtained from experiments on the production of a lepton pair and lepton-nucleon scattering[69]; the transverse momentum $P_\perp$ of the lepton pair is directly related to the transverse momentum of the partons. Such data indicate fairly large values of the momenta $k_\perp$, with mean values $\langle k_\perp \rangle \geq 1$ GeV/c (Fig. 29).[69-73]

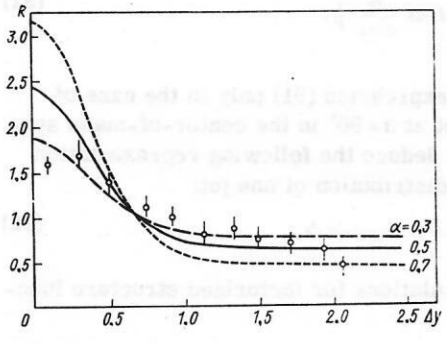

FIG. 28. The ratio $R(\Delta y)$. The theoretical curves are for $q_{\perp_2} = q_{\perp_3} = 1.05$ GeV/c and the experimental data are for $q_{\perp_2}$ and $q_{\perp_3} \geq 0.9$ GeV/c.[67]

TABLE I. Azimuthal acceptance functions $A_1(\Delta\phi, c_1, c_2)$ and $A_2(\Delta\phi, c_1, c_2, c_3)$ defined by Eqs. (A.27) and (A.33) for $q_{\perp_1} = 2.5$ GeV/c.

$q_{\perp_2}$	$A_1(\Delta\phi, c_1, c_2)$				
	$\Delta\phi = 0°$	27°	45°	63°	81°
0.2	0.10	0.30	0.48	0.63	0.75
0.6	0.29	0.74	0.94	0.991	0.999
1.0	0.45	0.93	0.997	~1	~1
1.4	0.57	0.98	~1	~1	~1
1.8	0.65	0.995	~1	~1	~1
$q_{\perp_2} = q_{\perp_3}$	$A_2(\Delta\phi, c_1, c_2, c_3)$				
0.2	0.01	0.09	0.23	0.40	0.56
0.6	0.08	0.54	0.88	0.98	0.998
1.0	0.20	0.86	0.99	~1	~1
1.4	0.33	0.96	~1	~1	~1
1.8	0.44	0.99	~1	~1	~1

It is also well known that the transverse momenta in hadron-hadron resonances and (or) clusters formed in the central region increase with increasing mass of these objects.[74] In the general case, $k_\perp$ can be a function of x and the mass Q of the lepton pair. To describe the functional dependence of $k_\perp(x)$, different models[75] have been proposed; in the papers of Landshoff[76] and Gunion[75] it is pointed out, for example, that in the covariant parton model the mean transverse momentum of the partons in a hadron changes with changing fraction x of their longitudinal momentum: the value of $k_\perp$ is smaller near $x = 0$ but increases to values of order 1 GeV/c as $x \to 1$. Other types of functional dependence were also considered.[75] Moreover, the dependence of the transverse momenta of the partons on Q can also be influenced by the Q dependence of the structure functions predicted by asymptotically free gauge theories. At the present time, fairly intensive investigations are being carried on in this direction, both theoretically and with a view to comparing the predictions with the

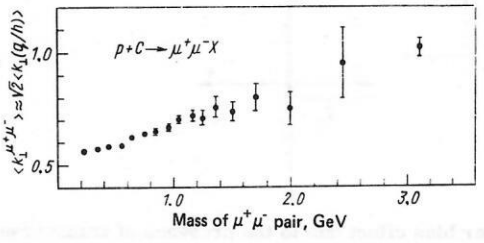

FIG. 29. Experimental evidence for the existence of transverse momenta of the partons within hadrons.[77]

results on the production of a lepton pair and hadron-hadron scattering at large $p_\perp$.

The importance of transverse momenta of the partons in hadrons for reactions with large $p_\perp$ follows from the trigger bias effect,[31,78] which is illustrated in Fig. 30a. The hard scattering cross section $d\sigma/d\hat{t}$ decreases rapidly with increasing transverse momentum $p_\perp$ of the parton k relative to the momentum of parton i. For fixed momentum $p_\perp$ of the trigger hadron C, the quantity $d\sigma/d\hat{t}$ enhances the configurations in which the internal transverse momenta $k_{\perp i}$ and $k_{\perp j}$ point in the direction of the momentum of hadron C. As is shown in Fig. 30b, this effect reduces the transverse momentum in the backward hemisphere. The configurations in Fig. 30b correspond to the same transverse momentum $P_{\perp C}$ of the trigger particle, but for the configuration of Fig. 30b this transverse momentum is increased by the above mechanism. According to the calculation of Fox,[31] this effect increases the single-particle cross sections by a factor of two and decreases by somewhat less the distributions of the particles of the backward hemisphere.

The influence of the transverse momenta of the partons on the form of the single-particle distributions has been investigated by many people.[79-82] We shall follow Ref. 82 and consider the single-particle distributions, and also their dependence on the parameter n_{eff}, since this dependence is modified when one takes into account the transverse momenta of the partons. In fact, we calculate the dependence on $p_\perp$ for the case of a single-jet distribution; it is to be expected that the single-particle distribution due to the jet fragmentation will have the same power behavior $p_\perp^{-n}$ as the jet distribution.[61,63,64]

In a parton-parton collision, there are formed two

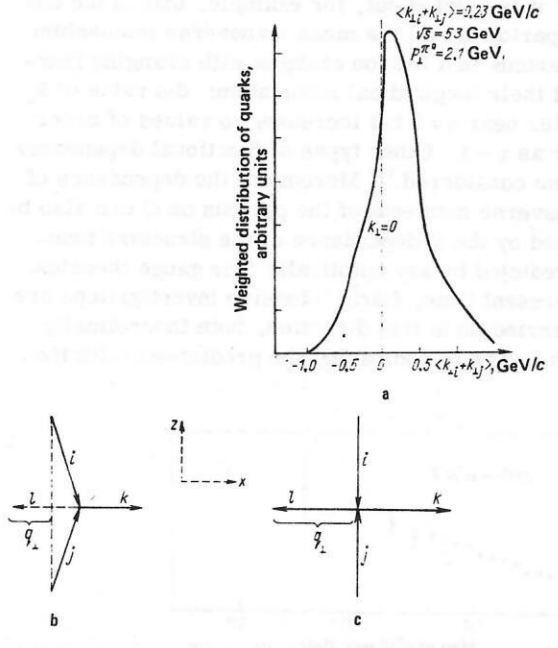

FIG. 30. Trigger bias effect due to the presence of transverse momenta of the partons (a) and hard collision of partons with (b) and without (c) allowance for transverse momenta.[31]

hadron jets with large $p_\perp$, the square of their energy in the parton-parton rest frame being equal to $\hat{s}$ and the square of the momentum transfer to $\hat{t}$. The system of two jets, which we shall call a "dijet," is characterized in the hadron-hadron center-of-mass system by the longitudinal momentum $P_\parallel = \sqrt{s}/2)(x_1 - x_2)$ or the rapidity Y and, if the partons originally had a transverse momentum, by the transverse momentum $\mathbf{p}_\perp = \mathbf{k}_{\perp_1} + \mathbf{k}_{\perp_2}$.

We use the asymptotic kinematics, in which

$$\left.\begin{aligned} &\hat{s} \approx x_1 x_2 s, \\ &x_1 = \exp(Y)\sqrt{\hat{s}/s}, \quad x_2 = \exp(-Y)\sqrt{\hat{s}/s}, \end{aligned}\right\} \tag{89}$$

where x_1 and x_2 are the fractions of the longitudinal momentum of partons 1 and 2. This kinematics means that the parton momenta satisfy $k_{\parallel i} \gg k_{\perp i}$.

The dijet production cross section, expressed in terms of the parton distributions $q(x, k_\perp) = (1/x)\mathcal{F}(x, \mathbf{k}_\perp)$ in the case when the dijet rapidity is small, $Y \approx 0$, and the produced jets are detected at $\vartheta = 90°$ in the center-of-mass system has the form

$$\frac{d\sigma}{d\hat{s}\, dY\, d^2P_\perp} \approx \frac{\text{const}}{\hat{s}^{n/2}} \sum_{i,j} \int d^2k_\perp \mathcal{F}_i(x_1, \mathbf{k}_\perp)\, \mathcal{F}_j(x_2, \mathbf{P}_\perp - \mathbf{k}_\perp). \tag{90}$$

We restrict the treatment to the kinematic region $\hat{s} \gg 1$ GeV^2 and $\hat{s} \gg P_\perp^2$. In the numerical calculations, we shall use $n = 4$ and 8.

For the investigation of the influence of the parton transverse momenta on the jet production, the dependence of the expression (90) on $P_\perp$ is more important than the dependence on Y or $P_\parallel$. Varying the dependence on $P_\parallel$, we can nevertheless expect appreciable effects due to the parton momenta $k_\perp$. In the special case of an isotropic dijet distribution (90), we can treat accurately the kinematics of its decay into two jets.[83] For the following treatment, we approximate the dijet cross section (90) by the isotropic cross section $(Ed^4\sigma/dsd^3\hat{P})_{\text{isotr}}$, which coincides with the expression (90) for $\vartheta = 90°$ ($Y = 0$).

From the isotropic dijet distribution we can readily obtain the energy distribution $d\sigma/d\hat{s}dE$ for the dijet. If in the rest frame the dijet decays isotropically into two jets i and j with momenta $|\mathbf{p}_i^*| = |\mathbf{p}_j^*| = \sqrt{\hat{s}}/2$ characterized by the polar angles ϑ_i and $\vartheta_j = \vartheta_i + \pi$, then the distribution of jet i in the center-of-mass system is determined by the expression[83]

$$\frac{d\sigma}{d\varepsilon^*} = \int_{E_0 = \varepsilon + \sqrt{\hat{s}}/4\varepsilon}^{E_1 = \sqrt{\hat{s}}/2} dE\, d\hat{s}\, \frac{d\sigma}{d\hat{s}\, dE}\, \frac{1}{P}. \tag{91}$$

We shall use the expression (91) only in the case of production of a jet at $\vartheta = 90°$ in the center-of-mass system. From it we deduce the following representation for the invariant distribution of one jet:

$$\varepsilon\,(d\sigma/d^3p_i)\big|_{\substack{\vartheta=90° \\ \mu_i = p_\perp}} = (1/2\pi p_i)\, d\sigma/d\varepsilon_i. \tag{92}$$

We make the calculations for factorized structure functions

$$\mathcal{F}(x, \mathbf{k}_\perp) = F(x)\, g(k_\perp), \tag{93}$$

ignoring in what follows the dependence of the function

$g(k_\perp)$ on x.

To investigate the effect of the parton transverse momenta, we use the following distributions:

a) the Gaussian distribution

$$g(k_\perp^2) = (1/2\pi\sigma^2)\exp(-k_\perp^2/2\sigma^2), \tag{94}$$

for which

$$\sqrt{\langle k_\perp^2\rangle} = \sqrt{2}\,\sigma;$$

b) the power-law distribution

$$g(k_\perp^2) = (N/\pi)(m^2)^{N-1}(k_\perp^2 + m^2)^{-N}, \tag{95}$$

which for $N \geq 3$ leads to the relation

$$\sqrt{\langle k_\perp^2\rangle} = [N/(N^2 - 3N + 2)]^{1/2} m;$$

c) the exponential distribution

$$g(k_\perp^2) = (a^2/2\pi)\exp(-ak_\perp), \tag{96}$$

for which

$$\sqrt{\langle k_\perp^2\rangle} = 6/a^2.$$

In the case of the Gaussian distribution (94), the integrations with respect to E and $k_\perp$ can be performed analytically, and we then obtain for the jet spectrum at $\vartheta = 90°$ an expression of the form

$$\varepsilon_i \frac{d^3\sigma}{d^3p_i}\Big|_{\vartheta=90°} = \frac{1}{2\pi P_{i_\perp}} \frac{\text{const}}{2\pi} \int \frac{d\hat{s}}{\hat{s}^{n/2}} \exp\left[-\frac{1}{4\sigma^2}\left(p_{i_\perp} - \frac{\hat{s}}{4p_{i_\perp}}\right)^2\right] \times \frac{1}{\sqrt{4\pi}\,\sigma} F_1\left(\sqrt{\frac{\hat{s}}{s}}\right) F_2\left(\sqrt{\frac{\hat{s}}{s}}\right). \tag{97}$$

The asymptotic estimate of this integral under the condition that $F_i(\sqrt{\hat{s}/s}) = \text{const}$ leads to the expression

$$\varepsilon d^3\sigma/d^3p \sim 1/p_\perp^n.$$

Thus, in the asymptotic behavior the exponent n is not changed. Numerical calculations for finite values of s and p indicate that for reasonable values of the means $\langle k_\perp^2\rangle$ the value of n_{eff} does not change significantly. As an illustration, we give graphs of the ratio

$$R\left(\sqrt{\langle k_\perp^2\rangle}\right) = \frac{\varepsilon \left.\frac{d^3\sigma}{d^3p_i}\right|_{\langle k^2\rangle \neq 0}}{\varepsilon \left.\frac{d^3\sigma}{d^3p_i}\right|_{\langle k^2\rangle = 0}} \tag{98}$$

(Fig. 31a) and the effective exponent n_{eff} (Fig. 31b) for the exponential distribution (96). The distributions (94) and (95) lead to similar results. In this example, we have used an expression for the hard scattering cross section that decreases as $p_\perp^{-4}$ (gluon exchange); the same results can also be obtained for large values of n.

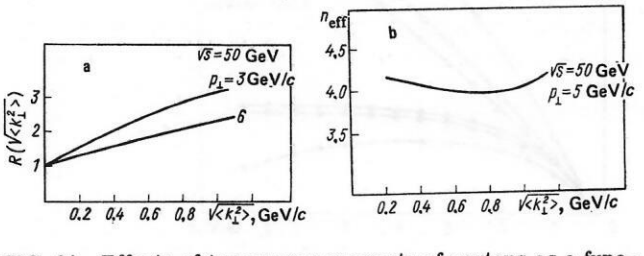

FIG. 31. Effects of transverse momenta of partons as a function of $\sqrt{\langle k_\perp^2\rangle}$ for the exponential distribution.[96] a) The function $(R\langle k_\perp\rangle)$; b) effective exponent n_{eff} for the cross section $\sim p^{-n_{\text{eff}}}$ in the case of large $p_\perp$.[82]

As can be seen from the curves, depending on the value of $p_\perp$, the collision energy $\sqrt{s}$, and the actual mean value of the transverse parton momentum $\sqrt{\langle k^2\rangle}$, the single-jet distribution at large $p_\perp$ is increased by a factor 2 to 3. According to the previous results,[61,63,64] it is expected that the single-particle spectrum will change in the same manner.

The influence of the transverse momenta of the partons on the correlation of the particles at large $p_\perp$ was investigated in Refs. 79 and 80. It was found that the two-particle cross section for the backward hemisphere does not depend very strongly on the parton transverse momenta. In addition, distributions such as dN/dp_{out} and dN/dx_e at $\sqrt{s} = 50$ GeV are well described even at large mean parton momentum $\langle k_\perp\rangle$ equal to 500 MeV/c; nevertheless, the departure from scaling observed in the measurement of this last quantity obviously cannot be explained solely by the transverse motion of the partons.[80]

Associative Multiplicities of the Forward and Backward Hemispheres. We calculate first the multiplicity of the hadrons in the jets. Integrating the distribution (79) over all intervals of y, φ, and $q_\perp$, we obtain the multiplicity of the hadrons of the jet:

$$\langle n\rangle_J = \int \frac{d^3n(\hat{s})}{dy\,d\varphi q_\perp\,dq_\perp} dy\,d\varphi q_\perp\,dq_\perp = A\left(\frac{\sqrt{s}}{2}\right)(F+1) \int_{b'\operatorname{ch}\hat{Y}_J}^{P_\perp} q_\perp\,eq_\perp \frac{1}{q_\perp^2}\left(1 - \frac{q_\perp}{P_\perp}\right)^F \times \int_{\hat{Y}_J-\Delta}^{\hat{Y}_J+\Delta} dy \int_{\Phi_J-\frac{\pi}{2}}^{\Phi_J+\frac{\pi}{2}} \frac{1}{c\sqrt{\pi}} \exp\left[-\frac{(\varphi-\Phi_J)^2}{c^2}\right] \frac{1}{c\sqrt{\pi}} \exp\left[\frac{(y-Y_J)^2}{c^2}\right]. \tag{99}$$

The transverse momentum $q_\perp$ varies in the intervals

$$b'_\perp \operatorname{ch}\hat{Y}_J < q_\perp < P_\perp, \quad P_\perp = \hat{E}_J/\operatorname{ch}\hat{Y}, \quad \hat{E}_J = \sqrt{s}/2, \tag{100}$$

where b' is the lower limit of the momenta for the jet system. In addition, the quantity Δ that appears in the limits of integration with respect to y is defined by

$$\Delta = \operatorname{arch}\left(\hat{E}_J/\sqrt{q_\perp^2 + m^2}\right) - \hat{Y}_J = \Delta(q_\perp), \tag{101}$$

where m is the mass of the particle.

An approximate integration in which the limits of integration with respect to y and φ tend to infinity gives for $F = 1$ or 2

$$\langle n\rangle_J = (F+1)\left[\ln\frac{\hat{E}_J}{b'} - F\left(1 - \frac{b'}{\hat{E}_J}\right) + \frac{1}{2}(F-1)\left(1 - \frac{b'^2}{\hat{E}_J^2}\right)\right]. \tag{102}$$

In Appendix 3, we determine by analogy with this the two-particle distribution for the jet fragmentation.

We make a calculation of the multiplicities for the case of one trigger particle with large transverse momentum. The detected particle is characterized by transverse momentum $q_\perp$ and rapidity y; we calculate the number of comoving particles for given rapidity y integrated over all transverse momenta $q_\perp$ in the interval of given acceptance with respect to the azimuthal angle φ in the forward hemisphere or in the hemisphere opposite the detected particle. These associative multiplicities will be investigated in detail in the

framework of a hard collision model that considers the particles of two jets. The associative multiplicities were investigated by Abad *et al.*[84]

In this paper, a detailed study is made of the associative multiplicities due to the background with small $q_\perp$, and for the component with large values of $q_\perp$ only the relation

$$\langle n\rangle_J \sim \langle P_\perp\rangle \tag{103}$$

was used, i.e., the multiplicity in the case of fragmentation of one jet is proportional to the mean transverse momentum of the jet.

We consider in more detail the multiplicities due to jets with large $P_\perp$, and we make the treatment consistent with the representation (79) for the jet fragmentation functions.

There are two possibilities for calculating the jet multiplicities for reactions with large $q_\perp$.

1. The jets are considered in the center-of-mass system corresponding to the elementary collision event of the two partons. Such jets are characterized by the energy $\sqrt{\hat{s}}/2$ and the jet multiplicities (102).

2. The jets are considered in the center-of-mass system corresponding to the total collision. Then the jet energy differs from $\sqrt{\hat{s}}/2$, and therefore the jet multiplicity also differs from case 1.

In what follows, we shall consider the first variant, since the total multiplicity in this case agrees with the multiplicity observed in e^+e^- annihilation described by means of quarklike jets.

After these preliminary considerations, we find the expressions for the associative multiplicities in the forward and backward hemispheres (only of the two-jet component). We discuss first the multiplicity in the backward hemisphere, the behavior of which is simpler. We begin with the basic expression (A.29) for the distribution of one trigger particle and one particle of the backward hemisphere. To calculate the multiplicity due to the jet of the backward hemisphere, we replace in the integrand the fragmentation function of the jet of the backward hemisphere by the expression (102) for the jet multiplicity.

The integrals with respect to $d\varphi_2$ and $d\Phi$ in the final expression factorize when the quantity $q_{\perp_2}$ in the term containing the azimuthal angle is replaced by its mean value. The integrals lead to the azimuthal acceptance function $A_1(\Delta\phi, c_1, c_2 = b/\langle q_{\perp_2}\rangle)$, which is determined by Eq. (A.27). Finally, to obtain the associative multiplicity, it is necessary to divide the result by the distribution of the trigger particle:

$$\frac{A_1\left(\Delta\phi, c_1, \frac{b}{\langle q_{\perp_2}\rangle}\right)\int_{q_{\perp_1}}^{\sqrt{\hat{s}}/2} dP_\perp \int_{Y_{0_1}}^{Y_{0_2}} dY_0 \int_{Y_{s_2}}^{Y_{s_2}} dY_s \frac{d^3\sigma_J}{dY_s dY_0 dP_\perp}\frac{d^3 n_s(\hat{s})}{dq_{\perp_1} dy_1 dq_1}\Big|_{\varphi_1=0}\langle n_0(\hat{s}, y_2)\rangle_J}{\int_{q_{\perp_1}}^{\sqrt{\hat{s}}/2} dP_\perp \int_{Y_{s_1}}^{Y_{s_2}} dY_s \int_{Y_{0_1}}^{Y_{0_2}} dY_0 \frac{d^3\sigma_J}{dY_s dY_0 dP_\perp}\frac{d^3 n(\hat{s})}{dq_{\perp_1} dy_1 dq_1}\Big|_{\varphi_1=0}}, \tag{104}$$

where

$$\langle n_0(\hat{s}, y_2)\rangle_J = \langle n_0(n_0(\hat{s})\rangle \frac{1}{\sqrt{\pi}\, b/\langle q_{\perp_2}\rangle}\exp\left[-\frac{(y_2 - Y_0)^2}{(b/\langle q_{\perp_2}\rangle)^2}\right]. \tag{105}$$

In the denominator, we have integrated with respect to $d\Phi$; for large $q_{\perp_1}$, this gives approximately unity. In the representation for the jet multiplicity $\langle n_0(\hat{s}, y_2)\rangle_J$ we have substituted the expression (102); for the jet fragmentation function we have used the formula (79) integrated over Φ_J, and we have replaced the jet production function by the expression (39) corresponding to hard scattering. We restrict the treatment to the elementary process $q+q \to q+q \to \text{jet}+\text{jet}$. For the quark distribution functions $f_{i/A}(x)$ we use the result of Barger and Phillips's fitting,[42] and for $d\sigma_{ij}/d\hat{t}$ we take the empirical parametrization of Kripfganz and Ranft[52]:

$$\left.\begin{aligned} &d\sigma_{ij}/d\hat{t} \sim f(\eta)/\hat{s}^4;\\ &f(\eta) = (1+\eta+1/\eta)^3. \end{aligned}\right\} \tag{106}$$

For the described integrands, the numerator and denominator of the expression (104) must be estimated numerically.

For the associative multiplicities of the forward hemisphere, we use similar approximations, describing the production and fragmentation of the jet in the same way as above. The final expression for the associative multiplicity in the forward hemisphere has the form

$$\frac{A_1\left(\Delta\phi, c_1, c_2\frac{b}{\langle q_{\perp_2}\rangle}\right)\int_{q_{\perp_2}}^{\sqrt{\hat{s}}/2} dP_\perp \int_{Y_0}^{Y_{0_2}} dY_0 \int_{Y_{s_1}}^{Y_{s_2}} dY_s \frac{d^3\sigma_J}{dY_s dY_0 dP_\perp}\left\{\frac{d^3 n_s(\hat{s})}{dq_{\perp_1} dy_1 dq_1}\Big|_{\varphi_1=0}\langle n_s(\hat{s}, y_2)\rangle_J\right\}}{\int_{q_{\perp_1}}^{\sqrt{\hat{s}}/2} dP_\perp \int_{Y_{0_1}}^{Y_{0_2}} dY_0 \int_{Y_{s_1}}^{Y_{s_2}} dY_s \frac{d^3\sigma_J}{dY_s dY_0 dP_\perp}\frac{d^3 n(\hat{s})}{dq_{\perp_1} dy_1 dq_1}\Big|_{\varphi_1=0}}. \tag{107}$$

The expression in the brackets is determined by Eq. (A.37). The integrals in Eq. (107) are again estimated numerically.

In Fig. 32, we plot the associative multiplicities (104) and (107) in the forward and backward hemispheres for $y_1 = y_2 = 0$ as functions of the transverse momentum $q_{\perp_1}$ of the detected particle for three values of $\sqrt{s}$.

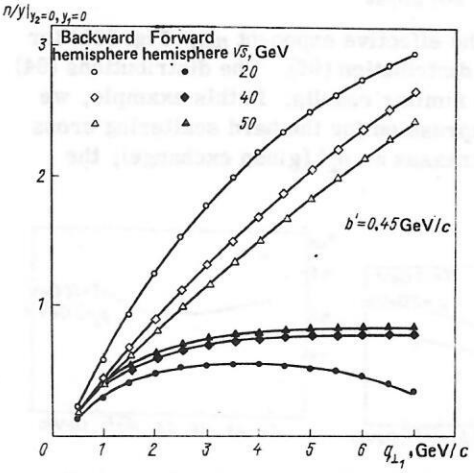

FIG. 32. Theoretical curves of the multiplicities in the forward and backward hemispheres per unit rapidity at $y_2 = y_1 = 0$ as a function of the transverse momentum $q_{\perp_1}$ of the trigger particle [Eqs. (94) and (97)].[67]

The associative multiplicity in the forward hemisphere is small and does not depend on the transverse momentum of the detected particle; the associative multiplicity in the backward hemisphere in the region of $q_{\perp_1}$ of current interest increases approximately linearly with increasing $q_{\perp_1}$. This result is a confirmation of the hypothesis (103) of Abad *et al.*[84]

In Fig. 33, we compare the results obtained by integrating the expression (107) with respect to y_2 with the data taken from Ref. 27.

In Fig. 34, we compare the predictions of formula (104) integrated with respect to y_2 with the data of Ref. 17.

The agreement with the data so far obtained shows that the absolute magnitude and also the dependence of the associative multiplicities on the transverse momentum of the trigger particle and the rapidity can be consistently described in the framework of the hard collision model.

3. SOME MODELS OF HARD COLLISIONS

We now discuss some of the presently known models of hard collisions.

1. Quark-Quark Elastic Scattering, $qq \to qq$ (Fig. 35a). The constituents i, j, k, and l are u, d, and s quarks or $\bar{u}$, $\bar{d}$, and $\bar{s}$ antiquarks in the hadrons. Originally, this model was proposed by Berman, Bjorken, and Kogut,[45] and it was investigated in detail by Ellis and Kislinger.[47]

On the basis of dimensional analysis it is expected that the single-particle inclusive cross section behaves as

$$E d^3\sigma/d^3p \approx (1/p_\perp^4) f(x_\perp, \theta_{cm}). \qquad (108)$$

However, experiment indicates a behavior of the type $p_\perp^{-8}$ [see Eqs. (1) and (2)]. Therefore, this model was forgotten for some time. It is quite possible that the behavior $p_\perp^{-4}$ is observed only at large $p_\perp$ or that the true behavior of the $p_\perp$ distribution can be established in experiments that measure the single-jet distributions by means of jet detectors. However, there are models in which a $p_\perp^{-8}$ behavior follows from energy-momentum conservation.[85]

A different possibility of explaining the experimental behavior of the cross section was considered by Hwa, Spiessbach, and Teper[86] and Fischbach and Look.[87] They proposed the introduction of quark form factors, which enabled them to describe the experimental data

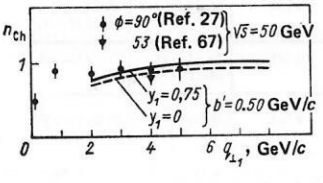

FIG. 33. Comparison of the multiplicity of the charged particles of the forward hemisphere as a function of the transverse momentum $q_{\perp_1}$ of the trigger particle with the data of Refs. 27 and 67.

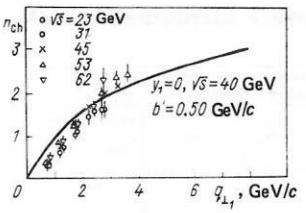

FIG. 34. Comparison of the multiplicity of the charged particles of the backward hemisphere as a function of the transverse momentum $q_{\perp_1}$ of this particle with the data of Refs. 17 and 67.

on single-particle production. Recently, this model was successfully regenerated by Field and Feynman,[51] who used purely phenomenological formulas for the cross sections of quark-quark elastic scattering and ignored the results of dimensional analysis.

2. Fusion of a Quark-Antiquark Pair into Mesons, $q\bar{q} \to MM$ (see Fig. 35b). The constituent i quarks are u, d, and s and the constituent j antiquarks are $\bar{u}$, $\bar{d}$, and $\bar{s}$. The outgoing constituents k and l carry meson quantum numbers corresponding to the quantum numbers of the ingoing quarks and antiquarks and also all the remainder denoted in Fig. 35b by the quark lines.

This model was proposed by Landshoff and Polkinghorne[58] (see also the reviews of Refs. 78 and 88). In accordance with the rules of dimensional analysis, this model predicts the correct behavior $p_\perp^{-8}$.

3. The Quark-Meson → Meson-Quark Constituent Interchange Model (CIM), $qM \to Mq$ (Fig. 35c). The meson production is considered in Fig. 35c, in which the constituents j and k are u, d, and s quarks or $\bar{u}$, $\bar{d}$, and $\bar{s}$ antiquarks. The constituents i and l are mesons with quantum numbers corresponding to the quantum numbers of the other quarks and the quarks j and k indicated in Fig. 35c by the quark lines. This model was proposed by Blankenbecler, Brodsky, and Gunion[89] (see also Refs. 48, 90, and 91). The rules of dimensional analysis give for the meson production cross section a dependence of the type $p_\perp^{-8}$, which is confirmed experimentally. Brodsky and Gunion[91] compared the predictions of Eqs. (50)–(53), which follow from dimensional analysis, with the experimental data. The results of their comparison are given in Table II, which is taken from Ref. 31; alongside, we give the prediction of model 1 of quark-quark elastic scattering, or rather the variant of this model proposed in Ref. 51.

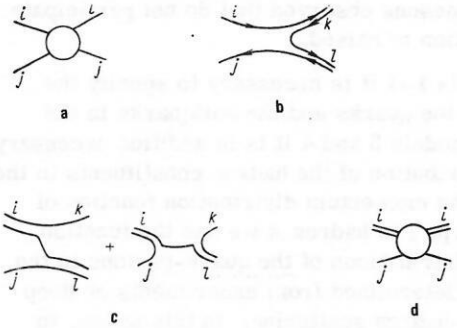

FIG. 35. Four hard collision models: a) $qq \to qq$; b) $q\bar{q} \to MM$; c) $qM \to Mq$ (CIM); d) $qM \to qM$ (gluon exchange).

TABLE II. Behavior of single-particle distributions in hard scattering models.[31]

Observed reaction	Hard scattering process		Scattering cross section at $\theta = 90°$; production cross section for $pp \to \pi^0$		
	qq scattering	CIM	qq scattering	CIM	Experimental data[12,21]
$pp \to \pi^0, \pi^+$	$qq \to qq$ $q \to \pi$	$qM^* \to qM^*$ $M^* \to \pi$	*	**	**
$pp \to \pi^-$	$qq \to qq$ $q \to \pi^-$	$qM^* \to qM^*$ $M^* \to \pi^-$	$(1-x_\perp)$	(?)	$(1-x_\perp)^{0.9}$
$pp \to \eta$	$qq \to qq$ $q \to \eta$	$qM^* \to qM^*$ $M^* \to \eta$	~ 0.5	const	~ 0.5
$pp \to K^+$	$qq \to qq$ $q \to K^+$	$qM^* \to qM^*$ $M^* \to K^+$	const	const	~ 0.5
$pp \to K^-$	$qq \to qq$ $(s, \bar{u})$-Quark $\to K^-$	$qM^* \to qM^*$ $M^* \to K^-$	$(1-x_\perp)^4$	$(1-x_\perp)^4$	$(1-x_\perp)^{2.9}$
	u-Quark $\to K^-$	$q\bar{q} \to K^+K^-$	$(1-x_\perp)^2$	$(1-x_\perp)^2$	
$pp \to \bar{p}$	$q\bar{q} \to q\bar{q}$ $\bar{q} \to \bar{p}$	$qM^* \to qM^*$ $M^* \to \bar{p}$	$(1-x_\perp)^7$	$(1-x_\perp)^6$	$(1-x_\perp)^{5.4}$
	$qq \to pq$ $q \to \bar{p}$	$q\bar{q} \to B^*\bar{B}^*$ $\bar{B}^* \to \bar{p}$	$(1-x_\perp)^7$	$p_\perp^{-4}(1-x_\perp)^2$	
$pp \to p$	$qp \to qp$		$p_\perp^{-4}(1-x_\perp)^{-4}$		$p_\perp^{-3.2}$
	$qq \to qq$ $q \to p$	$qB^* \to qB^*$ $B^* \to p$	$(1-x_\perp)^3$	$p_\perp^{-4}(1-x_\perp)^{-2}$	$(1-x_\perp)^{-2}$
	$q(qq) \to q(qq)$ $(qq) \to p$		$p_\perp^{-4}(1-x_\perp)^{-2}$		
$\pi^- p \to \pi^0$	$qq \to qq$ $q \to \pi^0$	$qM^* \to qM^*$ $M^* \to \pi^0$	$(1-x_\perp)^{-3}$	$(1-x_\perp)^{-2}$	$(1-x_\perp)^{-1.6}$

*The quark-quark scattering must be fitted in such a way as to ensure the $p_\perp$ dependence; in this case, one obtains a correct prediction for the $x_\perp$ dependence.
**The CIM predicts naturally the correct dependences on $p_\perp$ and $x_\perp$.

4. Quark-Meson Scattering with Gluon Exchange, $qM - qM$ (see Fig. 35d). The constituent i is a quark or antiquark; j carries meson quantum numbers.[33,52]

We consider two variants of each of the models 2, 3, and 4 for meson or baryon constituents participating in the hard collision process:

a) the detected meson may be one of the mesons produced directly in the hard collision process;

b) the detected meson was formed as a result of fragmentation of constituents with meson or quark quantum numbers. In ordinary experiments, because of selection by the trigger of events of special form, the fraction of mesons observed that do not participate in the framentation is raised.

For the models 1–4 it is necessary to specify the distributions of the quarks and the antiquarks in the hadrons. For models 3 and 4 it is in addition necessary to know the distribution of the hadron constituents in the hadrons. For the momentum distribution function of the partons of type i in hadron A we use the function $F_A^i(x)/x$. The distributions of the quark-partons in the hadrons can be determined from experiments on deep inelastic lepton-hadron scattering. In this sense, in the calculation of a reaction for large $p_\perp$ they are not free functions. However, it is true that at the present time the knowledge of these functions is unsatisfactory.

The quark and antiquark distribution functions in protons and neutrons have been deduced in many papers[41 42,52,92-96] from deep inelastic scattering data.

It must be recognized that the distributions so far obtained contain large uncertainties. From the experimental data on eN, μN, and νN collisions[90] it is known that there is a departure from scaling with respect to the variable x. At the same time, the data on the scattering of muons and neutrinos at energies greater than the SLAC energies do not lead as yet to such a consistent picture. Threrfore, in what follows we shall use distributions that scale exactly. With some exceptions that will be mentioned, our calculated distributions are almost insensitive to the exact form of the quark distributions and to a considerable extent depend on the hard scattering cross section. The distributions of the "sea" quarks are determined particularly unreliably from the existing data. McElhaney and Tuan[41] parametrized the distribution of the "sea" quarks by the function

$$P_A^z(x) = s(x)/x, \quad s(x) = 0.1(1-x)^{7/2}. \tag{109}$$

Barger and Phillips[42] proposed the function

$$s(x) = 0.145(1-x)^9. \tag{110}$$

The rules of dimensional analysis give

$$s(x) \sim (1-x)^7. \tag{111}$$

From data on lepton reactions it is impossible to deduce the quark distributions in mesons. Instead, it is necessary to use the distributions obtained on the basis of dimensional considerations.[93] For example, for the π^+ meson these distributions have the form

$$F_{\pi^+}^u(x) = F_{\pi^+}^{\bar{d}} = 2x(1-x) + 0.2(1-x)^5; \tag{112}$$

TABLE III. Momentum distributions $F_A^i(x)$ of the constituents in hadron A*.

i \ A	p	$\bar{p}$	n	π^+	π^-
π^+	$(1-x)^5(1-4x)$	$(1-x)^5$	$(1-x)^5$	1	$(1-x)^7$
π^-	$(1-x)^5$	$(1-x)^5(1+4x)$	$(1-x)^5(1+4x)$	$(1-x)^7$	1
π^0	$(1-x)^5(1+2x)$	$(1-x)^5(1+2x)$	$(1-x)^5(1+2x)$	$(1-x)^3$	$(1-x)^3$
u	$u_v(x)+s(x)$	$s(x)$	$d_v(x)+s(x)$	$2x(1-x)$ $+0.2(1-x)^5$	$0.2(1-x)^5$
d	$d_v(x)+s(x)$	$s(x)$	$u_v(x)+s(x)$	$0.2(1-x)^5$	$2x(1-x)$ $+0.2(1-x)^5$
s	$s(x)$	$s(x)$	$s(x)$	$0.2(1-x)^5$	$0.2(1-x)^5$
$\bar{u}$	$s(x)$	$u_v(x)-s(x)$	$s(x)$	$0.2(1-x)^5$	$2x(1-x)$ $+0.2(1-x)^5$
$\bar{d}$	$s(x)$	$d_v(x)+s(x)$	$s(x)$	$2x(1-x)$ $+0.2(1-x)^5$	$0.2(1-x)^5$
$\bar{s}$	$s(x)$	$s(x)$	$s(x)$	$0.2(1-x)^5$	$0.2(1-x)^5$

*As the distributions $u_v(x)$, and $d_v(x)$, and $s(x)$ one can use the parametrizations of Barger and Phillips[42] and McElhaney and Tuan.[41] The function $F_A^i(x)$ is defined by a relation analogous to (27): $P_A^i(x) = (1/x)F_A^i(x)$ (Ref. 33).

$$F^{d}_{\pi^+}(x)=F^{\bar{u}}_{\pi^+}=F^{s}_{\pi^+}(x)=F^{\bar{s}}_{\pi^+}=0.2\,(1-x)^5. \qquad (113)$$

Finally, for models 3 and 4 it still remains to specify the distribution functions of the pions in the hadrons. Once again, these distributions are not determined at all well. To find the form of these distributions, one can only use dimensional arguments.

In Table III we give the distribution functions $F_A^{(i)}(x)$ from Ref. 33. For models 1, 3, and 4 we require the function of the framentation of quark-partons into hadrons. For models 2, 3, and 4 we need the fragmentation functions for the constituents with meson quantum numbers.

In Table IV, which is taken from Ref. 33, we give the parton fragmentation functions. The distributions for the s and $\bar{s}$ quarks in Table IV are chosen in accordance with the assumption that all the distributions for the suppressed decays of the type $u\to\pi^-, d\to\pi^+, s\to\pi^\pm$, etc., are identical.[51] For the fragmentation of the meson constituents i into the mesons C we choose the momentum distribution of the mesons C in the form[62]

$$P^i_C(z)=(1/z)\,G^i_C(z)+K\delta_{iC}\delta\,(1-z), \qquad (114)$$

where the parameter K determines the fraction of mesons that do not fragment further. This quantity is small,[62] and therefore we shall take into account the nonfragmentation term only for the distinguished pion, since in this case its contribution is increased by the selection of events of special type by the trigger.

As the functions for the fragmentation of mesons into mesons, $G^i_C(z)$, we use the expressions obtained from dimensional analysis (see Table IV).

Usually, it is assumed that the cross section of parton-parton scattering must, in accordance with dimensional analysis, have the form

TABLE IV. Momentum distributions of the hadrons C produced by the fragmentation of parton i [the function $G^i_C(z)$ is defined by Eq. (17)].

i \ C	π^+	π^-	π^0
π^+	$1.6\,(1-z)^3$	$1.6\,(1-z)^7$	$1.6\,(1-z)^3$
π^-	$1.6\,(1-z)^7$	$1.6\,(1-z)^3$	$1.6\,(1-z)^3$
π^0	$1.6\,(1-z)^3$	$1.6\,(1-z)^3$	$1.6\,(1-z)^3$
u	$\frac{2}{3}-\frac{4}{15}z-\frac{2}{5}z^{8/3}$	$\frac{2}{3}-\frac{16}{15}z+\frac{2}{5}z^{8/3}$	$\frac{2}{3}-\frac{2}{3}z$
d	$\frac{2}{3}-\frac{16}{15}z-\frac{2}{5}z^{8/3}$	$\frac{2}{3}-\frac{4}{15}z-\frac{2}{5}z^{8/3}$	$\frac{2}{3}-\frac{2}{3}z$
s	$\frac{2}{3}-\frac{16}{15}z+\frac{2}{5}z^{8/3}$	$\frac{2}{3}-\frac{16}{15}z+\frac{2}{5}z^{8/3}$	$\frac{2}{3}-\frac{16}{15}z+\frac{2}{5}z^{8/3}$
$\bar{u}$	$\frac{2}{3}-\frac{16}{15}z+\frac{2}{5}z^{8/3}$	$\frac{2}{3}-\frac{4}{15}z-\frac{2}{5}z^{8/3}$	$\frac{2}{3}-\frac{2}{3}z$
$\bar{d}$	$\frac{2}{3}-\frac{4}{15}z+\frac{2}{5}z^{8/3}$	$\frac{2}{3}-\frac{16}{15}z+\frac{2}{5}z^{8/3}$	$\frac{2}{3}-\frac{2}{3}z$
$\bar{s}$	$\frac{2}{3}-\frac{16}{15}z+\frac{2}{5}z^{8/3}$	$\frac{2}{3}-\frac{16}{15}z+\frac{2}{5}z^{8/3}$	$\frac{2}{3}-\frac{16}{15}z+\frac{2}{5}z^{8/3}$

$$d\sigma/d\hat{t}\approx(1/\hat{s}^n)\,f\,(\hat{t}/\hat{s}). \qquad (115)$$

The experimentally observed behavior of the single-particle distributions at large momentum transfers requires that $n\approx 4$. The originally proposed model of quark-quark scattering with gluon exchange gave $n=2$ and did not agree with experiment. In considering mechanism A, $qq\to qq$, we shall not have recourse to the set of possible forms for $d\sigma/d\hat{t}$ discussed by Ellis and Kislinger in Ref. 47 but instead we shall use the expressions for the cross sections of hard quark-quark scattering obtained purely phenomenologically in Refs. 51, 52, 86, 87, and 97, in which $n=4$ in accordance with the experimental requirement.

In Table V we give some of the forms of the cross

TABLE V. Cross sections of parton-parton hard scattering in the case of different hard collision models

$$\eta=\frac{-\hat{t}/\hat{s}}{1+\hat{t}/\hat{s}}=\operatorname{tg}\frac{\theta_1}{2}\operatorname{ctg}\frac{\theta_2}{2}$$

(the models with the asterisk depend not only on $\hat{t}/\hat{s}$).

Hard collision model	$\frac{d\sigma}{d\hat{t}}\approx\frac{1}{\hat{s}^4}f\left(\frac{\hat{t}}{\hat{s}}\right)$	$f\left(\frac{\hat{t}}{\hat{s}}\right)=g(\eta)$	Comments and references
$1: qq\to qq$	$\approx\frac{1}{\hat{s}^4}\frac{(\hat{s}^2+\hat{u}^2)\hat{s}^2}{\hat{t}^4}$ (1.1)	$\left[\left(1+\frac{1}{\eta}\right)^2+\frac{1}{\eta^2}\right]\left(1+\frac{1}{\eta}\right)^2$	Ref. 51, quark form factors
	$=\frac{1}{\hat{s}^4}\frac{\hat{s}^3}{(-t)^3}\cdot 2.3\times 10^6\,\mu\text{b}\cdot\text{GeV}^2$ (1.2)	$\left(1+\frac{1}{\eta}\right)^3$	Ref. 97, given preference in Ref. 51
	$\approx\frac{1}{\hat{s}^4}\frac{\hat{s}^2}{(-\hat{t})^2}$ (1.3)	$\left(1+\frac{1}{\eta}\right)^2$	Ref. 51
	$\approx\frac{1}{\hat{s}^4}\frac{\hat{s}^2+\hat{u}^2}{\hat{t}^2}$ (1.4)	$\left(1+\frac{1}{\eta}\right)^2+\frac{1}{\eta^2}$	Ref. 97
*	$\approx\frac{1}{\hat{s}^2}\frac{\hat{s}^2+\hat{u}^2}{\hat{t}^2\left(1-\frac{\hat{t}}{\Lambda^2}\right)^4}$ (1.5)	$\left[\left(1+\frac{1}{\eta}\right)^2+\frac{1}{\eta^2}\right]\frac{\hat{s}^2}{\left(1-\frac{\hat{t}}{\Lambda^2}\right)^4}$	Refs. 86 and 98
	$\approx\frac{1}{\hat{s}^4}$ (1.6)		Ref. 65, isotropic
$2: q\bar{q}\to M\bar{M}$	$\approx\frac{1}{\hat{s}^4}\frac{\hat{s}^3}{\hat{t}^3}$ (2.1)	$\left(1+\frac{1}{\eta}\right)^3$	Ref. 86
$4: qM\to Mq$	$\approx\frac{1}{\hat{s}^4}\left(\frac{\hat{s}^2}{\hat{u}^2}+1\right)$ (4.1)	$(1+\eta)^2+1$	Ref. 97
$4: qM\to qM$	$\approx\frac{1}{\hat{s}^4}\frac{\hat{s}^3}{\hat{u}^3}$ (4.2)	$(1+\eta)^3$	Ref. 48
	$\approx\frac{1}{\hat{s}^4}\frac{\hat{u}}{\hat{s}}$ (4.3)	$\frac{1}{1-\eta}$	Ref. 48
	$\approx\frac{1}{\hat{s}^4}\frac{\hat{s}^2}{\hat{u}^2}$ (4.4)	$(1+\eta)^2$	Ref. 48
Empirical parametrization for all models	$\frac{1}{\hat{s}^4}f\left(\frac{\hat{t}}{\hat{s}}\right)$	$g(\eta)=g\left(\frac{1}{\eta}\right)=\left(a-\eta+\frac{1}{\eta}\right)^N$	Ref. 52

section $d\sigma/d\hat{t}$ encountered in the literature for models 1, 2, and 4. In Ref. 33, correlations of particles of the backward hemisphere were analyzed. Using the parametrization proposed in Ref. 52, we obtain

$$\left.\begin{aligned} &d\sigma/d\hat{t} = (1/\hat{s}^4)\, g(\eta);\\ &d\sigma/d\hat{u} = (1/\hat{s}^4)\, g(1/\eta);\\ &\eta = \frac{-t/\hat{s}}{1+\hat{t}/\hat{s}} = \operatorname{tg}(\theta_1/2)\operatorname{ctg}(\theta_2/2); \end{aligned}\right\} \tag{116}$$

$$g(\eta) + g(1/\eta) = (a+\eta+1)^N, \qquad a>0, \tag{117}$$

where the parameters a and N were determined in Ref. 33 from data on the rapidity correlations of particles of the backward hemisphere and were found to be $a=1$ and $N=3$ for model 1, and $a=0.5$ and $N=3$ for models 2, 3, and 4.

In accordance with Eq. (117), the function $g(\eta)$ can be determined if we retain all terms of the type $(1/\eta)^m$ for $m>0$ and the half-sum of terms with $m=0$:

$$g(\eta) = c_0/2 + \sum_{j=1}^{N} c_j (1/\eta)^j, \tag{118}$$

where

$$c_j = \sum_{k=0}^{(N-j)/2} \frac{k!}{(N-2k-j)!\,(k+j)!\,k!}\, a^{N-2k-j}. \tag{119}$$

The term $(1/\eta)^N$ dominates. We note that:

a) the empirically determined parametrizations of the cross section $d\sigma/d\hat{t}$ still require a proper justification from the theoretical point of view;

b) if we have specified a definite parametrization for the cross section $d\sigma/d\hat{t}$, consistency of the model of hard collisions requires that the same cross section describe all possible data on the production of particles in collisions at large momentum transfers.

TABLE VI. Elementary hard scattering processes in quantum chromodynamics and the differential cross sections corresponding to them in the lowest order*.

Process	Σ
$q_1q_2 \to q_1q_2$, $q_1\bar{q}_2 \to q_1\bar{q}_2$	$\frac{4}{9}\frac{s^2+u^2}{t^2}$
$q_1q_1 \to q_1q_1$	$\frac{4}{9}\left(\frac{s^2+u^2}{t^2}+\frac{s^2+t^2}{u^2}\right)-\frac{8}{27}\frac{s^2}{ut}$
$q_1\bar{q}_1 \to q_2\bar{q}_2$	$\frac{4}{9}\frac{t^2+u^2}{s^2}$
$q_1\bar{q}_1 \to q_1\bar{q}_1$	$\frac{4}{9}\left(\frac{s^2+u^2}{t^2}+\frac{t^2+u^2}{s^2}\right)-\frac{8}{27}\frac{u^2}{st}$
$q\bar{q} \to gg$	$\frac{32}{27}\frac{u^2+t^2}{ut}-\frac{8}{3}\frac{u^2+t^2}{s^2}$
$gg \to q\bar{q}$	$\frac{1}{6}\frac{u^2+t^2}{ut}-\frac{3}{8}\frac{u^2+t^2}{s^2}$
$qg \to qg$	$-\frac{4}{9}\frac{u^2+s^2}{us}+\frac{u^2+s^2}{t^2}$
$gg \to gg$	$\frac{9}{2}\left(3-\frac{ut}{s^2}-\frac{us}{t^2}-\frac{st}{u^2}\right)$

*The quantity Σ is defined by Eq. (120). Averaging (summation) is performed over the initial (final) colors and spins; q and g denote, respectively, the quark and the gluon. The indices 1 and 2 denote different flavors. The quantities s, t, and u are the Mandelstam variables for the elementary process.

4. PREDICTIONS OF QUANTUM CHROMODYNAMICS FOR THE CROSS SECTION OF HARD SCATTERING AT LARGE TRANSVERSE MOMENTA

Very recently[99,100] it has become possible in the framework of quantum chromodynamics—the gauge theory of color quarks and gluons based on the group $SU(3)$—to make some predictions concerning the behavior of the cross section $d\sigma/d\hat{t}$ of hard scattering with allowance for all contributions of the lowest orders to the supposedly dominant elementary processes of hard $2\to2$ scattering. These processes are given in Table VI. Since the gluons carry an appreciable fraction of the proton momentum, it is to be exprected that the contribution from hard scattering with the participation of gluons will be rather important. It can be shown that besides quark-quark scattering an important part is played by elastic quark-gluon and gluon-gluon scattering. In what follows, we shall consider the application of this approach to processes at large transverse momenta. In our exposition, we follow Ref. 99.

The differential cross section

$$d\sigma/d\hat{t} = \pi\alpha^2\Sigma/s^2 \tag{120}$$

for all processes of lowest order in quantum chromodynamics [i.e., or order $O(g^4)$] can be calculated; the results of the calculations for Σ are given in Table VI. As examples, we give in Fig. 36 the individual diagrams that contribute to the quark-gluon and gluon-gluon scattering.

For the inclusive distributions, we need not only the expressions for the different differential cross sections $d\sigma/d\hat{t}$ of hard scattering but also expressions for the structure functions F and the fragmentation functions G. In the general case the functions F and G depend on x (or, respectively, z), the parton transverse momenta $k_\perp$, and the square Q^2 of the momentum transfer. In this section, we shall completely ignore the dependence on the momenta $k_\perp$ (see Sec. 2).

For α, we take the asymptotic expression for the invariant charge corresponding to four-quark chromodynamics:

$$\alpha(Q^2) = 25/12\pi \lg(Q^2/\Lambda^2), \tag{121}$$

where $\Lambda \approx 0.3$ GeV.

The predictions of quantum chromodynamics for the quark and gluon distributions in the nucleons, in particular their Q^2 dependence, were recently investigated in detail, and analytic parametrizations were obtained[101,102] for the dependences. Simple expressions of

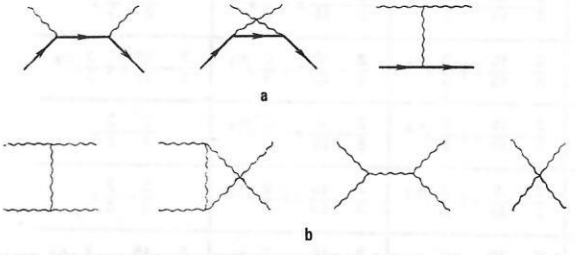

FIG. 36. Diagrams of lowest order for quark-gluon (a) and quark-gluon scattering (b).

the type[101]

$$F(x, Q^2) = A(Q^2)\, x^{a_1(Q^2)} (1-x)^{a_2(Q^2)} \qquad (122)$$

reproduce with an error of a few percent the predicted Q^2 dependence of the moments of the structure functions in a wide range of the variable Q^2, fairly good agreement with the deep inelastic scattering data being observed.

For the quark fragmentation functions we use Eqs. (35)–(36).[33,44] As the unknown gluon fragmentation function we choose the expression

$$G_g^{\pi^0}(z) = \frac{1}{3}(n_g + 1)(1-z)^{n_g}, \qquad (123)$$

in which n_g is as yet a free parameter. We shall not introduce into the fragmentation functions any dependence on Q^2 (a departure from scaling) since for this there is neither theoretical justification nor an experimental indication.

A problem arises: What is one to take as the effective square Q^2 of the momentum transfer? For example, if for each of the diagrams in Fig. 36a we use the true momentum passing through the internal propagator, the sum of the diagrams will no longer be gauge invariant, since they contain three different combinations of the constant α. Therefore, and also to simplify the calculations, we choose some general effective variable Q^2 defined by the equation

$$Q^2 = \sqrt[3]{\hat{s}\hat{t}\hat{u}}, \qquad (124)$$

where the quantities $\hat{s}$, $\hat{t}$, and $\hat{u}$ refer to the elementary process. We have found a number of important quantitative differences in the predictions for different choices of Q^2. For example, on the transition from the variable $Q^2 = \sqrt[3]{\hat{s}\hat{t}\hat{u}}$ to $Q^2 = (\hat{s} - \hat{t} - \hat{u})/3$, $-\hat{t}$ or $\hat{s}$ the total single-particle distributions change, but not by more

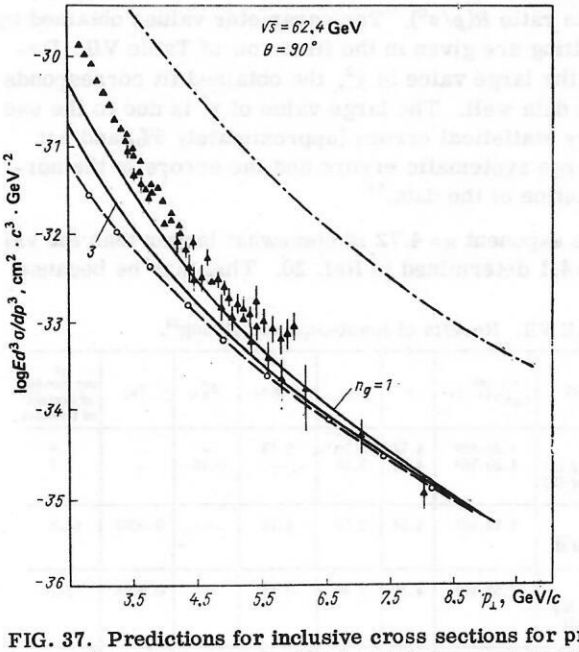

FIG. 37. Predictions for inclusive cross sections for production of π^0 (continuous curves) and jet (chain curve) in pp interactions. The curve with the open circles is the contribution of quark-quark scattering and the black triangles are the data of Ref. 12 on single-pion production.

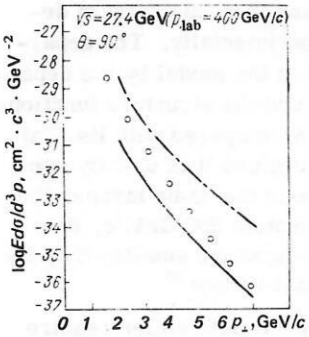

FIG. 38. Predictions for the inclusive cross sections for the production of π^0 (continuous curve) and jet (chain curve) in pp interactions; the open circles are the data of Ref. 19 on single-pion (π^-) production for θ near 90°.

than 25%.

The results of our calculations of the inclusive pion distributions and the total jet distributions (quark+gluon) for $\vartheta = 90°$ in the center-of-mass system and different energies and ranges of p_m are shown in Figs. 37–39. In Fig. 37, we compare the model with the data obtained on the CERN ISR at maximal energy. The two curves for the predicted inclusive cross section for π^0-meson production correspond to the choices $n_g = 1$ and 3 in Eq. (123). For some experimental points taken at momenta greater than $p_\perp \approx 6$ GeV/c good agreement is observed, but at smaller values of $p_\perp$ the theoretical curve passes below the experimental data. In this case, gluon effects are important, and therefore the form of the theoretical curve is very sensitive to the choice of the parameter n_g, but even for $n_g = 1$ the curve does not reach the experimental data; in what follows, we shall use $n_g = 2$. In Fig. 37 we also show separately the contribution from quark-quark scattering. The theoretical results are compared with the FNAL experimental data at momenta 400 GeV/c in Fig. 38. In this case, the predicted curve of the pion distribution passes appreciably lower than the experimental points. This is related to the fact that the model does not lead to the dis-

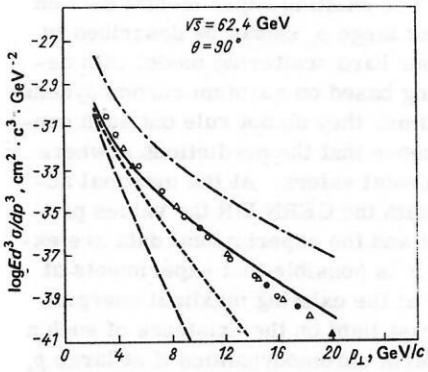

FIG. 39. Predictions for inclusive production of π^0 (continuous curve) and jet (chain curve) in pp interactions. The curve with short dashes is the contribution of quark-gluon scattering; the curve with long dashes is the contribution of gluon-gluon scattering. The points are the data of Ref. 19 on single-pion production at θ near 90°, which are extrapolated by the function $p_\perp^{-8} f(x_\perp)$. For greater clarity, the contribution of quark-quark scattering, which is dominant for $p_\perp > 4$ GeV/c, is not shown.

tribution $p_\perp^{-N} f(x_\perp)$ with $N = 8$, and it is this form of dependence that is observed experimentally. The departure from scaling determined in the model by the dependence of the invariant charge and the structure functions on Q^2 leads to an increase of N compared with its scaling value 4, but for different regions it is usually one or two units. If one calculates in the same manner the total jet cross section at momentum 200 GeV/c, it is approximately two orders of magnitude smaller than the recently presented experimental values.[30]

Thus, the existing experimental data either require the introduction of some additional contributions or may indicate the existence of a mechanism that appreciably increases the contributions, especially at low energies. It seems to us that in either case these must be nonasymptotic effects. As can be seen from Figs. 37 and 38, the basic processes of quantum chromodynamics become appreciable at higher energies and, probably, at larger $p_\perp$ values. The results of the experiment performed at CERN for transverse momenta up to $p_\perp = 20$ GeV/c and the maximal energy $\sqrt{s} = 62.4$ GeV/c of the CERN ISR are shown in Fig. 39. In this figure, we also plot the FNAL experimental points parametrized by the function $p_\perp^{-8} f(x_\perp)$. For $p_\perp > 10$ GeV/c, the predicted curve passes above these points, but the difference is not appreciable.

In Figs. 37 and 39 we also show the individual contributions to the π^0-meson production cross section due to the processes of (elastic) quark-quark, quark-gluon, and gluon-gluon scattering. The remaining contributions are given in Table VI, and they are not too important. At very small values of $x_\perp$ (less than 0.04) the term corresponding to gluon-gluon scattering is dominant. Above this value, but still at small $x_\perp$, the quark-gluon contribution begins to play a part. The mechanism of quark-quark scattering is dominant at intermediate and large $x_\perp$ values (greater than 0.15). The behavior at the intermediate points depends to a certain degree on the choice of the gluon fragmentation functions and the structure functions.

To summarize: The existing experimental data on hadron production at large $p_\perp$ cannot be described in the framework of our hard scattering model with departure from scaling based on quantum chromodynamics. At the same time, they do not rule out such contributions, in the sense that the predictions nowhere exceed the experimental values. At the maximal accessible energies with the CERN ISR the values predicted by the model and the experimental data are exceptionally close. It is possible that experiments at higher energies or at the existing maximal energies but larger $p_\perp$ will cast light on the existence of such a mechanism of quantum chromodynamics if at large $p_\perp$ a change in the scaling behavior of the cross section is observed.

5. SINGLE-PARTICLE DISTRIBUTIONS

The predictions of the four models considered in Sec. 3 were compared with the data on the single-particle distributions by Schiller *et al.*[34] In these models, the single-particle distributions are determined by Eq. (40), and also in Appendix 1. For the hard collision cross sections, one uses the representation

$$d\sigma/d\hat{t} = c^i (1/\hat{s}^n)\, g(\eta), \tag{125}$$

where the function $g(\eta)$ is parametrized by (117); the quantity c^i gives the absolute normalization of the cross section. To compare the four models with experiment, to make an optimal choice of the parameters, and also to compare the models with one another, least-squares fitting was carried out. The following data were used for this:

1) the production cross sections for the reactions $pp \to \pi^+ X$ and $pp \to \pi^- X$ at $\sqrt{s} = 19.4$, 23.8, and 27.4 GeV and $p_\perp > 3$ GeV/c (new, revised data) of the Chicago-Princeton group[19] and at $\sqrt{s} = 53$ GeV and $p_\perp > 2$ GeV/c of the British-Scandinavian group[15];

2) the π^0 production cross sections in the reaction $pp \to \pi^0 X$ at $\sqrt{s} = 52.7$ GeV and $p_\perp > 2.5$ GeV/c obtained by the CCR group[2];

3) the ratios $R(p/\pi) = (Ed^3\sigma/d^3p)_{pp\to\pi^0 X}/(Ed^3\sigma/d^3p)_{\pi^\pm p\to\pi^0 X}$ at $\sqrt{s} = 14.7$ and 19.4 GeV and $p_\perp > 1.5$ GeV/c obtained by the BNL-Caltech-LBL group.

Using the least-squares fitting, we obtained the following results for the four models.

Model 1, $qq \to qq$. *First fit.* For the quark distribution functions, we used Barger and Phillips's parametrization,[42] and the other distributions were chosen in accordance with Tables III and IV. For the fitting, we had the following free parameters: the normalization constant C and the exponent n in the expression (125) for the hard scattering cross section. In addition, assuming a difference in the absolute normalization of the data of different experiments, we used normalization parameters C^i for the π^0 distribution and $C(p/\pi^0)$ for the ratio $R(p/\pi^0)$. The parameter values obtained by the fitting are given in the first row of Table VII. Despite the large value of χ^2, the obtained fit corresponds to the data well. The large value of χ^2 is due to the use of only statistical errors (approximately 5%) and not the large systematic errors and the errors in the normalization of the data.[54]

The exponent $n = 4.72$ is somewhat larger than the value $n = 4.1$ determined in Ref. 20. This may be because

TABLE VII. Results of least-squares fitting[34].

Model	c^i, mb·GeV$^{2(n-1)}$	n	$c^i_{\pi^0}$	$C(p/\pi)$	F^π_{0u}	α_{nf}	χ^2 per number of degrees of freedom
1 $qq \to qq$ (1) $qq \to qq$ (2)	$1.38\cdot10^4$ $1.38\cdot10^4$	4.72 4.72	5.20 5.19	2.19 —	— 0.16	— —	7.8 7.7
2 $q\bar{q} \to M\bar{M}$	$1.14\cdot10^5$	4.51	2.56	4.76	—	0.0037	14.3
3 $qM \to Mq$ (CIM)	$2.52\cdot10^3$	4.32	2.20	3.16	—	0.0068	3.7
4 $qM \to qM$ (gluon exchange)	$4.94\cdot10^3$	4.45	2.51	2.44	—	0.011	6.14

only points with $p_\perp > 3$ GeV/c and additional data at $\sqrt{s} = 53$ GeV (Ref. 15) were used. We attempted to fit the data by taking $n = 4$, but then the value of χ^2 was five times as large. The normalization parameters C^i are approximately of the same order as those found by Field and Feynman[51] using different data. Unexpectedly, the normalization parameter of the π^0 distribution was found to be very large. The parameter value $C(p/\pi) = 2.19$ indicates that in the framework of the model the ratio $R(p/\pi)$ is only half of the experimental ratio.

What possibilities exist to increase this ratio in the model? The quark distribution functions are determined from deep inelastic scattering data and cannot be changed. The quark distribution functions for the pions given in Table III, $F^{\pi^+}_{\text{val}}(x) = 2x(1-x)$, are determined on the basis of dimensional analysis (see Ref. 93) and may be incorrect. The only thing that must be satisfied for the term corresponding to the contributions of the valence quarks is sum rules, for example,

$$\int_0^1 F^{\pi}_{u\ \text{val}}(x)\,\frac{dx}{x} = 1.$$

The hard scattering cross sections and the quark fragmentation functions are the same for the two reactions:

$$pp \to \pi^0 X \text{ and } \pi p \to \pi^0 X.$$

We first attempted to obtain $C(p/\pi) = 1$ by reducing the contribution of the "sea" quarks to the pion fragmentation function F^{π}_{q}. This did not give satisfactory agreement.

Second fit. By analogy with the functions $F^{\pi}_{q}(x)$ of Field and Feynman,[51] we replaced $F^{\pi}_{\text{val}}(x)$ for $x > x_0 > 0$ as follows:

$$F^{\pi}_{\text{val}}(x) = F^{\pi}_{0u} = \text{const}. \tag{126}$$

A good fit was obtained for $F^{\pi}_{0u} = 0.16$. The values of all the parameters for this fit are given in the second row of Table VII.

We arrive at the conclusion that the hard scattering model based on a phenomenological parametrization of the $qq \to qq$ scattering cross section gives a fairly good description of the single-particle distributions at $\theta_{\text{cm}} = 90°$. However, the observed value of $R(p/\pi)$ can be explained only by means of the constant distribution of valence quarks in pions introduced by Field and Feynman.[51] Equation (112) does not enable one to obtain a satisfactory description.

Model 2, $q\bar{q} \to MM$. The best fit is obtained using the quark distribution functions of McElhaney and Tuan.[41] The free parameters are the same as in the case of the first fit used in the model:

$$qq \to qq, \quad [c^i,\ n,\ c^i_{\pi^0},\ C\,(p/\pi)],$$

and also the fraction of nonfragmenting secondary mesons α_{nf}:

$$E\frac{d^3\sigma}{d^3p} = (1-\alpha_{nf})\,E\frac{d^3\sigma}{d^3p}\Big|_f + \alpha_{nf}E\frac{d^3\sigma}{d^3p}\Big|_{nf}. \tag{127}$$

The parameters corresponding to the best fit are given in Table VII. The value of χ^2 is large; the poorest description was obtained using Barger and Phillips's quark distributions[42] and the quark distributions in pions in the form (126). The large value of the parameter $C(p/\pi)$ indicates that it is difficult to fit the ratio $R(p/\pi)$ in the framework of this model. The form of the function $R(p/\pi)$ agrees with the data, but the difference in the normalization $C(p/\pi)$ is too large. An analogous though somewhat smaller discrepancy was also obtained by Combridge.[88]

The model describes the single-particle distributions at large $x_\perp$ rather poorly. In addition, it is known to be difficult to understand the ratio K^+/K^- measured at large $x_\perp$ in this model.

Model 3, $qM \to Mq$(CIM). As above, the free fitting parameters are c^i, n, $c^i_{\pi^0}$, $C(p/\pi)$, and α_{nf}. The results of the fit are given in Table VII. The value of χ^2 is the best of all the fits considered here. In accordance with the model, the ratio $R(p/\pi)$ differs from the data by the factor $C(p/\pi) = 3.16$. The model uses the functions of the fragmentation of protons and pions into meson constituents, $F^p_\pi(x)$ and $F^\pi_\pi(x)$, given in Table III, and the functions for the decay of mesons into pions, $G^\pi_\pi(z)$, given in Table IV. These functions are free functions of the model; in particular, the normalization of the functions $F(x)$ is not essentially restricted by sum rules. It therefore appears that the model is sufficiently flexible to give $C(p/\pi) = 1$ by means of a suitable modification of the fragmentation functions.

In the hard scattering model based on the mechanism $qM \to Mq$(CIM), the data on pion production at $\theta_{\text{cm}} = 90°$ are well described. However, this model uses a definite phenomenological representation of the hard scattering cross section with the function $g(\eta)$ given by (117) (allowance for the leading term gives $d\sigma/d\hat{t} \sim 1/\hat{s}\hat{t}^3$), which differs strongly, for example, from $d\sigma/d\hat{t} \sim 1/\hat{s}^2\hat{t}^2$ and the other originally proposed functions (see Table V).[48,97]

Model 4, $qM \to qM$ (Gluon Exchange). The parameters are the same as in model 3. The result of the fit is given in Table VII.

This model also satisfactorily describes pion production at $\theta_\perp = 90°$. The agreement is not so good as in model 3.

The fraction α_{nf} of nonfragmenting meson constituents determined for models 2, 3, and 4 is of the same order as the value found by Ellis, Jacob, and Landshoff[62] from an analysis of the correlations of particles of the opposite hemisphere.

In Fig. 40, we compare the predictions of the four models for the $p_\perp$ dependence of the ratios of the π^+-meson production cross sections to the π^--meson production cross section (for brevity, we write in what follows π^+/π^-) with the data of Ref. 20 obtained in pp collisions.

The $qq \to qq$ model leads to good agreement for $x_\perp > 0.3$ but seems to give a somewhat larger value for the ratio π^+/π^- for $0.1 < x_\perp < 0.3$.

The $q\bar{q} \to MM$ model agrees well with experiment at $x_\perp < 0.3$ but leads to a too small ratio π^+/π^- for large

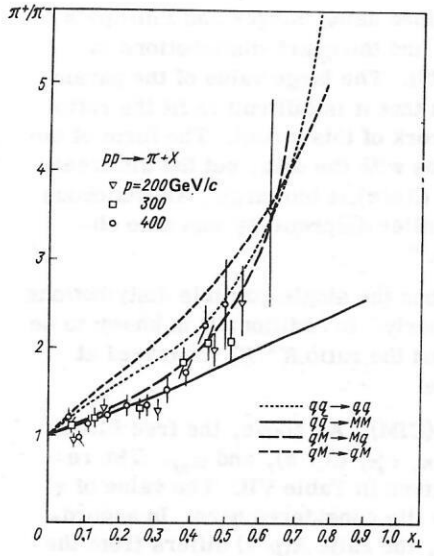

FIG. 40. Ratios π^+/π^- for pp collisions at 200, 300, and 400 GeV/c as functions of $x_\perp$. The data are taken from Ref. 20 and the comparison is made for the four models described in the text.[34]

values of $x_\perp$.

The $qM \to Mq$ (CIM) model gives a fairly good description of the data for all values of $x_\perp$.

This good fit is obtained through the introduction into the model of an additional degree of freedom compared with model 1. At small $p_\perp$, the term in which the mesons and quarks are regarded as fragmentation products is dominant. At large $p_\perp$, the term describing the nonfragmentation quarks and mesons is the principal term.

The $qM \to qM$ model (gluon exchange) agrees with experiment only at large $x_\perp$; at small $x_\perp$, it leads to a too large ratio π^+/π^-. Thus, from the point of view of explaining the ratios π^+/π^- the preferred models are the CIM and the models in which the $q\bar{q} \to MM$ mechanism is dominant at small $x_\perp$ and the $qq \to qq$ mechanism is dominant at large $x_\perp$.

The experimental data for the ratio π^+/π^- in pn collisions at $\theta_{cm} = 90°$ from Ref. 20 are compatible with the

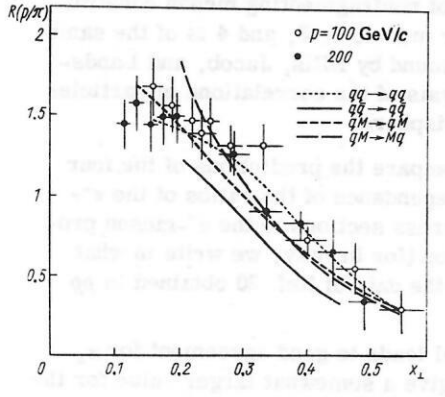

FIG. 41. Ratio of the invariant cross sections of the reactions $pp \to \pi^0 x$ and $\pi^- p \to \pi^0 X$ as a function of $x_\perp$. The data are from Ref. 21; the comparison is made for the four models described in the text.[34]

value $\pi^+/\pi^- = 1$ for all $x_\perp$. All the considered models agree with this observation, as can be seen from the expressions for the fragmentation functions $F_i^\pi(x)$ and $F_i^\eta(x)$ given in Table III. In Fig. 41, we compare with experiment the $x_\perp$ dependences of the ratios $R(p/\pi)$ predicted by the four models with the parameter values obtained from the fits (see Table III).

The $qq \to qq$ model (second fit) agrees very well with the experimental data in the complete region of $x_\perp$.

The $q\bar{q} \to MM$ model leads to the correct form of the dependence but, as we have already noted, it is hard to understand the discrepancy in the normalization.

The $qM \to Mq$ model (CIM) correctly predicts the form of the dependence for $x_\perp > 0.2$. This model has sufficient freedom to eliminate the discrepancy in the normalization. The increase in the predicted values of the ratio for $x_\perp$ below 0.2 may indicate that the model does not dominate at small $x_\perp$. Model 4 behaves like model 3, but at small $x_\perp$ it agrees somewhat better with the data.

The rapidity dependences of the single-particle distributions and of the ratios (π^+/π^-) predicted by models 1–4 were compared with the experimental data of Refs. 34 and 103.

So far, we have at our disposal only a limited amount of data on the rapidity dependence of the single-particle distributions, which were obtained in experiments using counters in the CERN ISR[9,15] and at FNAL.[104]

Recently, bubble-chamber data became available on π^+ and π^- production at $p_\perp > 1$ GeV/c in the reactions $\pi^- p \to \pi^+ \pi^- X$ at $\sqrt{s} = 5.6$ and 13.7 GeV[105] and 19.4 GeV,[106] and also $p\bar{p} \to \pi^+ \pi^- X$ at $\sqrt{s} = 5.6$ GeV.[107] These data correspond to rather small transverse momenta, so that we are definitely in the region in which the hard scattering mechanism is governed by small $p_\perp$ components. Nevertheless, the data indicate a strong increase of the (π^+/π^-) asymmetry with increasing transverse momentum. The observed (π^+/π^-) asymmetry corresponding to the data for $p_\perp > 1$ GeV/c is appreciably greater than the asymmetry measured at small $p_\perp$.

Note also that because of the low energy in this experiment the value of $x_\perp$ is fairly large ($0.1 \lesssim x_\perp \lesssim 0.4$). Therefore, we attempted to explain the asymmetry as the result of the hard scattering mechanism. In the framework of the quark fusion model, Combridge[78] also analyzed in this manner the data of Fretter *et al.*[106]

It should also be noted that according to the hard scattering models the π^+ and π^- rapidity distributions change fairly smoothly with increasing transverse momentum and already at $p_\perp = 1$ GeV/c acquire all the characteristic features.

In Fig. 42a, we give the rapidity dependences of the π^+ and π^- distributions in the reaction $\pi^- p \to \pi X$ at $\sqrt{s}$ = 20 GeV for the $qq \to qq$ model. At $p_\perp = 1$, 2.5, and 5.5 GeV/c the rapidity distributions shrink more and more with increasing transverse momentum, and the asymmetry is increased. In Fig. 42b, the same distributions are represented in the form of the ratio

$$\frac{\pi^-}{\pi^+} = E\frac{d^3\sigma}{d^3p}\Big|_{\pi^- p \to \pi^- X} \Big/ E\frac{d^3\sigma}{d^3p}\Big|_{\pi^- p \to \pi^+ X} \qquad (128)$$

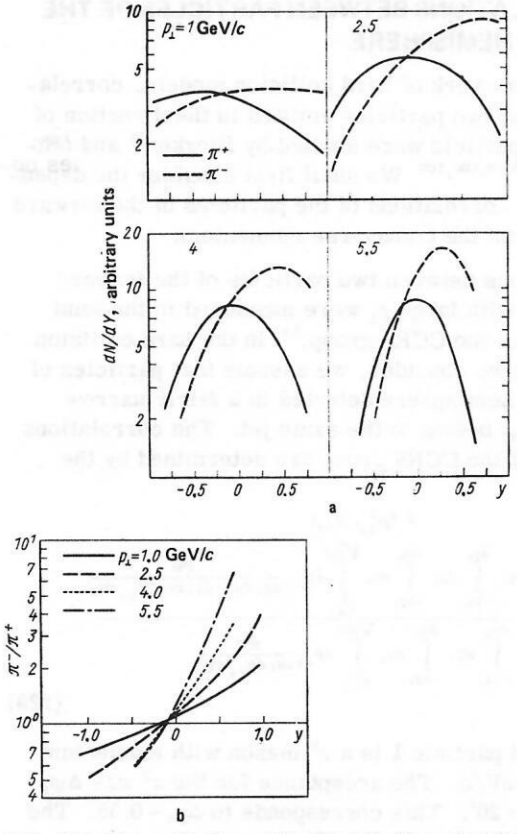

FIG. 42. Theoretical rapidity distributions for the reactions $\pi^- p \to \pi^+ X$ and $\pi^- p \to \pi^- X$ in the framework of the $qq \to qq$ hard scattering model. a) The invariant single-particle rapidity distribution; b) the ratio π^-/π^+ of the invariant single-particle rapidity distributions.[34]

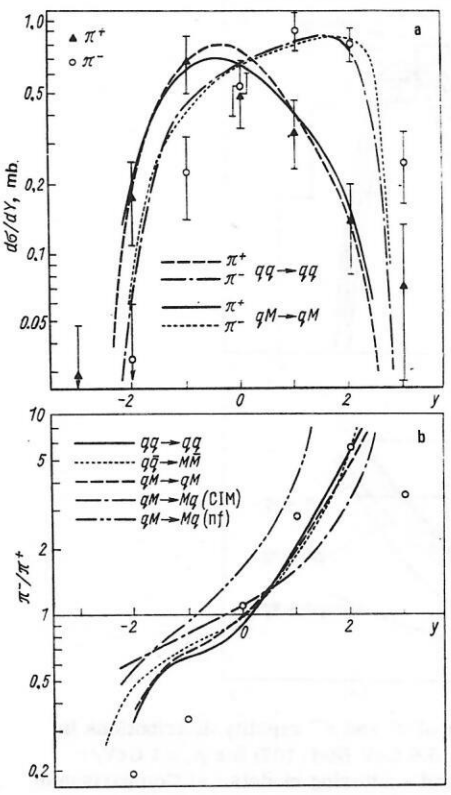

FIG. 43. Comparison of π^+ and π^- rapidity distributions in $\pi^- p$ collisions at $\sqrt{s}$ =19.4 GeV (Ref. 106) for $p_\perp > 1$ GeV/c with the predictions of the hard scattering models. a) Comparison of data with the rapidity distributions corresponding to the $qq \to qq$ and $qM \to qM$ (gluon exchange) models; b) comparison of data on the ratio π^-/π^+ with the results of calculations in the framework of the four considered models.[34]

as functions of the rapidity for the same $p_\perp$ values. This graph beautifully demonstrates the smooth increase in the asymmetry with increasing $p_\perp$. In Fig. 43, we compare the data on the π^+ and π^- distributions in $\pi^- p$ collisions at $\sqrt{s}$ = 19.4 GeV with the predictions of the hard scattering model, and in Fig. 44 with the data on pp collisions. In Fig. 44a, the experimental data on the π^+ and π^- rapidity distributions for $p_\perp > 1$ GeV/c are compared with the results of two hard scattering models. In each figure, we plot curves corresponding to the $qq \to qq$ model, and, in addition, in at least one of the figures curves for the other three models. In Fig. 44b, the data are given in the form of the ratios π^-/π^+ and are compared with the ratios calculated for all four models. For the hard scattering models 2–4, in which meson constituents also participate in the scattering, the given curves correspond to superposition of fragmenting mesons.

For the $qM - Mq$ model, the contributions of the fragmenting and nonfragmenting mesons differ appreciably. Therefore, in plotting the graphs for the ratios π^-/π^+ we also indicate separately these two contributions.

Comparing the results of the models with the experimental data, we see that the $qq \to qq$ model agrees well with the data of all experiments. The value of the (π^-/π^+) asymmetry is somewhat smaller than the experimental value; this effect arises because we ignored the transverse momenta for the jet fragmentation. Allowance for the dependence of the jet decay on the transverse momentum by, for example, the method described in Sec. 2 leads to a broadening of the calculated distributions. The predictions of the $q\bar{q} \to M\bar{M}$ and $qM \to qM$ (gluon exchange) models at $p_\perp = 1$ GeV/c are approximately the same as for the $qq \to qq$ model.

In the framework of the $qM - Mq$ model (CIM), the (π^-/π^+) asymmetry is smaller than the experimental value and the values predicted by the other models. This arises because for the given $p_\perp = 1$ GeV/c the contribution of the fragmenting mesons is dominant.

The calculated rapidity distributions depend very weakly on the parton distribution functions $F_A^i(x)$. For example, in the framework of the quark fusion model (for which this dependence is the strongest) we did not find any appreciable difference in the behavior when we used the distribution functions of Barger and Phillips[42] or McElhaney and Tuan.[41] So far, the results of our comparison with the data for the rapidity distributions at large $p_\perp$ do not allow us to give preference to any one of the hard collision models. At $p_\perp = 1$ GeV/c, the predictions of all the models are fairly similar. To investigate the difference in the predictions of the models at somewhat larger $p_\perp$, we have plotted in Fig. 45 the same π^+ and π^- rapidity distributions and the π^-/π^+ ratios in $\pi^- p$ collisions, but for $\sqrt{s} = 20$ GeV and $p_\perp = 5.5$ GeV/c. At such large $p_\perp$, the contributions of the non-

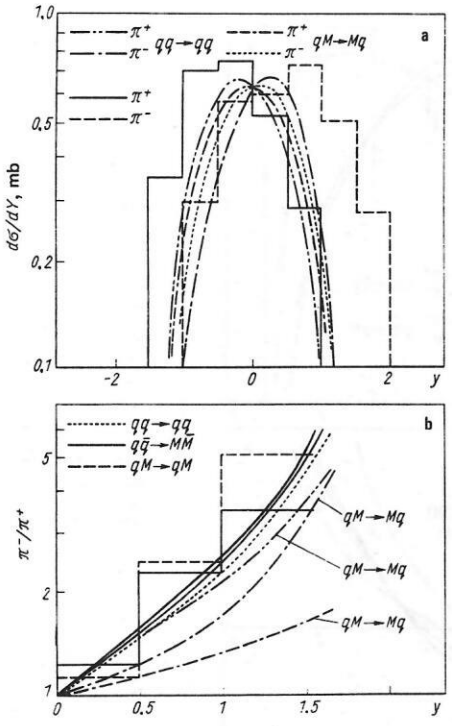

FIG. 44. Comparison of π^+ and π^- rapidity distributions in $\bar{p}p$ collisions at $\sqrt{s}$ = 6.6 GeV (Ref. 107) for $p_\perp > 1$ GeV/c with predictions of hard scattering models. a) Comparison of the data with the rapidity distributions corresponding to the $qq \to qq$ and $qM \to Mq$ models; b) comparison of the data on the ratio π^-/π^+ with the results of calculations in the framework of the four considered models.[34]

fragmenting mesons are dominant in models with meson constituents. There is a strong difference between the behaviors predicted by the $qq \to qq$ and $q\bar{q} \to M\bar{M}$ models, on the one hand, and the $qM \to qM$ and $qM \to Mq$ models on the other. In the case of the last two models, π^--meson production in the opposite direction is also dominant. Therefore, investigations of the rapidity distributions at large $p_\perp$ make it possible to distinguish better between these models.

6. CORRELATIONS BETWEEN PARTICLES OF THE FORWARD HEMISPHERE

In the framework of hard collision models, correlations between two particles emitted in the direction of the trigger particle were studied by Bjorken[61] and others.[62,63,65,79,98,108,109] We shall first consider the dependence of the correlations of the particles of the forward hemisphere on the transverse momentum.

Correlations between two particles of the forward hemisphere with large $p_\perp$ were measured in the joint experiment of the CCRS group.[12] In the hard collision model which we consider, we assume that particles of the forward hemisphere detected in a fairly narrow range $\Delta\varphi, \Delta\varphi$ belong to the same jet. The correlations measured by the CCRS group are determined by the function

$$\mathcal{F}(p^0_{\perp_1}, p_{\perp_2}) = \frac{\int_{-\Delta\varphi_1}^{\Delta\varphi_1} d\varphi_1 \int_{-\Delta\varphi_2}^{\Delta\varphi_2} d\varphi_2 \int_{-\Delta y_1}^{\Delta y_1} dy_1 \int_{-\Delta y_2}^{\Delta y_2} dy_2 \int_{p^0_{\perp_1}}^{\sqrt{s}/2} dp_{\perp_1} \frac{d^6\sigma}{dy_1\, dp_{\perp_1}\, d\varphi_1\, dy_2\, dp_{\perp_2}\, d\varphi_2}}{\int_{-\Delta\varphi_1}^{\Delta\varphi_1} d\varphi_1 \int_{-\Delta y_1}^{\Delta y_1} dy_1 \int_{p^0_{\perp_1}}^{\sqrt{s}/2} dp_{\perp_1} \frac{d^3\sigma}{dy_1\, dp_{\perp_2}\, d\varphi_1}}. \tag{129}$$

The detected particle 1 is a π^0 meson with momentum $p_{\perp_1} > p^0_{\perp_1} = 3$ GeV/c. The acceptance for the π^0 was $\Delta\varphi_1 = 7°$ and $\Delta\theta_1 = 20°$. This corresponds to $\Delta y_1 \approx 0.35$. The second particle is charged. The acceptance for this particle was $\Delta\varphi_2 = 8°$ and $\Delta\theta_2 = 28°$, which corresponds to $\Delta y_2 \approx 0.49$. In the calculations, we shall follow the jet model of Ref. 63.

We assume that the two-particle distributions for a jet with minimal correlations are determined by energy-momentum conservation. A suitable approximation has the form

$$\varepsilon_1\varepsilon_2 \frac{d^6n}{d^3p_1\, d^3p_2} = \frac{\langle n(n-1)\rangle_J}{\langle n\rangle_J^2} \varepsilon_1 \frac{d^3n}{d^3p_1} \varepsilon_2 \frac{d^3n}{d^3p_2}. \tag{130}$$

As in the calculation of the trigger bias effect in Sec. 2, we ignore the transverse momenta of the secondary particles with respect to the jet axis. In this approxi-

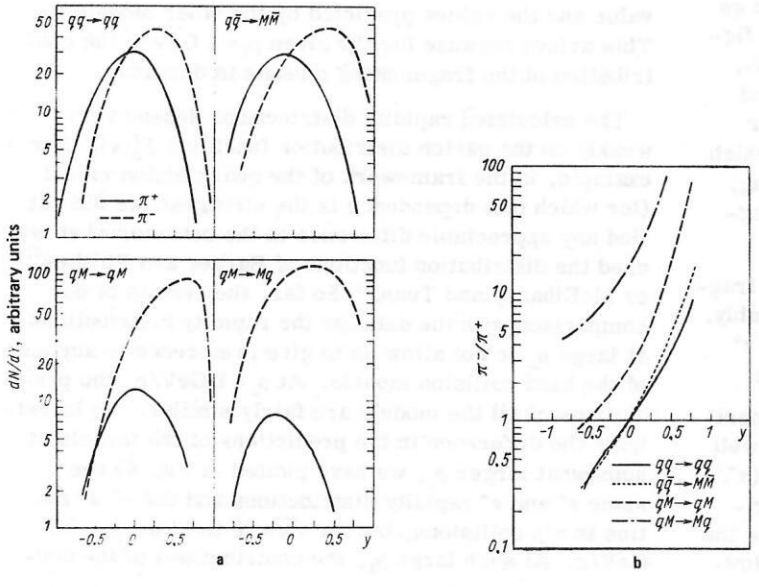

FIG. 45. Rapidity distributions of π^+ and π^- in the reactions $\pi^- p \to \pi^+ X$ and $\pi^- p \to \pi^- X$ at $\sqrt{s}$ = 20 GeV and $p_\perp$ = 5.5 GeV/c obtained for hard collision models. a) Rapidity distributions of π^+ and π^-; b) the ratios π^-/π^+ as functions of Y.[34]

mation, the two-particle distributions for the jet particles take the form

$$\frac{d^2n}{dp_1\,dp_2}=\frac{\langle n(n-1)\rangle_J}{\langle n\rangle_J^2}\frac{dn}{dp_1}\frac{dn}{dp_2}; \tag{131}$$

$$\frac{d^2n}{dp_1\,dp_2}=\frac{\langle n(n-1)\rangle_J}{\langle n\rangle_J^2}\frac{1}{P_{\perp J}^2}\frac{dn}{dx_1}\frac{dn}{dx_2}, \tag{132}$$

where the single-particle distributions dn/dx_i are determined by the expression

$$\frac{dn}{dx}=\pi^{3/2}bBP\left(1-\frac{x}{1+A^2/P}\right)^F\exp\left(-\frac{x^2p_2}{b^2+P^4/M^2}\right)\left[\operatorname{erf}\left(\frac{P}{b}\right)-\operatorname{erf}\left(\frac{xP}{b}\right)\right]\exp\left(\frac{x^2p_2}{b^2}\right). \tag{133}$$

In the central region of rapidities, for which the jet distribution in the form (66) holds, we obtain the following two-particle distribution with respect to the momenta of the particles from the decay of the jet:

$$\left.\frac{d^4\sigma}{dy_1\,d\varphi_1\,dp_{\perp_1}\,dp_{\perp_2}}\right|_{\substack{y_1=y_2=Y\\ \varphi_1=\varphi_2=\Phi}}=\int_{p_{\perp_1}+p_{\perp_2}}^{\sqrt{s}/2}dP_{\perp J}\frac{d^3\sigma_J}{dY\,d\Phi\,dP_{\perp J}}\frac{1}{P_{\perp J}^2}\frac{dn}{dx_1}\frac{dn}{dx_2}\frac{\langle n(n-1)\rangle_J}{\langle n\rangle_J^2}. \tag{134}$$

We calculated the integral in the expression (134) with the realistic single-particle distribution (133) numerically. To perform the integration in a closed form, we used the same approximation as in the derivation of (69) and (70):

$$\frac{d^2\sigma}{dp_{\perp_1}\,dp_{\perp_2}}=\frac{\Delta y\,\Delta\varphi\,(F+1)^2\,c}{p_{\perp_1}p_{\perp_2}}\int_{p_{\perp_1}+p_{\perp_2}}^{\sqrt{s}/2}dP_{\perp J}\frac{1}{P_{\perp J}^N}\times\exp\left(-\frac{2DP_{\perp J}}{\sqrt{s}}\right)\frac{\langle n(n-1)\rangle_J}{\langle n\rangle_J^2}(1-x_1-x_2+x_1x_2)^F. \tag{135}$$

We assume that the distribution with respect to the multiplicity in the jet is characterized by moments $\langle n(n-1)\rangle_J/\langle n\rangle_J^2$ that do not depend on the jet momentum (for example, a Poisson distribution). In addition, we ignore the term x_1x_2, which for $(x_1+x_2)<1$ is smaller than x_1 and x_2. In the framework of the adopted approximation, we go over to the new variable of integration $z=x_1+x_2$ and obtain

$$\frac{d^2\sigma}{dp_{\perp_1}\,dp_{\perp_2}}=\Delta y\,\Delta\varphi c\,(F+1)^2\frac{(p_{\perp_1}+p_{\perp_2})}{p_{\perp_1}p_{\perp_2}}\frac{1}{(p_{\perp_1}+p_{\perp_2})^N}\frac{\langle n(n-1)\rangle_J}{\langle n\rangle_J^2}I_2, \tag{136}$$

where

$$I_2=\int_0^1 dz z^{N-2}\exp\left[-\frac{2D}{\sqrt{s}}\frac{(p_{\perp_1}+p_{\perp_2})}{z}\right](1-z)^F. \tag{137}$$

This integral is analogous to the integral (70) and can be represented approximately as

$$I_2\approx\exp\left[-\frac{2D\,(p_{\perp_1}+p_{\perp_2})}{\sqrt{s}}\right]\frac{F!\,(N-1)!}{(F+N-1)!}. \tag{138}$$

The final result can be written in the form

$$\frac{d^2\sigma}{dp_{\perp_1}\,dp_{\perp_2}}=\Delta y\Delta\varphi c\frac{\langle n(n-1)\rangle_J}{\langle n\rangle_J^2}\frac{\exp\left(-\frac{2D\,(p_{\perp_1}+p_{\perp_2})}{\sqrt{s}}\right)}{p_{\perp_1}p_{\perp_2}(p_{\perp_1}+p_{\perp_2})^{N-1}}\times\frac{(F+1)\,(F+1)!\,(N-2)!}{(F+N-1)!}. \tag{139}$$

If the detector acceptance is large and sufficient to detect all pairs of jet particles, then for $p_\perp=p_{\perp_1}+p_{\perp_2}$ the two-particle distribution (139) can be expressed in terms of the single-particle distributions (74):

$$\frac{d^2\sigma}{dp_{\perp_1}\,dp_{\perp_2}}=\frac{\langle n(n-1)\rangle_J}{\langle n\rangle_J^2}(F-1)\frac{p_{\perp_1}-p_{\perp_2}}{p_{\perp_1}p_{\perp_2}}\frac{d\sigma}{dp}\Big|_{p_\perp=p_{\perp_1}+p_{\perp_2}}. \tag{140}$$

This corresponds to the invariant distribution

$$\varepsilon_1\varepsilon_2\frac{d^6\sigma}{d^3p_1\,d^3p_2}=\frac{\langle n(n-1)\rangle_J}{\langle n\rangle_J^2}(F-1)\frac{(p_{\perp_1}-p_{\perp_2})^2}{(p_{\perp_1}p_{\perp_2})^2}\varepsilon\frac{d^3\sigma}{d^3p_\perp}\Big|_{p_\perp=p_{\perp_1}+p_{\perp_2}}. \tag{141}$$

The behavior of the two-particle distributions of the type (141) was investigated in the experiment of the ACHM group (Aachen, CERN, Heidelberg, Munich) (see Fig. 7).[9] In analyzing the data, this group replaced the invariant cross section by a function of the transverse momentum of the system of two pions: $p_\perp=p_{\perp_1}+p_{\perp_2}$. An appreciable dependence on the difference $\Delta p_\perp$ between the transverse momenta of the two pions was not found. The distribution averaged over $\Delta p_\perp$ can be well represented by means of the parametrization

$$\left\langle\varepsilon_1\varepsilon_2\frac{d^6\sigma}{d^3p_1\,d^3p_2}\right\rangle_{\Delta p_\perp}=\frac{1}{p_-}f\left(\frac{2p_\perp}{\sqrt{s}}\right)\Big|_{p_\perp=p_{\perp_1}+p_{\perp_2}} \tag{142}$$

with exponent $N=7.1\pm0.5$, whose value is very close to the value of the parametrization of the single-particle distribution.[12]

The behavior of the two-particle distribution (141) is very characteristic of the jet model. Indeed, in the numerical integration of the expression (134) it was found that the two-particle distributions depend only on $p_{\perp_1}+p_{\perp_2}$. At small momenta, however, the ratio of the two- and single-particle distributions found in this manner behaves in a manner different from that predicted by Eq. (141).

The two-particle distribution (134) or its approximate forms (139) and (140) also serve as the basis for calculations of the correlations (129) between particles of the forward hemisphere. Integrating the single-particle distribution (74) with respect to $p_\perp$ and retaining only the principal term, we obtain

$$\int_{p_{-_1}^0}^{\sqrt{s}/2}dp_-\frac{d\sigma}{dp_-}\approx\frac{p_{-_1}^0}{N-1}\frac{d\sigma}{dp_{\perp_1}}\Big|_{p_{\perp_1}=p_\perp^0}. \tag{143}$$

In the same approximation, the integral with respect to $p_{\perp_2}$ of the two-particle distribution gives

$$\int_{p_{\perp_1}^0}^{\sqrt{s}/2}\frac{d^2\sigma}{dp_{-_1}\,dp_{-_2}}dp_{-_2}\approx\frac{p_{\perp_1}^0+p_{\perp_2}}{N-2}\frac{d^2\sigma}{dp_{\perp_1}\,dp_{\perp_2}}\Big|_{p_{\perp_1}=p_{\perp_1}^0}, \tag{144}$$

or, if we use (140),

$$\int_{p_{-_1}^0}^{\sqrt{s}/2}\frac{d^2\sigma}{dp_{\perp_1}\,dp_{\perp_2}}dp_{-_1}\approx\frac{\langle n(n-1)\rangle_J}{\langle n\rangle_J^2}\frac{(F+1)}{(N-1)}\frac{(p_{\perp_1}^0+p_{\perp_2})^2}{p_{\perp_1}^0p_{\perp_2}}\frac{d\sigma}{dp_\perp}\Big|_{p_\perp=p_{\perp_1}^0+p_{\perp_2}} \tag{145}$$

In the experiment of the CCRS group,[2] the single-particle and two-particle distributions were measured by means of a spectrometer having the same geometrical acceptance $\Delta\varphi$ and $\Delta\theta$ as that indicated after Eq. (129). In the framework of the approximation that we use for the jets, the secondary particles do not have transverse momentum relative to the jet axis, and therefore the correlation function (129) becomes independent of the detector acceptance; if the detector captures the detected particle, then all the particles of the jet are observed.

However, this approximation does not correspond to reality. We therefore introduce a correction factor $G(p_{\perp_2})$, which reflects the limitation for detection for the second particle:

$$G(p_{\perp_2},\ \Delta\theta,\ \Delta\varphi) = \operatorname{erf}(\Delta\theta p_{\perp_2}/\sqrt{2}\,b)\operatorname{erf}(\Delta\varphi p_{\perp_2}/\sqrt{2}\,b). \qquad (146)$$

This representation was obtained by means of the parametrization (37) for the jet fragmentation function. Using Eqs. (143), (144), and (146), we arrive at the following correlation function for the particles of the forward hemisphere:

$$\mathcal{F}(p^0_{\perp_1},\ p_{\perp_2}) = \frac{N-1}{N-1}\frac{p^0_{\perp_1}-p_{\perp_2}}{p^2_{\perp_1}}\left.\frac{d^2\sigma/dp_{\perp_1}dp_{\perp_2}}{d\sigma/dp_{\perp_1}}\right|_{p_{\perp_1}=p^0_{\perp_1}} G(p_{\perp_2},\ \Delta\theta,\ \Delta\varphi). \qquad (147)$$

We calculated the correlation (147) between the particles of the forward hemisphere by a numerical estimate of the two-particle distribution (134) and the single-particle distribution (68) using the reasonable distribution (133) for the jet particles.

In Fig. 46, we compare the calculated correlation with the data of the CCRS group. For the parameters c, N, and D in (66), we have used the values found by this group:

$$N = 7.6,\ D = 12.6,\ c = 14.8\ \text{mb}. \qquad (148)$$

The obtained results are in good agreement with the data, especially as regards the energy dependence. It should be emphasized that our model calculations do not contain arbitrary normalization parameters.

If we use the approximation (145), the correlation between the particles of the forward hemisphere can be expressed solely in terms of the single-particle distribution:

$$\mathcal{F}(p^0_{\perp_1},\ p_{\perp_2}) = \frac{\langle n(n-1)\rangle_J}{\langle n\rangle^2_J}\frac{(F+1)}{(N-2)(N-1)}\frac{(p^0_{\perp_1}-p_{\perp_2})^2}{p^2_{\perp_2}}\frac{(d\sigma/pp_\perp)|_{p_\perp=p^0_{\perp_1}+p_{\perp_2}}}{(d\sigma/dp_\perp)|_{p_\perp=p^0_{\perp_1}}} \times G(p_{\perp_2},\ \Delta\theta,\ \Delta\varphi). \qquad (149)$$

An expression similar to (149), including data on the single-particle distributions, was used by Bjorken[61] to explain the energy dependence of the correlations of particles of the forward hemisphere.

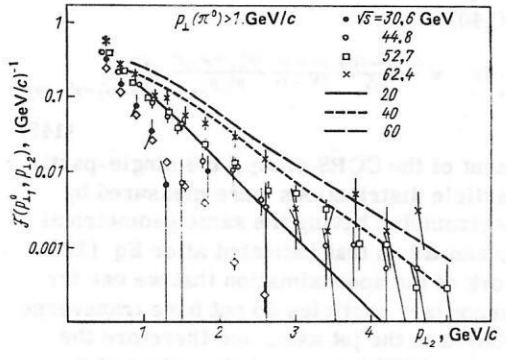

FIG. 46. Correlation function for forward hemisphere at large momentum transfers defined by Eq. (129) and calculated in the framework of the jet models in accordance with the expressions (134) and (147) for $F=2$ (Ref. 63).

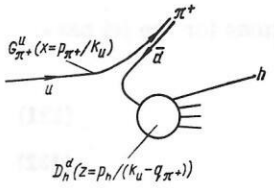

FIG. 47. Scheme for calculating the correlations in the forward hemisphere in the framework of the quark scattering model.

The rapidity dependence of the correlations between the particles of the forward hemisphere has already been discussed in Sec. 2. Here we shall merely emphasize that the presence of strong correlations between the detected particle and the second particle of the forward hemisphere eliminates variants of the models such as the quark fusion model 2 (see Sec. 3) and the constituent interchange model 3 if the meson constituent does not fragment. Only the variants of these models in which the meson constituents also decay like a jet or resonance agree with the data on the correlations between the particles of the forward hemisphere.

The magnitude of the correlation between the particles of the forward hemisphere, in particular the ratio h^+h^-/h^-h^- of the correlations, was investigated in Ref. 79. The data of the CCHK group are given in Fig. 11. A sharp peak is observed in the rapidity distribution of the trigger particle. For the $qq \to qq$ model, a qualitative analysis can be based on the scheme indicated in Fig. 47. For example, if the π^+ meson is created by a u quark, then it is assumed that the remaining hadrons of the jet can be regarded as decay products of a d quark carrying the momentum of the original quark with the momentum of the detected π^+ meson subtracted. Thus, considering the decay of the d quark for the detected π^+ meson, we find that among the comoving particles there will be more negative hadrons than positive hadrons.

In Figs. 48 and 49 we compare the theory with the data of an experiment in which a π^- meson was detected; $\theta_{cm} = 45°$. The model reproduces the experimental ratio $h^+h^-/h^-h^- \approx 3$.

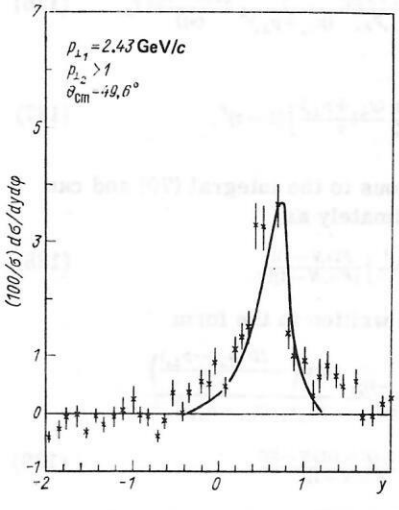

FIG. 48. Comparison of correlations between negatively charged trigger particle and positive secondary particle[79] with the data of the CCHK group.[7,8] The background at 45° has been subtracted from the data.[31]

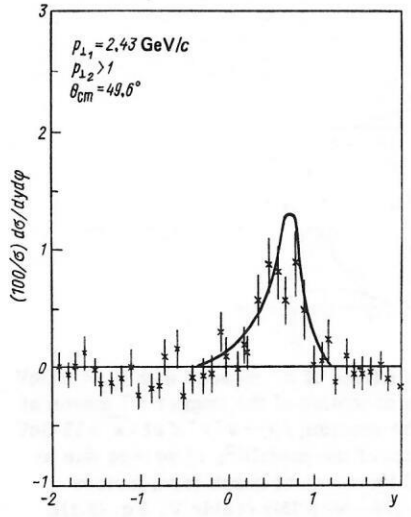

FIG. 49. The same as in Fig. 48 but for negatively charged trigger and secondary particles.[31]

7. CORRELATIONS FOR PARTICLES OF THE BACKWARD HEMISPHERE

The dependence of the correlation of the particles of the backward hemisphere on the transverse momentum is usually represented in the form of the distribution dN/dx_e, where $x_e = p_{\perp_2}/p_{\perp_1}$ is the ratio of the transverse momentum of the particle of the backward hemisphere to the transverse momentum of the trigger particle.

Figure 14 shows the data of the experiment of Ref. 10. These data were analyzed for the first time by Ellis *et al.*[62] The two-particle distribution in the case when one of the particles is emitted in the opposite direction, integrated over all angles, has the form

$$\left(\frac{d^2\sigma}{dp_{\perp_1}dp_{\perp_2}}\right)_{\text{op}} = 2\int_{p_{\perp_1}}^{\infty}\frac{dP_\perp}{P_\perp^2}\Phi(P_\perp,\sqrt{s})\,D_1^i\left(\frac{p_{\perp_1}}{P_\perp}\right)D_2^i\left(\frac{p_{\perp_2}}{P_\perp}\right) \quad (p_{\perp_1}>p_{\perp_2}), \tag{150}$$

where $\Phi(P_\perp,\sqrt{s})$ is the jet production cross section [see, for example, (66)], and $D_h^i(z)$ are the jet fragmentation functions (27). Then the distribution dN/dx_e for the opposite hemisphere is

$$\frac{dN}{dx_e} = \frac{\sum_{\text{ch}}\int dp_{\perp_2}\delta\left(x_e-\frac{p_{\perp_2}}{p_{\perp_1}}\right)\left(\frac{d^2\sigma}{dp_{\perp_1}dp_{\perp_2}}\right)_0}{\frac{d\sigma}{dp_{\perp_1}}}. \tag{151}$$

Ellis *et al.*[62] found that if one uses the fragmentation function

$$D_h^i(z) = B^h(1-z)^m/z, \tag{152}$$

the calculated distribution is too large, exceeding the experimental one by about a factor two. They showed that agreement with experiment is possible only if one adds to the function (152) a term corresponding to nonfragmenting mesons of the jet:

$$D_h^i(z) = B^h\frac{(1-z)^m}{z} + K^h\delta(z-1), \quad K^h \ll B^h. \tag{153}$$

The last term is only a few percent of the total probability. In Fig. 50, the results of their fit are compared with the data of Ref. 10. It is, however, emphasized in Ref. 66 that better agreement with experiment is obtained without the term containing the δ function but using jet fragmentation functions (37) that take into account the departure from scaling (Fig. 51). This also leads to a small departure from scaling for the distributions with respect to x_e. In addition, as was shown by Preparata and Rossi,[109] a jet model with nonvanishing invariant mass also leads to better agreement with experiment.

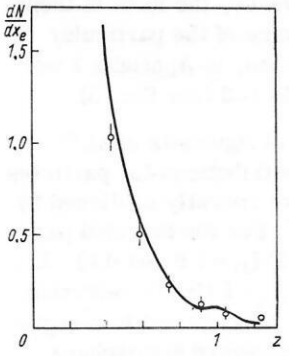

FIG. 50. Comparison of the distribution dN/dx_e of backward hemisphere particles obtained in Ref. 62 with data of the experiment of Ref. 10. In the calculation of the curves it was assumed that the probability of finding only one particle in the jet is very small. This corresponds to a δ function smeared around the point $x_e = 1$.

A clear departure from scaling in the behavior of the dN/dx_e distribution was obtained by the CCHK group (see Fig. 15).[18] At the present time, none of the hard scattering models is capable of explaining this nonscaling behavior.

In Sec. 2, we have already considered the rapidity correlations between particles of the backward hemisphere. The rapidity distribution for a particle opposite to the detected particle with large $p_\perp$ was used by many authors to study the dynamics of the hard collision process.[33,52,59,65,79,97,98] The two-particle distributions for the backward hemisphere are calculated in

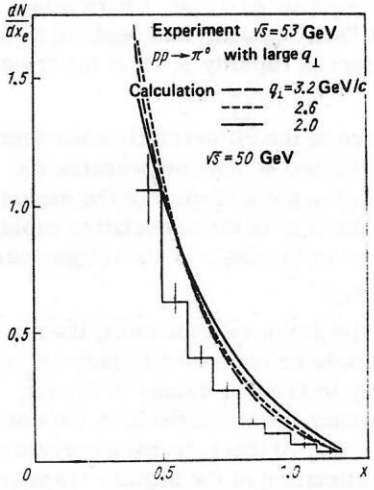

FIG. 51. Comparison of the experimental data on the distribution dN/dx_e of particles in the backward hemisphere[10] with the results obtained using our parametrization for the jet fragmentation function.

accordance with Eq. (61). However, the form of these expressions depends on the choice of the particular hard scattering model. Therefore, in Appendix 1 we give the expressions for models 1–3 (see Sec. 3).

We shall follow the analysis of Ilgenfritz *et al.*[33] Detailed data on the rapidity distributions for particles of the opposite hemisphere were recently published by the CCHK group (see Fig. 12).[7] For the detected particle $x_{\perp_1} = 0.1$, and $\theta_1 = 20$ and $40°$ ($y_1 \approx 1.6$ and 0.8). In the analysis, only the data for $p_{\perp_2} < 1$ GeV/c referring to a negatively charged trigger particle and to a negatively charged particle of the backward hemisphere were used. There is a hope that in this channel the effects of the leading particle are minimal. In addition, we have restricted ourselves to comparing the form of the calculated distributions for the backward hemisphere with the form of the experimental dependence. We have already discussed the problems associated with the absolute normalization when considering the distribution dN/dx_e. Restrictions on the hard scattering cross sections follow only from the form of the distributions. The stability of the maximum of the distribution for the backward hemisphere at $y_2 = 0$ for $x_{\perp_1} \approx 0.1$, irrespective of the rapidity y_1 of the trigger particle, is striking.

Data on correlations for particles of the opposite hemisphere were also published in Refs. 10, 11, and 17. There are a number of indications that the maximum of the correlations is shifted with a change in the $x_{\perp_1}$ of the detected particle.[11,17] It was shown in Ref. 52 that this is in agreement with the predictions of hard scattering models.

The picture of the correlations for the opposite hemisphere is made up of a number of different effects:

1) dominance of the region of low energies in the elementary collision event; this increases the correlations in the region $y_1 y_2 > 0$ (back-to-antiback correlation);

2) a comparative broadening of the rapidity distribution in the center-of-mass system for the elementary collisions in the case of scattering of nonsymmetric constituents (say, $qM \to qM$ or $q\bar{q} \to MM$, where q is a valence quark and $\bar{q}$ a "sea" quark); this leads to a splitting of the maximum at rapidity $y_1 \approx 0$ of the trigger particle;

3) a peripheral nature of the differential cross section for the elementary collision, which compensates the low-energy effect from the point of view of the experimentally established stability of the associative rapidity distribution with regard to the angle of the trigger particle (rapidity) at low $x_{\perp_2}$;

4) the possibility of jet fragmentation along the direction of the trigger particle or transition to large $x_{\perp_1}$ values, leading effectively to large x_1 values of the jet; this establishes a tendency for an increase in the correlations in the region $y_1 y_2 < 0$ (back-to-back correlation) and a sharper collimation of the angular (rapidity) distributions for the particle of the backward hemisphere.

These tendencies are confirmed by our calculations.

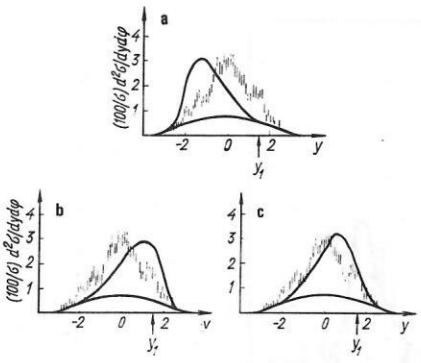

FIG. 52. Rapidity distributions of π^- mesons with $p_{\perp_2} \geq 1$ GeV opposite to the direction of motion of the trigger π^- meson at $y_1 = 1.6$ and $x_{\perp_1} = 0.1$ in the reaction $pp \to \pi^- \pi^- X$ at $\sqrt{s} = 53$ GeV compared with the results of the models[33]; a) $qq \to qq$ due to gluon exchange modified by means of quark form factors [Table V, Eq. (1.1)]; b) $qM \to Mq$ (CIM) [Table V, Eq. (2.1)]; c) $qq \to qq$ with phenomenological expressions for the cross section [Table V, Eq. (1.3)].

They show that the correlations for the scattering angles $\theta_1 = 45$ or $90°$ of the detected particles may be a decisive test for these models, which have already passed the test for angles $\theta_1 = 20°$.

In Fig. 52, we compare the predictions of three models with the data at $y_1 = 1.6$ and $x_{\perp_1} = 0.1$. In Fig. 52a, we give the result obtained for the quark-quark scattering model including quark form factors,[51] which change the gluon exchange cross section [see Table V, (1.1)]. The resulting cross section is to a large degree peripheral, as is indicated by the appearance of a sharp peak in the region $y_1 y_2 < 0$. We established that this feature is characteristic of models in which the principal term in $1/\eta$ and η has exponent $N = 4$. We should therefore like to eliminate from consideration all the variants in which the $p_\perp^{-8}$ behavior of the meson production cross section in the framework of quark-quark scattering models with gluon exchange is associated with a modification of the structure functions[86] or the amplitudes[87] through approximate quark form factors. This leads to a fairly strong peripherality, which distorts the correlation functions. In the framework of the model of Hwa *et al.*,[86] this was demonstrated in Ref. 98 for scattering angle $90°$ of the detected particle, and it was accompanied by the appearance of clearly defined peripheral peaks in the distributions for the backward hemisphere.

From Fig. 52b, we conclude that the $qM \to Mq$ model using the expression for the hard scattering cross section [see Table V, (4.1)] proposed originally in the CIM model is to a large degree nonperipheral, which leads to a peak in the region $y_1 y_2 > 0$. This conclusion differs from the one drawn earlier in Ref. 97, since at that time the experimental data of Ref. 8 were not yet available, but it agrees with the conclusions of Fox.[31] Such qualitatively incorrect behavior does not depend on the concrete constituent exchange mechanism. If one parametrizes in the same manner the quark-quark scattering cross section [see Table V, (1.3)], the same type of correlations in Fig. 52c is obtained. Thus, the inapplicability of both models is due to the incorrect ex-

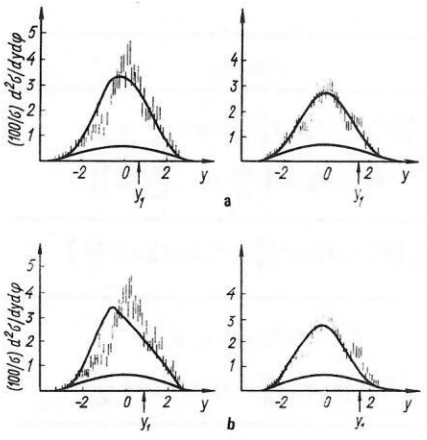

FIG. 53. The same as in Fig. 52 for two rapidities of the trigger particle ($y_1 = 0.8$ and 1.6, $\theta_1 = 45°$ and 20°) compared with the results of the $qq \to qq$ models using Ref. 33; a) phenomenological expression for the cross section (117) with $a = 1$, $N = 3$; b) phenomenological expression for the cross section (1.2) from Table V.

ponent in the expression (117): $N = 2$. The data for $\theta = 20°$ can be successfully described by means of the models 1–4 (see Sec. 3) using the empirical parametrization (117) of the hard scattering cross section with exponent $N = 3$. This is also true of the expressions for the cross sections proposed by Field and Feynman[51] [see Table V, (1.2)] and Baier *et al.*[98] [see Table V, (2.1)]. The leading term of all these parametrizations has the form $d\sigma/d\hat{t} \approx 1/\hat{s}\hat{t}^3$. The parameter a in Eq. (117) realizes the subsequent control of the degree of peripherality introduced with $N = 3$. The best agreement with the experimental data is achieved when $a = 1$ for the process $qq \to qq$ and $a = 0.5$ for the other elementary processes. In Fig. 53, we make a comparison with the data only for the $qq \to qq$ model.

As a result of these investigations, we conclude that the currently existing data do not enable us to distinguish between the models, but they do give the possibility of predicting that a difference will be found in experiments with large transverse momenta of the detected particle, with different species of detected particles (for example, K^-), and corresponding data on the correlations for different clusters of particles.

TABLE VIII. Results of comparison of hard scattering models with experimental data*.

	Compared quantities	$qq \to qq$	$q\bar{q} \to MM$	$qM \to Mq$ (CIM)	$qM \to qM$
Single-particle distributions	$p_\perp$-dependence in pp	Good agreement	Problems with π^+/π^-	Good agreement; for the ratio π^+/π^- superposition of f and nf mesons must be taken into account	Good agreement
	Ratio $R(p/\pi)$	Good agreement but constant $F^q_{\pi\text{ val}}$ required	Problems with absolute value	Good agreement	Good agreement
	y-distribution in πp and $p\bar{p}$ at $p_\perp = 1$ GeV/c	Good agreement	Good agreement	π^+/π^- asymmetry too small	Good agreement
	Production of $K^\pm$, p, $\bar{p}$	$K^\pm$, good agreement	Problems with K^+/K^- at large $p_\perp$	Good agreement	Probably everything in order
	Compared quantities	$qq \to qq$	$q\bar{q} \to MM$	$qM \to Mq$ (CIM)	$qM \to qM$
Correlations for the opposite hemisphere	y dependence, form	Good agreement; quark form factors eliminated	Good agreement; detected particle preferentially f	Good agreement; detected particle preferentially nf. The dependence $d\sigma/dt \sim \sim 1/\hat{s}^2\hat{u}s + 1/\hat{s}^4$ eliminated	Good agreement; preferentially detected particle from f
	dN/dx_e and normalization of y dependence	In all models, problems with the absolute normalization; proposed corrections: departure from scaling for $\sigma(z)$, superposition of f and nf, allowance for transverse momenta of partons in the hadrons and of the hadrons in the jets			
	CCHK, departure from scaling for dN/dx_e	Problems in all models; weak departure from scaling in $G(z)$			
	Correlations and associative multiplicities for the forward hemisphere	Good agreement	Good agreement only with allowance for the contributions of the f mesons for the forward hemisphere		

*f contribution of fragmenting mesons; nf, contribution of nonfragmenting mesons.

CONCLUSIONS

The majority of the experimental data so far obtained are consistent with the predictions of hard scattering models. For this reason, it appears to us that the hard scatterig model is justified. There is a fairly good proof of the existence of jets in reactions with large $p_\perp$, which is also predicted by these models. However, the complete picture is by no means fully understood. We have already mentioned the empirical nature of the expressions for the hard collision cross sections in the majority of models, the absence of a deep theoretical understanding of the interconnection between the problem of quark confinement and the jet production effect, and the fact that as yet we are not capable of making a final choice between the hard scattering models.

In Table VIII we summarize the situation in the different hard scattering models considered in this review.

APPENDIX 1. TWO-JET DISTRIBUTION AND THE SINGLE-PARTICLE AND TWO-PARTICLE DISTRIBUTIONS FOR THE OPPOSITE HEMISPHERE IN THE HARD COLLISION MODELS

In this appendix, we collect together the concrete expressions encountered in the models that we consider.

In Tables A.I–A.IV we take

$$\tau_{ik}=1, \tag{A.1}$$

if quark i is a constituent of meson k, and

$$\tau_{ik}=0 \tag{A.2}$$

otherwise.

In Fig. A.1 we define the quark lines used in Fig. A.2.

Single-Particle Distributions with Fragmenting Constituents. The single-particle distribution has the form

$$E_C\frac{d^3\sigma}{d^3p_C}\approx\frac{4}{xp_{\perp c}^3}\int\int dx_1\,dx_2\,X(x_1,x_2,z)\frac{\eta}{(1+\eta)_2}. \tag{A.3}$$

TABLE A. I.

Elementary process	$X(x_1, x_2, z)$
$qq\to qq$ (Fig. A.2a)	$\sum_i\sum_j F_A^i(x_1)F_B^j(x_2)\left[\frac{d\sigma}{d\hat t}G_C^i(z)+\frac{d\sigma}{d\hat u}G_C^j(z)\right]$
$q\bar q\to MM$ (Fig. A.2b)	$\sum_{i,j,k}\left(F_A^i(x_1)F_B^j(x_2)\left[\frac{d\sigma}{d\hat t}G_C^k(z)\tau_{ik}+\frac{d\sigma}{d\hat u}G_C^k(z)\tau_{jk}\right]+F_A^j(x_1)F_B^i(x_2)\left[\frac{d\sigma}{d\hat t}G_C^k(z)\tau_{jk}+\frac{d\sigma}{d\hat u}G_C^k(z)\tau_{ik}\right]\right)$
$qM\to qM$ (Fig. A.2c)	$\sum_{i,j}\left(F_A^j(x_1)F_B^i(x_2)\left[\frac{d\sigma}{d\hat t}G_C^j(z)+\frac{d\sigma}{d\hat u}G_C^i(z)\right]+F_A^i(x_1)F_B^j(x_2)\left[\frac{d\sigma}{d\hat t}G_C^i(z)+\frac{d\sigma}{d\hat u}G_C^j(z)\right]\right)$
$qM\to Mq$ (Fig. A.2d)	$\sum_{i,j,k,l}\tau_{il}\tau_{kj}\delta_{(Q_i+Q_j-Q_l-Q_k),\,0}\times\left[F_A^j(x_1)F_B^i(x_2)\left(\frac{d\sigma}{d\hat t}G_C^k(z)+\frac{d\sigma}{d\hat u}G_C^l(z)\right)+F_A^i(x_1)F_B^j(x_2)\left(\frac{d\sigma}{d\hat t}G_C^l(z)+\frac{d\sigma}{d\hat u}G_C^k(z)\right)\right]$

TABLE A. II.

Elementary process	$Y(x_1, x_2)$
$q\bar q\to MM$ (Fig. A.2e)	$\sum_{i,j}(F_A^i(x_1)F_B^j(x_2)\left[\frac{d\sigma}{d\hat t}\tau_{iC}+\frac{d\sigma}{d\hat u}\tau_{iC}\right]+F_A^j(x_1)F_B^i(x_2)\left[\frac{d\sigma}{d\hat t}\tau_{jC}+\frac{d\sigma}{d\hat u}\tau_{iC}\right])$
$qM\to qM$ (Fig. A.2f)	$\sum_i\left(F_A^C(x_1)F_B^i(x_2)\frac{d\sigma}{d\hat t}+F_A^i(x_1)F_B^C(x_2)\frac{d\sigma}{d\hat u}\right)$
$qM\to Mq$ (Fig. A.2g)	$\sum_{i,j,k}\tau_{iC}\tau_{kj}\delta_{(Q_i+Q_j-Q_j-Q_k),\,0}\times\left(F_A^i(x_1)F_B^j(x_2)\frac{d\sigma}{d\hat t}+F_A^j(x_1)F_B^i(x_2)\frac{d\sigma}{d\hat u}\right)$

The function $X(x_1, x_2, z)$ for different elementary processes is defined in Table A.I.

The corresponding kinematic relations can be written in the form

$$\left.\begin{aligned}\eta&=(x_1/x_2)\,\mathrm{tg}^2(\theta_C/2);\\ z&=(x_{\perp C}/2)\,(1+\eta)/x_1\,\mathrm{tg}\,(\theta_C/2).\end{aligned}\right\} \tag{A.4}$$

The limits of integration are

$$\left.\begin{aligned}&x_1x_{\perp C}\,\mathrm{tg}\,(\theta_C/2)/[2x_1-x_{\perp C}\,\mathrm{ctg}\,(\theta_C/2)]\leqslant x_2\leqslant 1;\\ &x_{\perp C}\,\mathrm{ctg}\,(\theta_C/2)/[2-x_{\perp C}\,\mathrm{tg}\,(\theta_C/2)]\leqslant x_1\leqslant 1.\end{aligned}\right\} \tag{A.5}$$

Single-Particle Distributions with Nonfragmenting Mesons. The single-particle distribution has the form

TABLE A. III.

Elementary process	$V(x_1, x_2, z_1, z_2)$
$qq\to qq$ (Fig. A.2a)	$\sum_i\sum_j F_A^i(x_1)F_B^j(x_2)\left[\frac{d\sigma}{d\hat t}G_C^i(z_1)G_D^j(z_2)+\frac{d\sigma}{d\hat u}G_C^j(z_1)G_D^i(z_2)\right]$
$q\bar q\to M\bar M$ (Fig. A.2b)	$\sum_i\sum_j\sum_k\sum_l\delta_{(Q_i+Q_j-Q_k-Q_l),\,0}\left(F_A^i(x_1)F_B^j(x_2)\times\left[\frac{d\sigma}{d\hat t}G_C^k(z_1)G_D^l(z_2)\tau_{ik}\tau_{jl}+\frac{d\sigma}{d\hat u}G_C^k(z_1)G_D^l(z_2)\tau_{il}\tau_{jk}\right]+F_A^j(x_1)F_B^i(x_2)\left[\frac{d\sigma}{d\hat t}G_C^k(z_1)G_D^l(z_2)\tau_{il}\tau_{ik}+\frac{d\sigma}{d\hat u}G_C^k(z_1)G_D^l(z_2)\tau_{ik}\tau_{jl}\right]\right)$
$qM\to qM$ (Fig. A.2c)	$\sum_{ij}\left(F_A^i(x_1)F_B^j(x_2)\left[\frac{d\sigma}{d\hat t}G_C^i(z_1)G_D^j(z_2)+\frac{d\sigma}{d\hat u}G_C^j(z_1)G_D^i(z_2)\right]+F_A^j(x_1)F_B^i(x_2)\times\left[\frac{d\sigma}{d\hat t}G_C^j(z_1)G^i+\frac{d\sigma}{d\hat u}G_C^i(z_1)G_D^j(z_2)\right]\right)$
$qM\to Mq$ (Fig. A.2d)	$\sum_{i,j,kl}\delta_{(Q_k+Q_j-Q_i-Q_l),\,0}\left\{\tau_{ik}\tau_{jl}\left[F_A^j(x_1)F_B^k(x_2)\times\left(\frac{d\sigma}{d\hat t}G_C^l(z_1)G_D^i(z_2)+\frac{d\sigma}{d\hat u}G_C^i(z_1)G_D^l(z_2)\right)+F_A^k(x_1)F_B^j(x_2)\left(\frac{d\sigma}{d\hat t}G_C^i(z_1)G_D^l(z_2)+\frac{d\sigma}{d\hat u}G_C^l(z_1)G_D^i(z_2)\right)\right]+\tau_{jk}\tau_{il}\left[F_A^j(x_1)F_B^k(x_2)+F_A^k(x_1)F_B^j(x_2)\right]\left(\frac{\partial\sigma^*}{\partial t}\right)(G_C^i(z_1)G_D^l(z_2)+G_C^l(z_1)+G_C^l(z_1)G_D^i(z_2))\right\}$

TABLE A. IV.

Elementary process	$U(x_1, x_2, z_2)$
$q\bar{q} \to MM$ (Fig. A.2e)	$\sum_{i,j,l} \delta_{(Q_i \dotplus Q_j - Q_C - Q_l),\,0} \Big(F_A^i(x_1) F_B^j(x_2) \times \Big[\frac{d\sigma}{d\hat{t}} G_D^l(z_2) \tau_{iC}\tau_{jl} \dotplus \frac{d\sigma}{d\hat{u}} G_D^l(z_2) \tau_{il}\tau_{jC} \Big] \dotplus F_A^j(x_1) F_B^i(x_2) \Big[\frac{d\sigma}{d\hat{t}} G_D^C(z_2) \tau_{il}\tau_{jC} \dotplus \frac{d\sigma}{d\hat{u}} G_D^C(z_2) \tau_{iC}\tau_{jl} \Big] \Big)$
$qM \to qM$ (Fig. A.2f)	$\sum_i \Big(F_A^C(x_1) F_B^i(x_2) \frac{d\sigma}{d\hat{t}} G_D^i(z_2) \dotplus F_A^i(x_1) F_B^C(x_2) \frac{d\sigma}{d\hat{u}} G_D^i(z_2) \Big)$
$qM \to Mq$ (Fig. A.2g)	$\sum_{i,j,k} \Big(\delta_{(Q_k+Q_i-Q_j-Q_C),\,0} \tau_{jk}\tau_{iC} \Big[F_A^i(x_1) F_B^k(x_2) \times \frac{d\sigma}{d\hat{t}} G_D^j(z) \dotplus F_A^k(x_1) F_B^i(x_2) \frac{d\sigma}{d\hat{u}} G_D^j(z_2) \Big] \dotplus \delta_{(Q_k+Q_j-Q_i-Q_C),\,0} \tau_{jk}\tau_{iC} [F_A^k(x_1) F_B^j(x_2) \dotplus F_A^j(x_2) F_B^k(x_2)] \frac{d\sigma^*}{d\hat{t}} G_D^i(z_2) \Big)$

$$E_C \frac{d^3\sigma}{d^3p_C} \approx \frac{2}{x_{\perp C}\pi} \int \frac{dx_1 \operatorname{tg}(\theta_C/2)}{\Big[1 - \frac{x_{\perp C}}{2} \frac{1}{x_1} \operatorname{ctg}(\theta_C/2)\Big]^2} \frac{\eta}{(1 \dotplus \eta)^2} Y(x_1, x_2). \tag{A.6}$$

For the different elementary processes, the function $Y(x_1, x_2)$ is defined in Table A.II. The corresponding kinematic relations are given by

$$\left.\begin{aligned} &\eta = (x_1/x_2)\operatorname{tg}^2(\theta_C/2);\quad x_2 = (x_{\perp C})\operatorname{tg}(\theta_C/2) \\ &\times [1 - (x_{\perp C}/2)(1/x_1)\operatorname{ctg}(\theta_C/2)]^{-1}. \end{aligned}\right\} \tag{A.7}$$

The limits of integration are

$$x_{\perp C} \operatorname{ctg}(\theta_C/2)/[2 - x_{\perp C} \operatorname{tg}(\theta_C/2)] \leqslant x_1 \leqslant 1. \tag{A.8}$$

Two-Particle Distributions; All Constituents Fragment. The two-particle distribution can be represented in the form

$$E_C E_D \frac{d^6\sigma}{d^3p_C d^3p_D} \frac{16}{\pi s x_{\perp C}^2 x_{\perp D}^2} \times \int \frac{x_1 dx_1}{(\operatorname{ctg}(\theta_1/2) \dotplus \operatorname{ctg}(\theta_2/2))^2} V(x_1, x_2, z_1, z_2). \tag{A.9}$$

The function $V(x_1, x_2, z_1, z_2)$ for the different elementary processes is given in Table A.III.

The kinematic relations that we need have the form

$$\left.\begin{aligned} &\eta = \operatorname{tg}(\theta_C/2)\operatorname{ctg}(\theta_D/2); \\ &x_2 = x_1 \operatorname{tg}(\theta_C/2)\operatorname{tg}(\theta_D/2); \\ &z_1 = z_{\perp C}(1 \dotplus \eta)/2x_1 \operatorname{tg}(\theta_C/2); \\ &z_2 = x_{\perp D}(1 - \eta)/2x_1 \operatorname{tg}(\theta_C/2). \end{aligned}\right\} \tag{A.10}$$

The limits of integration are determined by the inequality

$$\max\Big(\frac{x_{\perp C}(1 \dotplus \eta)}{2\operatorname{tg}(\theta_C/2)}, \frac{x_{\perp D}(1 \dotplus \eta)}{2\operatorname{tg}(\theta_C/2)}\Big) \leqslant x_1 \leqslant \min(1, \operatorname{ctg}(\theta_C/2)\operatorname{ctg}(\theta_D/2)). \tag{A.11}$$

Two-Particle Distributions; the Detected Meson does not Fragment. The two-particle distribution is represented by

$$E_C E_D \frac{d^6}{d^3p_C d^3p_D} \approx \frac{2}{\pi s x_{\perp D}^2} U(x_1, x_2, z_2). \tag{A.12}$$

The function $U(x_1, x_2, z_2)$ for the different elementary processes is given in Table A.IV. The kinematic relations are

$$\left.\begin{aligned} &x_1 = (x_{\perp C}/2)[\operatorname{ctg}(\theta_C/2) \dotplus \operatorname{ctg}(\theta_D/2)]; \\ &x_2 = (x_{\perp C}/2)[\operatorname{tg}(\theta_C/2) \dotplus \operatorname{tg}(\theta_D/2)]; \\ &z_2 = x_{\perp D}(1 \dotplus \eta)/2x_1 \operatorname{tg}(\theta_C/2). \end{aligned}\right\} \tag{A.13}$$

Two-Jet Distribution. The two-jet distribution has the form

$$E_l E_k \frac{d^3\sigma_J}{d^3p_l d^3p_k} = \frac{1}{\pi} \sum_{i,j} F_A^i(x_1) F_B^j(x_2) \frac{d\sigma}{d\hat{t}} \delta^{(2)}(p_{\perp l} + p_{\perp k}). \tag{A.14}$$

The kinematic variables $\hat{s}$ and $\hat{t}$ describing the parton-parton collision are determined by

$$\hat{s} \approx p_\perp^2 [1 \dotplus \operatorname{tg}(\theta_l/2)\operatorname{ctg}(\theta_k/2)][1 \dotplus \operatorname{tg}(\theta_k/2)\operatorname{ctg}(\theta_l/2)]; \tag{A.15}$$

$$\hat{t} \approx -p_\perp^2 [1 \dotplus \operatorname{tg}(\theta_l/2)\operatorname{ctg}(\theta_k/2)]. \tag{A.16}$$

The fractions of the longitudinal momenta x_1 and x_2 of the incident partons are given by

$$x_1 = (p_\perp/\sqrt{\hat{s}})[\operatorname{ctg}(\theta_l/2) \dotplus \operatorname{ctg}(\theta_k/2)]; \tag{A.17}$$

$$x_2 = (p_\perp/\sqrt{\hat{s}})[\operatorname{tg}(\theta_l/2) \dotplus \operatorname{tg}(\theta_k/2)]. \tag{A.18}$$

APPENDIX 2. APPROXIMATE EXPRESSIONS FOR INCLUSIVE DISTRIBUTIONS AT LARGE TRANSVERSE MOMENTA

In this appendix, we give approximate expressions for the inclusive distributions, using a simple approximation with no correlations for the cross section for the production of two jets (21) and the jet fragmentation functions (10) and (A.1). We take

$$A_1(\sqrt{\hat{s}}/2) = A_2(\sqrt{\hat{s}}/2) = 1.$$

Inclusive Single-Particle Distribution. The inclusive single-particle distribution has the form

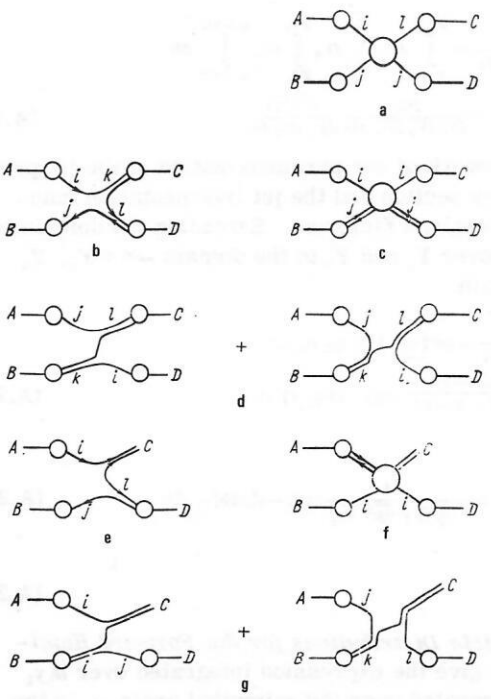

FIG. A.2.

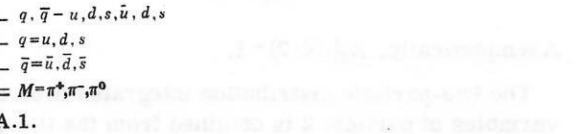

FIG. A.1.

$$\frac{d^3\sigma}{dy_1\,dq_{\perp_1}\,d\varphi_1}=\int_{q_{\perp_1}}^{\sqrt{s}/2}dP_\perp\int_{Y_{s_1}}^{Y_{s_2}}dY_s\int_{Y_{0_1}}^{Y_{0_2}}dY_0\int_{\varphi_2-\pi/2}^{\varphi_1+\pi/2}d\Phi$$
$$\times\frac{d^4\sigma_J}{dY_s\,dY_0\,dP_\perp\,d\Phi}\,\frac{d^3n(\hat{s})}{dq_{\perp_1}\,d\varphi_1\,dy_1}. \tag{A.19}$$

In the framework of our parametrization of the jet production cross section and the jet fragmentation function, four integrals factorize. Extending the domain of integration over Y_s and Y_0 to the domain $-\infty\leq Y_s,\ Y_0\leq\infty$, we obtain

$$\frac{d^3\sigma}{dy_1\,dq_{\perp_1}\,d\varphi_1}=\operatorname{erf}\left(\frac{\pi}{2c_1}\right)W_1(y_1,B_s,c_1)$$
$$\times\frac{CF!\,(N-2)!}{q_{\perp_1}^{N-2}\,(F+N-1)!}\exp(-2Dq_{\perp_1}/\sqrt{s}). \tag{A.20}$$

Here

$$W_1(y_1,B_s,c_1)=\frac{1}{\sqrt{\pi}\,\sqrt{2B_s^2+c_1^2}}\exp\left[-y_1^2/(2B_s^2+c_1^2)\right] \tag{A.21}$$

and

$$c_i=b/q_{\perp_i}. \tag{A.22}$$

Two-Particle Distributions for the Forward Hemisphere. We give the expression integrated over $d(y_1+y_2)$ and integrated over the azimuthal angle φ_2 in the interval $\varphi_1-\Delta\phi\leq\varphi_2\leq\varphi_1+\Delta\phi$:

$$\frac{d^4\sigma}{dq_{\perp_1}\,dq_{\perp_2}\,d(y_1-y_2)\,d\varphi_1}=\int_{\varphi_1-\Delta\Phi}^{\varphi_1+\Delta\Phi}d\varphi_2\int_{-\infty}^{\infty}d(y_1+y_2)\int_{q_{\perp_1}+q_{\perp_2}}^{\sqrt{s}/2}dP_\perp\int_{Y_{0_1}}^{Y_{0_2}}dY_0$$
$$\times\int_{\varphi_{\max}=\frac{\pi}{2}}^{\varphi_{\min}+\frac{\pi}{2}}d\Phi\,\frac{d^4\sigma_J}{dY_s\,dY_0\,dP_\perp\,d\Phi}\,\frac{d^6n(\hat{s})}{dq_{\perp_1}\,dq_{\perp_2}\,dy_1\,dy_2\,d\varphi_1\,d\varphi_2}; \tag{A.23}$$

$$\varphi_{(\min)}^{\max}=\max_{(\min)}(\varphi_1,\varphi_2). \tag{A.24}$$

Proceeding as before, we obtain

$$\frac{d^4\sigma}{dq_{\perp_1}\,dq_{\perp_2}\,d(y_1-y_2)\,d\varphi_1}=A_1(\Delta\phi,c_1,c_2)\,W_2((y_1-y_2),B_s,c_1,c_2)\,\frac{(F+1)^2}{q_{\perp_1}q_{\perp_2}}$$
$$\times\frac{1}{(q_{\perp_1}+q_{\perp_2})^{N-1}}\exp\left(-\frac{2D\,(q_{\perp_1}+q_{\perp_2})}{\sqrt{s}}\right)\frac{CF!\,(N-2)!}{(F+N-1)!}. \tag{A.25}$$

Here, we have adopted the abbreviation

$$W_2((y_1-y_2),B_s,c_1,c_2)=\frac{1}{\sqrt{\pi}\,\sqrt{c_1^2c_2^2/2B_s^2+c_1^2+c_2^2}}$$
$$\times\exp\left[-\frac{(y_1-y_2)^2}{c_1^2c_2^2/2B_s^2+c_1^2+c_2^2}\right]. \tag{A.26}$$

The azimuthal acceptance is determined by

$$A_1(\Delta\phi,c_1,c_2)=\int_{-\Delta\phi}^{\Delta\phi}d\varphi_2\,\frac{1}{2\sqrt{\pi}}\,\frac{1}{\sqrt{c_1^2+c_2^2}}\exp\left[-\frac{\varphi_2}{c_1^2+c_2^2}\right]$$
$$\times\left\{\operatorname{erf}\left[\frac{\pi}{2}\sqrt{\frac{1}{c_1^2}+\frac{1}{c_2^2}}-\frac{\varphi_2}{c_2^2\sqrt{\frac{1}{c_1^2}+\frac{1}{c_2^2}}}\right]\right.$$
$$\left.-\operatorname{erf}\left[\left(\varphi_2-\frac{\pi}{2}\right)\sqrt{\frac{1}{c_1^2}+\frac{1}{c_2^2}}-\frac{\varphi_2}{c_2^2\sqrt{\frac{1}{c_1^2}+\frac{1}{c_2^2}}}\right]\right\}. \tag{A.27}$$

For sufficiently large $\Delta\phi$ and for sufficiently large transverse momenta $q_{\perp_1}$ and $q_{\perp_2}$

$$A_1(\Delta\phi,c_1,c_2)\approx 1. \tag{A.28}$$

Distribution for One Trigger Particle and One Particle of the Opposite Hemisphere. We give the expression obtained by integrating over the azimuthal angle in the interval $\varphi_1+\pi-\Delta\phi\leq\varphi_2\leq\varphi_1+\pi+\Delta\phi$:

$$\frac{d^5\sigma}{dq_{\perp_1}\,dq_{\perp_2}\,d\varphi_1\,dy_1\,dy_2}=\int_{\varphi_1+\pi-\Delta\Phi}^{\varphi_1+\pi+\Delta\Phi}d\varphi_2\int_{q_{\perp_1}}^{\sqrt{s}/2}dP_\perp\int_{Y_{0_1}}^{Y_{0_2}}dY_0\int_{Y_{s_1}}^{Y_{s_2}}dY_s\int_{\varphi_{\max}-\pi/2}^{\varphi_{\min}+\pi/2}d\Phi$$
$$\times\frac{d^4\sigma_J}{dY_s\,dY_0\,dP_\perp\,d\Phi}\,\frac{d^3n_s(\hat{s})}{dq_{\perp_1}\,dy_1\,d\varphi_1}\,\frac{d^3n_0(\hat{s})}{dq_{\perp_2}\,dy_2\,d\varphi_2}, \tag{A.29}$$

where

$$\varphi_{(\min)}^{\max}=\max_{(\min)}(\varphi_1+\pi,\varphi_2). \tag{A.30}$$

As above, we obtain

$$\frac{d^5\sigma}{dq_{\perp_1}\,dq_{\perp_2}\,dy_1\,dy_2\,d\varphi_1}=A_1(\Delta\phi,c_1,c_2)\,W_1(y_1,B_s,c_1)\,W_1(y_2,B_0,c_2)$$
$$\times\frac{C\,(F+1)^2}{q_{\perp_1}q_{\perp_2}}\int_{q_{\perp_1}}^{\sqrt{s}/2}dP_\perp\,\frac{1}{P_\perp^N}\exp\left(-\frac{2DP_\perp}{\sqrt{s}}\right)\left(1-\frac{q_{\perp_1}}{P_\perp}\right)^F\left(1-\frac{q_{\perp_2}}{P_\perp}\right)^F. \tag{A.31}$$

Distribution for the Detected Particle and Two Particles of the Opposite Hemisphere. We give the expression integrated over $d(y_2+y_3)$ and the azimuthal angles φ_2 and φ_3 in the interval $\varphi_1+\pi-\Delta\phi\leq\varphi_i\leq\varphi_1+\pi+\Delta\varphi$, $i=2,3$:

$$\frac{d^6\sigma}{dq_{\perp_1}\,dq_{\perp_2}\,dq_{\perp_3}\,dy_1\,d(y_2-y_3)\,d\varphi_1}=A_2(\Delta\phi,c_1,c_2,c_3)$$
$$\times W_1((y_1,B_s,c_1)\,W_2(y_2-y_3),B_0,c_2,c_3)\,\frac{C\,(F+1)^3}{q_{\perp_1}q_{\perp_2}q_{\perp_3}}\int_{q_{\perp_1}}^{\sqrt{s}/2}dP_\perp\,\frac{1}{P_\perp}$$
$$\times\exp\left(-\frac{2DP_\perp}{\sqrt{s}}\right)\left(1-\frac{q_{\perp_1}}{P_\perp}\right)^F\left(1-\frac{q_{\perp_2}+q_{\perp_3}}{P_\perp}\right)^F. \tag{A.32}$$

The azimuthal acceptance is given by

$$A_2(\Delta\phi,c_1,c_2,c_3)=\frac{1}{\pi\sqrt{c_1^2c_2^2+c_1^2c_3^2+c_2^2c_3^2}}$$
$$\times\int_{-\Delta\phi}^{\Delta\phi}d\varphi_2\int_{-\Delta\phi}^{\Delta\phi}d\varphi_3\exp\left[-\frac{c_3^2\varphi_2^2+c_2^2\varphi_3^2+c_1^2(\varphi_2-\varphi_3)^2}{c_1^2c_2^2+c_1^2c_3^2+c_2^2c_3^2}\right](1/2)$$
$$\times\left\{\operatorname{erf}\left[\left(\varphi_{\max}-\frac{\pi}{2}\right)\sqrt{1/c_1^2+1/c_2^2+1/c_3^2}-\frac{\varphi_2/c_2^2+\varphi_3/c_3^2}{\sqrt{1/c_1^2+1/c_2^2+1/c_3^2}}\right]\right.$$
$$\left.-\operatorname{erf}\left[(\varphi_{\min}+\pi/2)\sqrt{1/c_1^2+1/c_2^2+1/c_3^2}-\frac{\varphi_2/c_2^2+\varphi_3/c_3^2}{\sqrt{1/c_1^2+1/c_2^2+1/c_3^2}}\right]\right\}. \tag{A.33}$$

APPENDIX 3. INCLUSIVE TWO-PARTICLE DISTRIBUTION FOR JET FRAGMENTATION

As in Sec. 2, we determine the two-particle distribution for fragmentation of one jet in the overall center-of-mass system:

$$\frac{d^6n(\hat{s})}{dq_{\perp_1}\,dq_{\perp_2}\,dy_1\,dy_2\,d\varphi_1\,d\varphi_2}=\frac{(F+1)^2}{P_\perp q_{\perp_1}q_{\perp_2}}\,A_2\left(\frac{\sqrt{s}}{2}\right)\left(1-\frac{q_{\perp_1}+q_{\perp_2}}{P_\perp}\right)^F$$
$$\times(1/\pi c_1c_2)\exp\left[-\frac{(y_1-Y_J)^2}{c_1^2}-\frac{(y_2-Y_J)^2}{c_2^2}\right](1/\pi c_1c_2)$$
$$\times\exp\left[-(\varphi_1-\Phi_J)^2/2-(\varphi_2-\Phi_J)^2/2\right]. \tag{A.34}$$

Here and in what follows we use the abbreviation $c_i=b/q_{\perp_i}$, $i=1,2,3$.

The normalization function $A_2(\sqrt{\hat{s}}/2)$ is found from the sum rule for the transverse momenta:

$$\int_0^{P_\perp-q_{\perp_1}}dq_{\perp_2}q_{\perp_2}\int dy_2\,d\varphi_2\,\frac{d^6n(\hat{s})}{dq_{\perp_1}\,dq_{\perp_2}\,dy_1\,dy_2\,d\varphi_1\,d\varphi_2}=(P_\perp-q_{\perp_1})$$
$$\times\frac{d^3n(\hat{s})}{dq_{\perp_1}\,dy_1\,d\varphi_1}. \tag{A.35}$$

Asymptotically, $A_2(\sqrt{\hat{s}}/2)\sim 1$.

The two-particle distribution integrated over the variables of particle 2 is obtained from the two-parti-

cle distribution (A.1):

$$\left\{\langle n_2(\hat{s})\rangle_{q_{\perp_1}} \frac{d^3n(\hat{s})}{dq_{\perp_1}\,dy_1\,d\varphi_1}\right\}$$

$$= \int_{\frac{b'}{\mathrm{ch}\hat{Y}_J}}^{\frac{\hat{E}_J}{\mathrm{ch}\hat{Y}_J}-q_{\perp_1}} dq_{\perp_2} \int_{Y_L(\hat{Y}_J,q_1)}^{Y_U(\hat{Y}_J,q_1)} dy_2 \int_{\Phi_L(\Phi_J,q_1)}^{\Phi_U(\Phi_J,q_1)} d\varphi_2 \times \frac{d^6n(\hat{s})}{dq_{\perp_1}\,dq_{\perp_2}\,dy_1\,dy_2\,d\varphi_1\,d\varphi_2}. \quad (A.36)$$

We replace the purely kinematic limits of integration over y_2 and φ_2 by $Y_L \to -\infty$, $Y_U \to \infty$ and $\Phi_L \to -\infty$, $\Phi_U \to \infty$; in this approximation for $F=1$ or 2 we obtain the result

$$\left\{\langle n_2(\hat{s})\rangle_{q_1} \frac{d^3n(\hat{s})}{dy_{\perp_1}\,dy_1\,d\varphi_1}\right\} \sim \frac{1}{c_1\sqrt{\pi}} \exp\left[-\frac{(y_1-Y_J)^2}{c_1^2}\right] \frac{1}{c_1\sqrt{\pi}} \times \exp\left[-\frac{(\varphi_1-\Phi_J)^2}{c_1^2}\right] \left\{\left(1-\frac{q_{\perp_1}}{P_\perp}\right)^F \ln\left[\frac{\hat{E}_J}{b'}\left(1-\frac{q_{\perp_1}}{P_\perp}\right)\right]\right. \quad (A.37)$$

$$\left. -F\left(1\frac{q_{\perp_1}}{P_\perp}-\frac{b'}{\hat{E}_J}\right)\left(1-\frac{q_{\perp_1}}{P_\perp}\right)^{F-1}+\frac{F-1}{2}\left[\left(1-\frac{q_{\perp_1}}{P_\perp}\right)^2-\frac{b'^2}{\hat{E}_J^2}\right]\right\}.$$

where

$$b'/\hat{E}_J < (1-q_{\perp_1}/P_\perp). \quad (A.38)$$

The curly brackets on the left-hand side of the above expression indicate that the given term is *not* the product of a single-particle distribution and the jet multiplicity.

[1]F. W. Büsser *et al.*, in: Proc. of the Sixteenth Intern. Conf. on High Energy Physics, FNAL, Batavia, Vol. 3 (Eds. J. D. Jackson and A. Roberts), Batavia (1972), p. 317.
[2]F. W. Büsser *et al.*, Phys. Lett. **B46**, 471 (1973.
[3]R. Cottrell *et al.*, Phys. Lett. **B55**, 341 (1975).
[4]M. Della Negra *et al.*, Phys. Lett. **B59**, 481 (1975).
[5]M. Della Negra *et al.*, Phys. Lett. **B59**, 401 (1975).
[6]M. Della Negra *et al.*, Nucl. Phys. **B104**, 365 (1976).
[7]M. Della Negra *et al.*, Contribution to the Tbilisi Conf.; Preprint CERN-EP/PHYS 76–35; 76–43 (1976).
[8]M. Della Negra, in: Proc. of the Seventh Intern. Symposium on Many Particle Production, Tutzing, German Federal Republic, June 21–26, 1976, p. 189.
[9]K. Eggert *et al.*, Nucl. Phys. **B98**, 49 (1975).
[10]P. Darriulat *et al.*, Nucl. Phys. **B107**, 429 (1976).
[11]K. Eggert *et al.*, Nucl. Phys. **B98**, 73 (1975).
[12]F. W. Büsser *et al.*, Nucl. Phys. **B106**, 1 (1976).
[13]B. Alper *et al.*, Phys. Lett. **B17**, 275 (1973).
[14]B. Alper *et al.*, Nucl. Phys. **B87**, 19 (1975).
[15]B. Alper *et al.*, Nucl. Phys. **B100**, 237 (1975).
[16]M. Banner *et al.*, Phys. Lett. **B44**, 537 (1973).
[17]R. Kephart *et al.*, Phys. Rev. D **14**, 2909 (1976).
[18]R. Sosnowski, in: Proc. of the Eighteenth Intern. Conf. on High Energy Physics, Tbilisi, July, 1976, p. A4–3.
[19]D. Antreasyan *et al.*, Phys. Rev. Lett. **38**, 112 (1977).
[20]D. Antreasyan *et al.*, Phys. Rev. Lett. **38**, 115 (1977).
[21]G. Donaldson *et al.*, Phys. Rev. Lett. **36**, 1110 (1976).
[22]C. Donaldson *et al.*, "Inclusive production at large transverse momentum for $\pi^{\pm}p$ and pp interactions at 100 and 200 GeV/c," contribution to the Tbilisi Conference.
[23]D. C. Carey *et al.*, Phys. Rev. Lett. **32**, 24 (1974); **33**, 327 (1974).
[24]J A. Appel *et al.*, Phys. Rev. Lett. **33**, 719, 722 (1974).
[25]J. W. Cronin *et al.*, Phys. Rev. Lett. **31**, 1426 (1973); Phys. Rev. D **11**, 3105 (1975).
[26]F. W. Büsser *et al.*, Phys. Lett. **B51**, 306 (1974).
[27]P. Darriulat, in: Proc. of the Eighteenth Intern. Conf on High Energy Physics, Tbilisi, July, p. A4–23.
[28]J. T. Dakin *et al.*, Phys. Rev. D **10**, 1401 (1974).
[29]P. Capiluppi *et al.*, Nucl. Phys. **B79**, 189 (1974).
[30]C. Bromberg *et al.*, Phys. Rev. Lett. **38**, 1447 (1977).
[31]G. C. Fox, California Institute of Technology Preprint CALT-68-573 (1976).
[32]S. J Brodsky, Talk at the Eighth Colloquium on Many Particle Production, Kaiserberg, France, June 1977.
[33]E.-M. Ilgenfritz *et al.*, Karl-Marx-University, Preprint KMU–HEP 77-C1(1977).
[34]A. Schiller *et al.*, Acta Phys. Pol. B (1977).
[35]M. Gell–Mann, Phys. Lett. **8**, 214 (1964); G. Zweig, Preprint CERN–TH 401, 412 (1964).
[36]J. J. Kokkedee, The Quark Model, Benjamin, New York (1968) (Russian translation published by Mir, Moscow (1971)).
[37]R. H. Dalitz, in: Proc. of the Seventh Intern. Conf. on Few Body Problems in Nuclei and Particle Physics (1975–76), North-Holland, Amsterdam–NewYork–Oxford (1976); H. J. Lipkin, Phys. Rep. C **8**, 173 (1973).
[38]R. P. Feynman, Phys. Rev. Lett. **23**, 1415 (1969); Photon–Hadron Interactions, Benjamin, New York (1972).
[39]J. D. Bjorken, Phys. Rev. **179**, 1547 (1969).
[40]R. E. Taylor, in: Proc. of the 1975 Intern. Symposium on Lepton and Photon Interactions at High Energies, Stanford, August 1975.
[41]R. McElhaney and S. F. Tuan, Phys. Rev. D **8**, 2267 (1973).
[42]V. Barger and R. J. N. Phillips, Nucl. Phys. **B73**, 269 (1974).
[43]L. M. Sehgal, Nucl. Phys. **B90**, 471 (1975).
[44]J. Kripfganz (unpublished, see Ref. 33).
[45]S. M. Berman, J. D. Bjorken, and J. B. Kogut, Phys. Rev. D **4**, 3388 (1971).
[46]J. D. Bjorken, Phys. Rev. D **8**, 4098 (1973).
[47]S. D. Ellis and M. B. Kislinger, Phys. Rev. D **9**, 2027 (1974).
[48]D. Sivers, S. Brodsky, and R. Blankenbecler, Phys. Rep. Phys. Lett. **23C**, 1 (1976).
[49]V. A. Matveev, R. M. Muradyan, and A. N. Tavkhelidze, Lett. Nuovo Cimento **7**, 719 (1973).
[50]S. J. Brodsky and G. R. Farrar, Phys. Rev. Lett. **31**, 1153 (1973).
[51]R. D. Field and R. P. Feynman, California Institute of Technology Preprint CALT 68–565 (1976).
[52]J. Kripfganz and J. Ranft, Nucl. Phys. B124, 353 (1977).
[53]V. N. Gribov and L. N. Lipatov, Phys. Lett. **B37**, 78 (1971).
[54]P. M. Fishbane and J. D. Sullivan, Phys. Rev. D **6**, 3568 (1972).
[55]Y. Eylon and Y. Zarmi, Nucl. Phys. B83, 475 (1974).
[56]C. H. Llewellyn-Smith, Phys. Rev. D **4**, 2392 (1972).
[57]J. F. Gunion, S. J. Brodsky, and R. Blankenbecler, Phys. Lett. **B39**, 649 (1972); Phys. Rev. D **8**, 287 (1973); **6**, 2652 (1972); Phys. Lett. **B42**, 461 (1972).
[58]P. V. Landshoff and J. C. Polkinghorne, Phys. Rev. D **8**, 4157 (1973); Phys. Lett. B45, 361 (1973); Phys. Rev. D **10**, 891 (1974).
[59]R. O. Raitio and G. A. Ringland, Phys. Rev. D **14**, 2291 (1976).
[60]J. D. Bjorken, Acta Phys. Pol. **B5**, 893 (1974).
[61]J. D. Bjorken, in: Proc. of the Summer Institute in Particle Physics, SLAC 191 (1975), p. 85.
[62]S. D. Ellis, M. Jacob, and P. V. Landshoff, Nucl. Phys. B108, 93 (1976).
[63]J. Ranft and G. Ranft, Nucl. Phys. B110, 493 (1976).
[64]M. Jacob and P. V. Landshoff, Preprint CERN–TH 2181 (1976).
[65]W. Furmanski and J. Wosiek, University of Cracow Preprints TU JU 76–7, 76–8, 76–13 (1976).
[66]G. Ranft and J. Ranft, Acta Phys. Pol. **B8**, 179 (1977).
[67]G. Ranft and J. Ranft, Acta Phys. Pol. **B8**, 275 (1977).
[68]E. M. Levin and M. G. Ryskin, Zh. Eksp. Teor. Fiz. **69**, 1537 (1975) [Sov. Phys. JETP **42**, 783 (1975)].
[69]K Kajantie, Rapporteur's Talk at the European Conf. on Elementary Particles, Budapest, July (1977).
[70]M. Gronau and Y. Zarmi, Preprint Technion PH–77–30 (1977).

[71]K. J. Anderson *et al.*, Phys. Rev. Lett. **37**, 799 (1976).
[72]J. G. Branson *et al.*, Phys. Rev. Lett. **38**, 1334 (1977).
[73]L. M. Lederman and B. G. Pope, Phys. Lett. **B66**, 486 (1977).
[74]F. Hayot, F. S. Henyey, and M. Lebellac, Nucl. Phys. **B80**, 77 (1974); J. Kripfganz and G. Ranft, Karl–Marx–University Report KMU–HEP 74–13 (1974); R. Kirachner (to be published).
[75]F. E. Close, F. Halzen, and D. M. Scott, Phys. Lett. **B68**, 447 (1977); J. F. Gunion, Preprint UCD–76–8 (1976); D. E. Soper, Phys. Rev. Lett. **38**, 461 (1977); J. B. Kogut, Phys. Lett. **B65**, 377 (1976); A. C. Davis and E. J. Squires, Durham University Preprint (May 1977); J. C. Polkinghorne, Preprint CERN TH–2333 (June 1977).
[76]P. V. Landshoff, Phys. Lett. **B66**, 452 (1977); J. F. Gunion, Preprint UCD–76–8 (1976).
[77]K. J. Anderson *et al.*, FNAL Preprint (1976); D. C. Hom *et al.*, Phys. Rev. Lett. **37**, 1374 (1976).
[78]B. L. Combridge, Phys. Rev. D **12**, 2893 (1975).
[79]R. P. Feynman, R. D. Field, and G. C. Fox, CALT–69–595 (1978).
[80]M. Fontannaz and D. Schiff, Orsay Preprint (June 1977).
[81]M. Della Negra *et al.*, CCHK Colloboration; Preprint CERN/EP/PHYS 77–10–Rev (March 1977).
[82]G. Ranft and J. Ranft, Preprint CERN–TH 2363 (August 1977).
[83]R. Hagedorn, Relativistic Kinematics, Benjamin, New York (1963).
[84]J. Abad, A. Cruz, and J. L. Alonso, Nucl. Phys. **B115**, 533 (1976).
[85]C. Michael and L. Vanryckeghen, Liverpool University Preprint LTH–24 (1976).
[86]R. C. Hwa, A. J. Spiessbach, and M. J. Teper, Phys. Rev. Lett. **36**, 1418 (1976).
[87]E. Fischbach and G. W. Look, in Purdue University Preprint (1976).
[88]B. L. Combridge, Phys. Lett. **B62**, 222 (1976).
[89]R. Blankenbecler, S. J. Brodsky, and J. F. Gunion, Phys. Lett. **B42**, 461 (1972); Phys. Rev. D **6**, 2652 (1972).
[90]S. J. Brodsky, Preprint SLAC–Pub. 1733 (1976).
[91]S. J. Brodsky and J. F. Gunion, Preprint SLAC–Pub. 1804 (1976).
[92]R. Blankenbecler *et al.*, Preprint SLAC–Pub. 1513 (1975).
[93]G. R. Farrar, Nucl. Phys. **B77**, 429 (1974).
[94]G. Altarelli *et al.*, Nucl. Phys. **B69**, 531 (1974).
[95]J. Okada, S. Pakvasa, and S. F. Tuan, Lett. Nuovo Cimento **16**, 555 (1976).
[96]V. Barger, T. Weiler, and R. J. N. Phillips, Nucl. Phys. **B102**, 439 (1976).
[97]R. Raitio, Wisconsin University Preprint COO–545 (1976).
[98]R. Baier *et al.*, Nucl. Phys. **B118**, 139 (1977).
[99]B. L. Combridge, J. Kripfganz, and J. Ranft, Preprint CERN–TH–2343.
[100]R. Culter and D. Sivers, Preprint ANL–HEP–PR–40 (June 1977); A. P. Contofouris, R. Gaskell, and A. Nicolaidis, McGill University Reports (1977).
[101]A. J. Buras and K. J. F. Gaemers, Preprint CERN–TH 2322 (1977).
[102]I. Hincpliffe and C. H. Llewellyn-Smith, Oxford Preprint OUTP 77–36 (1977); M. Glück and E. Reya, Mainz Report MZ–TH 77–3 (1977).
[103]A. Shklovskaya *et al.*, Dubna–Leipzig Collaboration, Karl–Marx–University, Preprint KMU–HEP 77–03 (1977).
[104]D. C. Carey *et al.*, Phys. Rev. Lett. **33**, 327 (1974).
[105]J. Bartke *et al.*, Nucl. Phys. **B117**, 293 (1976).
[106]W. B. Fretter *et al.*, Phys. Lett. **B57**, 197 (1975).
[107]E. G. Boos *et al.*, Alma-Ata—Dubna—Moscow—Košice—Prague—Helsinki Collaboration, Paper 903, contribution to the Eighteenth Intern. Conf. on High Energy Physics, Tbilisi (1976).
[108]J. Gasser and U. P. Sukpatme, Cambridge University Preprint DAMTP 76–3 (1976).
[109]G. Preparata and G. Rossi, Nucl. Phys. **B111**, 111 (1976).

Translated by Julian B. Barbour